DEVELOPMENT, USE, AND VALIDATION OF THE CFD TOOL FLACS FOR HYDROGEN SAFETY STUDIES

Prankul Middha

A dissertation submitted in partial fulfilment of the requirement for the degree of philosophiae doctor (PhD)

Institute of Physics and Technology
University of Bergen
Bergen, Norway
2010

Acknowledgements

I would like to thank my advisors Olav Roald Hansen and Bjørn Arntzen for their advice, contributions and feedback on papers. Thanks are also due to my colleagues at GexCon, especially Trygve Skjold and Idar Storvik for their invaluable input, discussions and support during my PhD work. The experiments to determine the burning velocity of hydrogen-air mixtures would not have been possible without the help of Trygve Skjold.

Thanks are also due to Norwegian Research Council (NFR) for their funding for this PhD study. The author is also involved in the International Energy Agency (IEA) Task 19 on Hydrogen Safety that is also funded by NFR. A lot of this work was done as a part of GexCon's involvement in the EU-sponsored Network of Excellence, HySafe. I developed good cooperation with several researchers there which have also played a significant role in this PhD study.

Finally, I wish to thank my wife Prachi and my daughters Prarthna and Prapti for their support, patience and love. Without you, it would not have been possible.

Bergen, Spring 2010
Prankul Middha

Abstract

Computational Fluid Dynamics (CFD) calculations for gas explosion safety have been widely used for doing risk assessments within the oil and gas industry for more than a decade. Based on predicted consequences of a range of potential accident scenarios a risk level is predicted. The development of applications using hydrogen as a clean energy carrier has accelerated in recent years, and hydrogen may be used widely in future. Due to the very high reactivity of hydrogen, safe handling is critical. To be able to perform proper consequence modelling as a part of a risk assessment, it is essential to be able to model the physical processes well. CFD tools have the potential to model the relevant physics and predict well, but without proper user guidelines based on extensive validation work, very mixed prediction capability can be expected. This PhD thesis deals with the development and validation of the Computational Fluid Dynamics (CFD) tool FLACS for hydrogen safety applications. Significant validation work against several experiments has been carried out in order to increase the confidence of predictions of scenarios relevant to hydrogen safety. The validation studies have included dispersion, explosion and combined dispersion and explosion studies. A range of different dispersion experiments is simulated, including low momentum releases in a garage, sub-sonic jets in a garage with stratification effects and subsequent slow diffusion, low momentum and subsonic horizontal jets influenced by buoyancy, and free jets from high-pressure vessels. LH_2 releases are also considered. Some of the simulations are performed as blind predictions. FLACS uses a utility program in order to model releases from high-pressure reservoirs. Work has been carried out in order to extend the models in the utility program in order to include real gas effects. Validation against explosion experiments in geometries ranging from smooth and obstructed pipes, refuelling station, tunnel, vented vessels, jet-ignited lane, etc. have been successfully performed. However, CFD tools must be validated against representative experimental data, involving combined release and ignition scenarios, in order to have a real predictive capability in accidental situations. Therefore, a detailed study involving release and ignition experiments from FZK has been carried out.

Work has also been done for developing risk analysis methods specific to hydrogen applications. Quantitative Risk Assessments (QRA) of hydrogen applications presents new challenges due to a large difference in properties of hydrogen and natural gas, namely in reactivity, flammability limits, buoyancy and transport properties. However, it is not realistic to perform an extensive risk assessment for all hydrogen applications similar to that carried out for petrochemical installations. On the other hand, simplified tools and techniques based on codes and standards likely have a limited applicability, as these are not able to represent actual geometry and physics of the explosion. A 3-step approach is proposed, in which the CFD-tool FLACS is used to estimate the risk. The initial approach is to carry out a "worst-case" calculation evaluating the consequences if a full stoichiometric gas cloud is ignited. Mitigation measures can also be considered. As a second step, if potential consequences of the initial approach are not acceptable, the assumptions are refined and more calculations are performed to make the evaluations more realistic and reduce unnecessary conservatism of the chosen worst-case scenarios. Typically a number of dispersion calculations are performed to generate likely gas clouds, which are subsequently ignited. If estimated consequences are still not acceptable, a more comprehensive study, including ventilation, dispersion and explosion, is performed to evaluate the probability for unacceptable events. Calculation examples have been used to illustrate the different approaches. The proposed approach is thus very flexible, and can be tailored to the scenario under consideration.

However, in many of these scenarios, especially involving reactive gases such as hydrogen, deflagration to detonation transition (DDT) may be a significant threat. Another main part of this thesis has been the development of models in order to enable FLACS to provide indications about the possibility of a deflagration-to-detonation transition (DDT). The likelihood of DDT

has been expressed in terms of spatial pressure gradients across the flame front. This parameter is able to visualize when the flame front captures the pressure front, which is the case in situations when fast deflagrations transition to detonation. Reasonable agreement was obtained with experimental observations in terms of explosion pressures, transition times, and flame speeds for several practical geometries. The DDT model has also been extended to develop a more meaningful criterion for estimating the likelihood of DDT by comparison of the geometric dimensions with the detonation cell size.

In the end, several practical studies have been carried out. This includes a very detailed simulation study to examine what, if any, is the explosion risk associated with hydrogen vehicles in tunnels. Its aim was to further our understanding of the phenomena surrounding hydrogen releases and combustion inside road tunnels, and furthermore to demonstrate how a risk assessment methodology described above could be applied to the current task. A study to determine the relative risk of methane, hydrogen and hythane (a blend of hydrogen and methane) has also been performed.

The work performed in the dissertation has resulted in 18 publications (journal articles + conference proceedings). 12 of them are included in the appendix and the complete list of publications (including 4 other conference papers connected with the work done in this thesis) is presented in the next pages.

Thus, this dissertation presents the extensive work that has been carried out to develop and validate FLACS-Hydrogen to pave the way to use the tool for applications related to hydrogen safety.

List of Publications associated with this PhD study

Paper 1
P. Middha, O.R. Hansen, I.E. Storvik, (2009). Validation of CFD-model for hydrogen dispersion. *Journal of Loss Prevention in Process Industries*, 22(6), 1034-1038.

Paper 2
P. Middha, M. Ichard, B.J. Arntzen, (2010). Validation of CFD modelling of LH_2 spread and evaporation against large-scale spill experiments. *International Journal of Hydrogen Energy*, doi:10.1016/j.ijhydene.2010.03.122.

Paper 3
A.G. Venetsanos, E. Papanikolaou, M. Delichatsios, J. Garcia, O.R. Hansen, M. Heitsch, A. Huser, W. Jahn, T. Jordan, J.-M. Lacome, H.S. Ledin, D. Makarov, **P. Middha**, E. Studer, A.V. Tchouvelev, A. Teodorczyk, F. Verbecke, M.M. Van der Voort, (2009). An inter-comparison exercise on the capabilities of CFD models to predict the short and long term distribution and mixing of hydrogen in a garage. *International Journal of Hydrogen Energy* 34(14), 5912-5923.

Paper 4
P. Middha, T. Skjold, A.E. Dahoe, (2006). Turbulent and laminar burning velocities from constant volume expansions in a 20-litre vessel, 31st International Symposium on Combustion, Heidelberg, Germany, August 6-11, 2006.

Paper 5
P. Middha, O.R. Hansen, (2009). Using computational fluid dynamics as a tool for hydrogen safety studies. *Journal of Loss Prevention in the Process Industries* 22(3), 295-302.

Paper 6
P. Middha, O.R. Hansen, M. Groethe, B.J. Arntzen, (2007). Hydrogen Explosion Study in a Confined Tube: FLACS CFD Simulations and Experiments, In: Proceedings of the 21st International Colloquium of Dynamics of Explosions and Reactive Systems, Poitiers, France, July 23-27, 2007.

Paper 7
D. Makarov, F. Verbecke, V. Molkov, O. Roe, M. Skotenne, A. Kotchourko, A. Lelyakin, J. Yanez, O. R. Hansen, **P. Middha**, S. Ledin, D. Baraldi, M. Heitsch, A. Efimenko, A. Gavrikov, (2009). An inter-comparison exercise on CFD model capabilities to predict a hydrogen explosion in a simulated vehicle refuelling environment. *International Journal of Hydrogen Energy* 34(6), 2800-2814.

Paper 8
P. Middha, O.R. Hansen, J. Grune, A. Kotchourko, (2010). Validation of CFD calculations against ignited impinging hydrogen jet experiments. *Journal of Hazardous Materials*, 179(1-3), 84-94.

Paper 9
P. Middha, O.R. Hansen, I.E. Storvik, (2006). Prediction of deflagration to detonation transition in hydrogen explosions, In: AIChE Spring National Meeting and 40th Annual Loss Prevention Symposium, Orlando, FL, April 23-27, 2006.

Paper 10
P. Middha, O.R. Hansen, (2008). Predicting deflagration to detonation transition in hydrogen explosions. *Process Safety Progress* 27(3), 192-204.

Paper 11

O.R. Hansen, **P. Middha**, (2008). CFD-based risk assessment for hydrogen applications. *Process Safety Progress* 27(1), 29-34.

Paper 12

P. Middha, O.R. Hansen, (2009). CFD simulation study to investigate the risk from hydrogen vehicles in tunnels. *International Journal of Hydrogen Energy* 34(14), 5875-5886.

Other Journal articles

1. D. Baraldi, A. Kotchourko, A. Lelyakin, J. Yanez, **P. Middha**, O.R. Hansen, A. Gavrikov, A. Efimenko, F. Verbecke, D. Makarov, V. Molkov, (2009). An inter-comparison exercise on CFD model capabilities to simulate hydrogen deflagrations in a tunnel. *International Journal of Hydrogen Energy*, 34(18), 7862-7872.
2. A.G. Venetsanos, E. Papanikolaou, **P. Middha**, O.R. Hansen, J. Garcia, M. Heitsch, D. Baraldi, P. Adams, (2010). HySafe Standard benchmark Problem SBEP-V11: Predictions of hydrogen release and dispersion from a CGH2 bus in an underpass. *International Journal of Hydrogen Energy*, 35(8), 3857-3867.
3. P. Middha, D. Engel, O.R. Hansen, (2009). Can the addition of hydrogen to natural gas reduce the explosion risk? In: Proceedings of 3rd International Conference of Hydrogen Safety, Corsica, France, September 16-18, 2009. International Journal of Hydrogen Energy, doi:10.1016/j.ijhydene.2010.04.132.

Other Selected Conference Publications

1. **P. Middha**, O.R. Hansen, H. Schneider, (2007). Deflagration to Detonation Transition (DDT) in Jet Ignited Hydrogen-Air Mixtures: Large Scale Experiments and FLACS CFD Predictions. In: 12th International Loss Prevention Symposium, Edinburgh, UK, May 22-24, 2007.
2. T. Jordan, J. Xiao, **P. Middha**, J. Travis, J. Garcia, J., O.R. Hansen, V. Molkov, F. Verbecke, A.G. Venetsanos, (2007). Results of the HySafe CFD validation Benchmark SBEP-V5. In: 2nd International Conference of Hydrogen Safety, San Sebastian, Spain, September 11-13, 2007.
3. **P. Middha**, C.J.M. van Wingerden, O.R. Hansen, (2008). On the possibility of DDT in vapour cloud explosions. In: 42nd Annual Loss Prevention Symposium, New Orleans, USA, April 6-10, 2008.
4. **P. Middha**, O.R. Hansen, (2008). Hydrogen safety research at GexCon. In: Norwegian Hydrogen Seminar 2008, Bergen, September 25-26, 2008.
5. O.R. Hansen, **P. Middha**, (2008). Blind prediction of dispersion and explosion experiments using CFD. In: 2nd World Conference on Safety of Oil & Gas Industry, College Station, TX, October 28-29, 2008.
6. **P. Middha**, C.J.M. van Wingerden, (2009). On the use of consequence models for accident investigations. In: 43rd Annual Loss Prevention Symposium, Tampa, FL, USA, April 26-30, 2009.
7. T. Jordan, et al., **P. Middha**, et al. (46 authors), (2009). Achievement of the EC Network of Excellence HySafe, In: Proceedings of 3rd International Conference of Hydrogen Safety, Corsica, France, September 16-18, 2009. *International Journal of Hydrogen Energy*, under review.

Nomenclature

Latin Symbols

a	Model constant (Able-Nobel EOS)
A	Area
A_f	Flame surface element
c	Speed of sound
C_p	Heat capacity (constant pressure)
C_v	Heat capacity (constant volume)
dP/dx	Spatial pressure gradient
g	Gibb's free energy
h	Enthalpy
k	Turbulent kinetic energy
K_u	Stretch rate
Ka	Karlovitz number
Le	Lewis number
l_I	Integral length scale
L_M	Markstein length
$\dot{m}$	Mass Flow rate
M	Mach number
Ma	Markstein number
n	Effective specific heat ratio for non-ideal gases (= γ for ideal gases)
P	Pressure
Pr	Prandtl number
$Q9$	Equivalent stoichiometric gas cloud
R	Gas constant
Re	Reynolds number
R_F	Flame radius
s	Entropy
S_L	Laminar Burning Velocity
S_{QL}	Quasilaminar burning velocity
S_T	Turbulent Burning Velocity
t	Time
T	Temperature
T_f	Flame temperature
v	Velocity
V	Flammable volume
$\underline{V}$	Specific volume
X_{CV}	Control volume size
Z	Compressibility factor

Greek Symbols

α	Thermal diffusivity
β	Flame thickness adjustment factor (in flame model)
δ_L	Laminar flame thickness
ε	Turbulent dissipation
γ	Specific Heat Ratio
ρ	Density
σ	Volume expansion
υ	Dynamic viscosity

Table of Contents

1 Introduction

The possibility of using hydrogen as an energy carrier has increasingly caught interest of both public and government policy makers in recent times due to the concerns about the possible impact of greenhouse gases and the finite nature of fossil fuel reserves. The expected scarcity of fossil fuels and the fear of carbon induced climate changes make the deployment of hydrogen in combination with renewable energy sources and possibly nuclear energy an interesting alternative (Winter, 2009). Hydrogen combustion does not produce any greenhouse gases that are responsible for local and global environmental concerns. Even if the large majority of research for the ushering in of a "hydrogen economy" involves developing effective production and storage techniques, the safety of hydrogen during production and subsequent large-scale usage remains a significant concern (e.g. Brewer, 1978; Hord, 1978; Astbury, 2008). The nuclear industry has also been particularly interested in evaluating hydrogen safety, especially due to accidents like Chernobyl (e.g. Balanov, 2007) and Three Mile Island (e.g. Henrie and Postma, 1983), and the potential increase in use of nuclear power. Compared to offshore oil exploration accidents, where consequences will be mainly local, the consequences from nuclear accidents can be more global.

The hazards from hydrogen primarily stem from its wide flammability range, extremely fast burning rate (order of magnitude larger compared to natural gas), and the considerable amount of energy released when it burns or explodes (Astbury, 2008). This leads to consequences that are much more severe as compared to hydrocarbons. This is clearly shown by experiments carried out in the late 1980s in a wedge shaped geometry (Bjerketvedt, Bakke and van Wingerden, 1997) that show the overpressures generated on the combustion of a stoichiometric fuel-air mixture for various gases (results are shown in Figure 1.). Hydrogen is also quite different from natural gas in certain other ways, some of which actually help to reduce the risk of using the gas. Hydrogen is much lighter than air and therefore, has very strong buoyancy that will quickly remove the gas in an unconfined situation. However, any leakage of hydrogen in confined space frequented by motor vehicles such as parking garages and tunnels poses a significant hazard. Further, much lower energies are needed to ignite hydrogen and mitigation methods traditionally used for natural gas seldom work in case of hydrogen. The safety issue is further worsened by the wide detonability limits and the propensity of flames to accelerate rapidly due to the very high laminar burning velocity of hydrogen. Clearly, hydrogen has many characteristics that are significantly different from conventional gaseous fuels such as natural gas, propane, etc. The HySafe project website, www.hysafe.org, contains an updated view of hydrogen safety considerations. These must be accounted for before designing and installing any systems such as fuel cells, dispensers, etc. that will form a part and parcel of any future society that uses hydrogen as an energy carrier. These are described in some detail below.

Physical and Chemical Characteristics

At atmospheric temperature and pressure, hydrogen is colourless, odourless, non-toxic and non-corrosive, which is physiologically not dangerous in principle. One of its most important and positive characteristics is its low density (it is the lightest of all elements). It is positively buoyant above a temperature of 22 K. Hydrogen gas has a very high diffusivity and a high buoyant velocity. Therefore, it mixes rapidly with ambient air upon release. This is a favourable safety effect in unconfined and well-ventilated areas where it helps to reduce the likelihood of a flammable mixture forming in the vicinity of a release. However, if leaks occur in (partially) confined or poorly ventilated spaces, the concentration of hydrogen can reach dangerous levels in higher regions, for example, underneath a roof. The risk of explosion can then be considerable if ignition sources are present. Hydrogen molecules have a small size, small molecular weight, and a

low viscosity. As a result, hydrogen can permeate through materials and pass through smaller leak paths as compared to other gases. This increases the likelihood of the formation of a flammable gas cloud. Hydrogen gas does not have a flash point as it is already a gas at ambient conditions. Therefore, cryogenic hydrogen will flash at all temperatures above its boiling point of 20 K.

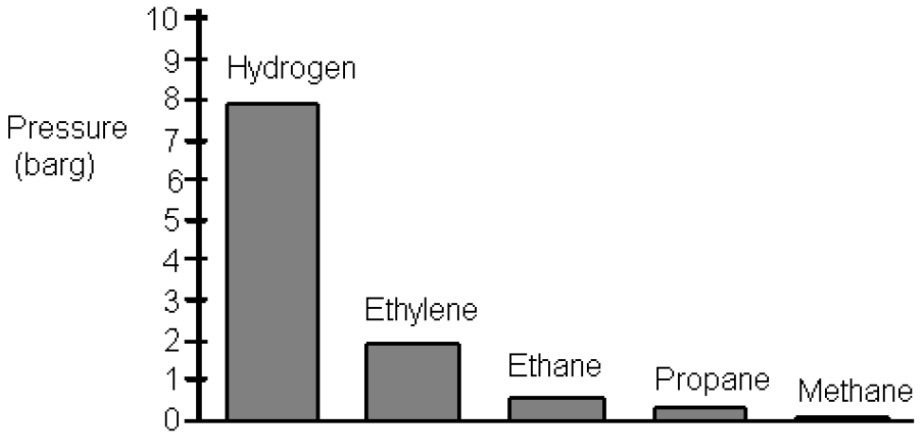

Figure 1.1 – Comparison of explosion overpressure for various stoichiometric gas-air mixtures in a 10 m wedge shaped vessel (from Bjerketvedt, Bakke and van Wingerden, 1997)

Ignition

The auto-ignition temperature for hydrogen, which is the minimum temperature of a hot surface that can ignite a flammable mixture, is 858 K. It is relatively high (higher than natural gas that has a value of 813 K). Over the flammable range of hydrogen-air mixtures, the minimum ignition energy varies by almost three orders of magnitude and can be as low as 0.017 mJ, a value that is an order of magnitude lower than that of hydrocarbon-air mixtures. Even very small sparks such as those produced by wearing certain types of clothing are enough to ignite a hydrogen-air mixture. However, it must be pointed out that in practical release situations the lower ignition energy of hydrogen may not be as significant a differentiation between the fuels as it first seems. The minimum ignition energy tends to be for mixtures at around stoichiometric composition (29.5 % for hydrogen). At the LFL the ignition energy for hydrogen is similar to that of methane. In addition many so called weak ignition sources such as electrical equipment sparks, electrostatic sparks or sparks from striking objects involve more energy than is required to ignite methane or propane.

In addition, spontaneous ignition is much more commonly observed with hydrogen. There have been several explanation propounded to explain this effect. One of these is that hydrogen exhibits a positive Thompson-Joule effect at temperatures above 193 K, the inversion temperature. This means that the temperature of hydrogen gas increases upon depressurisation, which in turn may lead to ignition. This makes hydrogen more susceptible to ignition after sudden release from high pressure containment. Another explanation is "diffusion ignition" whereby a shock wave from expansion of high-pressure gas into air is postulated to cause local auto-ignition. This is currently an area of research and many groups around the world are involved in studying this phenomena currently (see, e.g. Dryer, et al., 2007; Groethe, et al., 2005). Golub and coworkers (2007; 2008) conclude that self-ignition of the hydrogen-air mixture occurs at the contact surface of the hydrogen and oxidant mixture and is a result of temperature increase produced by the shock wave (the shock wave is in turn produced in front of the high-pressure hydrogen gas propagating in a tube). It has also been found that the downstream geometry

following a discharge from a high-pressure source also plays a role in whether or not self-ignition occurs (Dryer, et al., 2007; Mogi, et al., 2008). Attempts have also been made to study this phenomenon experimentally using direct numerical simulations (DNS) such as the work done by Yamada, et al. (2009). Golub and coworkers have also carried out numerical simulations of their own using detailed kinetics of hydrogen oxidation (Xu, et al., 2008; Golub, et al., 2009). However, a detailed analysis of this phenomenon is beyond the scope of this dissertation. Nonetheless, attempts are made to include this in the risk analysis methods presented in Chapter 9.

Combustion Properties

Hydrogen burns in a non-luminous, almost invisible pale blue, hot flame to water vapour (and there is no release of CO_2 or soot). A hydrogen fire is next to impossible to detect with naked eye and there is very limited radiation due to the absence of soot. The low emissivity of a hydrogen flame reduces the heat transfer by radiation to objects near the flame. Thus, a hydrogen fire is potentially less dangerous than a natural gas fire.

The flammability range of hydrogen (at room temperature) is between 4–75 % vol. in air (Coward & Jones, 1952; Lewis & von Elbe, 1987), whereas the maximum flame temperature of a burning (premixed stoichiometric) hydrogen-air mixture is 2403 K (Glassman, 1987). In comparison, the flammability range of natural gas at room temperature is between 5–15 % vol. in air. The burning velocity of hydrogen in air at stoichiometric ambient conditions is around 2.5 m/s reaching a maximum of approximately 3 m/s at a concentration of 40.1 %, which would even increase to 11.75 m/s in pure oxygen. (In comparison, the value for natural gas is of the order of 0.4 m/s). These values are higher than the ones of hydrocarbon fuel-air mixtures due to the fast chemical kinetics and high diffusivity of hydrogen. This leads to consequences (upon ignition) that are much more severe compared to natural gas.

The detonability limits of hydrogen lie in the range of 18 % (as low as 11 % in some experiments) to 59 % of hydrogen concentration in air by volume. There is also a high sensitivity to a transition to detonation (DDT). Detonation can potentially cause a much severe damage as compared to an ordinary explosion (deflagration). A measure of the sensitivity of a mixture is the detonation cell size. The detonation cell size for a stoichiometric hydrogen-air mixture is of the order of 10–15 mm. In comparison, the value for a methane-air mixture is as large as 330 mm. More details on this are given in Chapter 7.

Thus, it can be established that the use of hydrogen represents many potential hazards even if it does have some favourable properties such as high buoyancy. This points to the need for establishing viable tools to carry out the required safety and risk analyses connected with the use of hydrogen infrastructure (LaChance, Tchouvelev & Ohi, 2007). It is possible to use both simplified methods (venting guidelines, etc.) and advanced tools such as those based on Computational Fluid Dynamics (CFD) in order to carry out the required safety analyses. For safety analysis of hydrogen systems, there is also a significant focus on regulations, codes, and standards (RCS) e.g. safety distance rules (e.g. Schjølberg and Østdahl, 2008; Marangon, Carcassi, Engebø & Nilsen, 2007; Rosyid, Jablonski & Hauptmanns, 2007). However, only CFD tools have the potential to model the relevant physics involved in safety analyses. With CFD, it is possible to take account of effects of buildings, mitigation measures, piping and vessel arrangements, etc. which have been found to have a strong influence on the consequences of any accident or unwanted incident. Due to these reasons, CFD has been used more and more in recent years as a part of QRA studies in the oil and gas and associated chemical industry (NORSOK, 2001; Herrmann, 2007). A primary requirement for the use of any such tool, in addition to the models capturing the correct physics, is extensive validation against available small- and large-scale experiments (with studies on variations of various important parameters that may affect

explosion loads and hence risk). The validation should be an integrated part of development. Clear user guidelines must exist to enable user independency, even when predicting blind. Without proper user guidelines based on extensive validation work, very mixed prediction capability can be expected. More details on these requirements are presented in Chapter 8 and paper 11. This study seeks to improve the reliability, efficiency, and the applicability of FLACS for hydrogen safety applications and pave the way for the use of risk studies in a potential "hydrogen economy".

A significant portion of this work has been done as a part of GexCon's involvement in the EU-sponsored Network of Excellence (NoE) HySafe. This network consisted of 25 partners from all over Europe (and 1 in Canada) including research organizations, governmental agencies, university and industry. The objectives of the network included (a) Contribution to common understanding and approaches for addressing hydrogen safety issues, (b) Integration of experience and knowledge on hydrogen safety in Europe, (c) Integration and harmonisation of the fragmented research base, (d) Contribution to EU safety requirements, standards and codes of practice, (e) Contribution to an improved technical culture on handling hydrogen as an energy carrier, and (f) Promotion of public acceptance of hydrogen technologies. A summary of all the achievements of this five year long NoE activity is presented in Jordan, et al. (2009). The work done by the author included several CFD benchmarks and practical applications of CFD to risk and safety analyses.

2 The CFD tool FLACS

Since it is well-known that CFD analyses are very useful to provide consistent and accurate estimates of risk associated with process industry (Holen, 2001), this work has focused on the development and use of the CFD tool FLACS for problems associated with hydrogen safety. The Computational Fluid Dynamics (CFD) tool FLACS has been developed by Chr. Michelsen Institute (CMI), Christian Michelsen Research (CMR) and currently GexCon since 1980, primarily aimed at simulating the dispersion of flammable gas in process areas, and subsequent explosions of gas-air mixtures. FLACS solves the compressible conservation equations for mass, momentum, enthalpy, and mass fraction of species on a 3-*D* Cartesian grid using a finite volume method. Hjertager (1985, 1986) describes the basic equations used in the FLACS model, and Hjertager, Bjørkhaug & Fuhre (1988a,b) present the results of explosion experiments to develop and validate FLACS initially. During the course of more than 25 years of development and evaluation of the FLACS software, the numerical methods have been steadily modified and revised.

The inherent capability of FLACS has been performing explosion and dispersion calculations to help in the improvement of oil and gas platform safety with initial focus on the North Sea. Significant experimental validation activity has contributed to the wide acceptance of FLACS as a reliable tool for prediction of natural gas explosions in real process areas offshore and onshore (Hansen, Storvik & van Wingerden, 1999). Some of the significant efforts include simulations of the 180 m^3 British Gas (Advantica) box (Catlin, Gregory, Johnson & Walker, 1993), 27 m^3 CMR (GexCon) 3D-corner, 50 m^3 CMR (GexCon) M24 module (Hjertager, Bjørkhaug & Fuhre, 1988a; 1988b), Shell SOLVEX chambers (2.5 m^3, 550 m^3), 1–250 m^3 TNO and British Gas MERGE experiments (Mercx, 1996) and 1600–2700 m^3 British Gas (Advantica) BFETS (Selby & Burgan, 1998)/ HSE Phase 3A (Al-Hassan & Johnson, 1998)/ Phase 3B full-scale tests (Johnson, Cleaver, Puttock & van Wingerden, 2002). FLACS is also used as an accident investigation tool. A summary of some past accident investigations has recently been presented by Middha & van Wingerden (2009).

The numerical model uses a second order central differencing scheme for resolving diffusive fluxes and a second-order "kappa" scheme (hybrid scheme with weighting between 2nd order upwind and 2nd order central difference, with delimiters for some equations) to resolve the convective fluxes. The solver is implicit in nature. The time stepping scheme used in FLACS is a first order backward Euler scheme. Second order schemes in time have been implemented, but are generally not used due to short time steps. Based on extensive validation, guidelines for time stepping have been established in order to get accurate results. These are based on CFL (Courant-Friedrich-Levy) numbers based on speed of sound (CFLC) and flow velocity (CFLV). The discretized equations are solved using the BiCGStab in the SIMPLE pressure correction algorithm (Patankar, 1980). The SIMPLE algorithm has been extended to handle compressible flows with additional source terms for the compression work in the enthalpy equation.

FLACS uses a k-ε model in order to model the convection, diffusion, production, and dissipation of turbulence (see, e.g. Harlow & Nakayama, 1967; Launder & Spalding, 1974). However, the standard k-ε model has been modified by adding source terms for turbulence production by velocity gradients to achieve independent and rapid build-up of the turbulent flow field and representative turbulence production from objects not resolved by the computational grid (subgrid objects). In addition, several other modifications have been implemented (Arntzen, 1998) including (a) Modification of the discretization for production of turbulent energy for objects with width equal to about one control volume (CV), (b) Wall functions with no slip condition for solid surfaces, and (c) Source terms for the production of turbulent energy due to Rayleigh–Taylor instabilities (when buoyant gas is accelerating denser gas due to gravity). With

the close coupling between sub-grid modelling and turbulence model, it is not believed that replacing k-ε model with a more advanced turbulence model with more equations and constants will give increase the accuracy for typical simulations carried out with FLACS.

In order to model gas explosions, FLACS contains a combustion model that assumes that the flame in an explosion can be regarded as a collection of flamelets. The ignition process is modelled by artificially forcing the initial chemical reactions in a small volume at the beginning of the calculation. One-step reaction kinetics is assumed, with the laminar burning velocity being a measure of the reactivity of a given mixture. A chemical equilibrium model is used to estimate the composition of the combustion products. These include H_2O and CO_2, but also increasing amounts of H_2, CO and OH for rich concentrations and high temperatures. Heat is added due to combustion and the heat capacities for different gases depend strongly on temperature. The model consists of two parts: a three-step burning velocity model and a flame model.

Since a grid size that is significantly finer than realistically possible is needed to fully resolve the flame, it is common in numerical methods to artificially thicken the flame so that its structure is fully resolved and coarse grids may be used. This method is used in the β flame model in FLACS (Butler and O'Rourke, 1976). The factor β used in FLACS is proportional to the grid size and inversely proportional to the integral length scale (Arntzen, 1998). The flame model gives the flame a constant flame thickness (equal to 3 grid cells) independent of propagation mode and the grid resolution and assures that the flame propagates into the reactant with the specified velocity that is based on a series of parameters. The flame is propagated based on the transport of "products" into new cells and subsequently "burns" with a specified velocity (calculated using the burning velocity model). The real flame area is properly described. A number of correction models are made to compensate for weaknesses due to flame thickness, including (a) Proper estimation of initial stages must be estimated (before 3 control volume flame thickness is reached), (b) Correction for flames with high curvature, (c) Combustion towards walls, and (d) Flame folding behind subgrid objects. These models ensure good results for a range of grid resolutions. The burning velocity model consists of the following three models (Arntzen, 1998):

(a) A laminar burning velocity model that describes the laminar burning velocity as a function of gas mixture, concentration, temperature, pressure, oxygen concentration in air and amount of inert diluents.

(b) A model describing quasi-laminar combustion in the first phases of flame propagation after ignition. Due to flame instabilities e.g. Rayleigh-Taylor and thermal-diffusive instabilities and body forces, the observed burning velocity increases as the flame propagates away from ignition (due to flame wrinkling). This is mathematically represented as:

$$S_{QL} = S_L\sqrt{1 + C_{QL}R_F} \tag{2.1}$$

where S_{QL} is the quasilaminar burning velocity, C_{QL} is the adjustment factor depending on the fuel composition, and R_F is the flame radius. All flame wrinkling at scales less than the grid size is represented by sub-grid models, which is important for flame interaction with objects smaller than the grid size.

(c) A model that describes turbulent burning velocity as a function of turbulence parameters (intensity and length scale). The model is based on a broad range of experimental data (Abdel-Gayed, Bradley & Lawes, 1987). Bray (1990) found that the data from Abdel-Gayed et al. could be represented in a reasonable manner by the following empirical expression:

$$\frac{S_T}{S_L} = 0.875Ka^{-0.392}\frac{u'}{S_L} \tag{2.2}$$

Here, *Ka* is the Karlovitz stretch factor, S_T is the turbulent burning velocity, and S_L is the laminar burning velocity. By introducing the definition for the Karlovitz stretch factor, in terms of the turbulent Reynolds number ($\mathrm{Re}_T = u' l_I / \nu$, where ν is the kinematic viscosity), this can be reformulated to obtain the default correlation for the turbulent burning velocity in FLACS:

$$S_T = 0.875\left\{0.1573\left(\frac{u'}{S_L}\right)^2\left(\frac{u' l_I}{\upsilon}\right)^{-0.5}\right\}^{-0.392} u' \qquad (2.3)$$
$$= 1.81\, u'^{0.412} S_L^{0.784} l_I^{0.196} \upsilon^{-0.196}$$

However, the length scale used here is not directly obtained from the turbulence model, but is rather a function of the geometry and flame travel distance. With very strong turbulence compared to length scale, a relation limiting the reaction rate (Karlovitz "quench" criterion) is also implemented. The effect of Lewis number (*Le*) that is a dimensionless quantity defined as the thermal diffusivity divided by the mass diffusion coefficient is also included (also see below).

A good description of geometry and the coupling of geometry to the flow, turbulence, and flame is one of the key elements in the modelling. Since even small details of the obstacles on a petrochemical installation can have a significant impact on flame acceleration and hence explosion overpressures, the proper representation of the obstacles has been a key aspect of the development of the FLACS code (Bjerketvedt, Bakke & van Wingerden, 1997). The FLACS code uses a distributed porosity concept which enables the detailed representation of complex geometries (in some cases with up to 400.000 objects) using a Cartesian grid (as shown in Figure 2.). Large objects and walls are represented on-grid, and smaller objects are represented sub-grid. This enables geometrical details to be characterized while maintaining reasonable simulation times. This approach represents geometrical details as porosities (opposite of blockage) for each control volume. Each CV surface or each CV volume is fully open, fully blocked or partly blocked. For the partly blocked surfaces or volumes, the porosity is defined as the fraction of the area/volume that is available for fluid flow. Sub-grid objects contribute to flow resistance, turbulence generation and flame folding in the simulation as it is important to model the turbulence correctly for partly porous and "sub-grid" objects to obtain good results. In case of small objects, the flow kinetic energy lost due to drag is compensated as a source term for turbulent energy. The flame folding contribution is very important for explosion calculations. The geometry representation has been optimized so that the dependency on grid size, shape, and translation is as low as possible. Hjertager (1985, 1986) and Arntzen (1998) describe this concept in more detail.

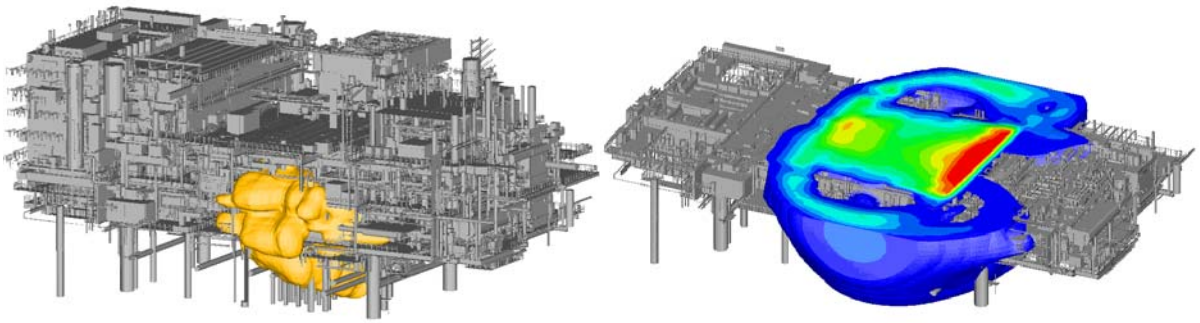

Figure 2.1 – Representation of the detailed geometry is important for the quality of the predictions for explosion and dispersion studies. In FLACS this is handled with a porosity concept.

Previous hydrogen work at GexCon

Despite some sporadic explosion tests at GexCon (CMI) with hydrogen before 1990, the main focus was natural gas explosions. Through the 1990s when the validity of FLACS for natural gas dispersion and explosion predictions improved, the limitations when handling hydrogen became more visible. This particularly applied for lean concentrations of hydrogen, for which the reactivity of FLACS was far too low and lower flammability limit (LFL) too high. With increasing interest in hydrogen safety in recent years, a significant effort has been required to learn more about hydrogen explosions and improve FLACS. A dedicated R&D project was carried out from 2001–04 to improve the validation basis for FLACS-HYDROGEN with support from Statoil and Norsk Hydro (now merged into Statoil) and later Ishikawajima Heavy Industries (IHI) in Japan. Numerous small-scale explosion and dispersion tests were carried out (some examples are presented in Figure 2.2). The experimental tests included:

- Small-scale 3*D*-corner tests (obstacle array of 37 cm × 37 cm × 37 cm) with 3 different obstruction densities. Two ignition positions and 3–6 gas concentrations were applied (Renoult & Wilkins, 2003a).
- GexCon channel (1.4 m × 0.30 m × 0.30 m) experiments with 4 different baffle configurations, 2 ignition locations and 3–6 gas mixtures with air (Renoult & Wilkins, 2003a).
- GexCon dispersion chamber (1.2 m × 0.90 m × 0.20 m), low and high momentum releases were performed in 3 different geometry configurations. Transient gas concentrations were measured at 12 locations (Renoult & Wilkins, 2003b).

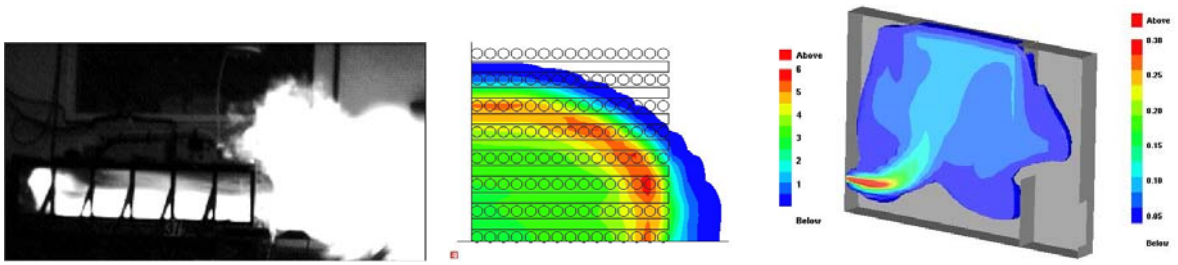

Figure 2.2 – Picture and plots illustrating test series from the hydrogen safety project 2001–2004: Explosion in the 1.4 m channel (left), simulated pressure distribution (barg) of one of the 3*D*-corner tests (centre) and volume fraction H_2 in a dispersion test (right).

FLACS simulations for all the tests were carried out and compared against experimental data. These tests were used for identification and improvement of any existing weaknesses in the FLACS code for modelling hydrogen explosions and establishment of the relevant guidelines. There were several problems seen initially. Too low overpressures were seen for lean mixtures while the overpressures for rich mixtures were too high. Inclusion of Lewis number effects on the burning velocity for hydrogen-air mixtures resolved this weakness. This is especially important for hydrogen as lean mixtures have a Lewis number smaller than one and rich mixtures have a Lewis number larger than one (that increases strongly with increasing concentration of hydrogen). This is due to the large difference in the diffusivity of hydrogen and air.

Using the experimental data on the effect of gas concentration on explosion overpressures for a range of test geometries obtained as a part of this project, weaknesses in previous versions of FLACS for carrying out simulations of hydrogen explosions were identified by Hansen and coworkers. Lower flammability limit was lowered, and the significant difference in flame wrinkling between lean flames and rich flames was adjusted. Modifications to ensure correct flame speed for curved flames were carried out. Laminar flames will wrinkle due to instabilities.

For hydrogen, the laminar flame speeds are increased by a factor up to 3.5 with distance due to wrinkling (This factor was lower in previous releases of FLACS, and too low flame speeds were therefore seen). More wrinkling is assumed for lean hydrogen flames than for rich due to Lewis number effects. This is due to the fact that the thermo-diffusive instability is very important for hydrogen-air mixtures. If the Lewis number (*Le*) is greater than 1, i.e. the thermal diffusivity is larger than the diffusivity of the deficient reactant, the flame temperature T_f is locally reduced, and if $Le < 1$; i.e. the diffusivity of the deficient reactant is larger, T_f increases. This causes an increase in the local flame speed and any perturbation to the system grows in the upstream direction. This can cause higher flame temperatures and hence higher overpressures for lean mixtures. Similarly, Lewis numbers less than unity are also associated with negative Markstein numbers (*Ma*) that lead to increased wrinkling of a flame front and significantly greater flame acceleration as compared to positive values of *Ma* (Bradley, Sheppard & Wolley, 2001). Bradley has also shown that the thermal-diffusive effects cannot withstand the Landau-Darrieus instability mechanisms in case of a negative *Ma* and the thermal-diffusive instability may destabilize of the flame front (Bradley, 1999).

Using the improved models, the simulations agreed reasonably well with experimental data. Figure 2.3 presents comparisons between simulations and experimental results for the 1.4 m channel equipped with 4 baffles (BR = 0.17) with 24 % H_2 in air ignited in the inner end. Most aspects of the simulated pressure traces (maximum pressures, development of pressure and more) correspond very well to the observations although it can be seen that the simulated arrival time is somewhat sooner than observed. Simulation and experimental results for other tests compare reasonably well.

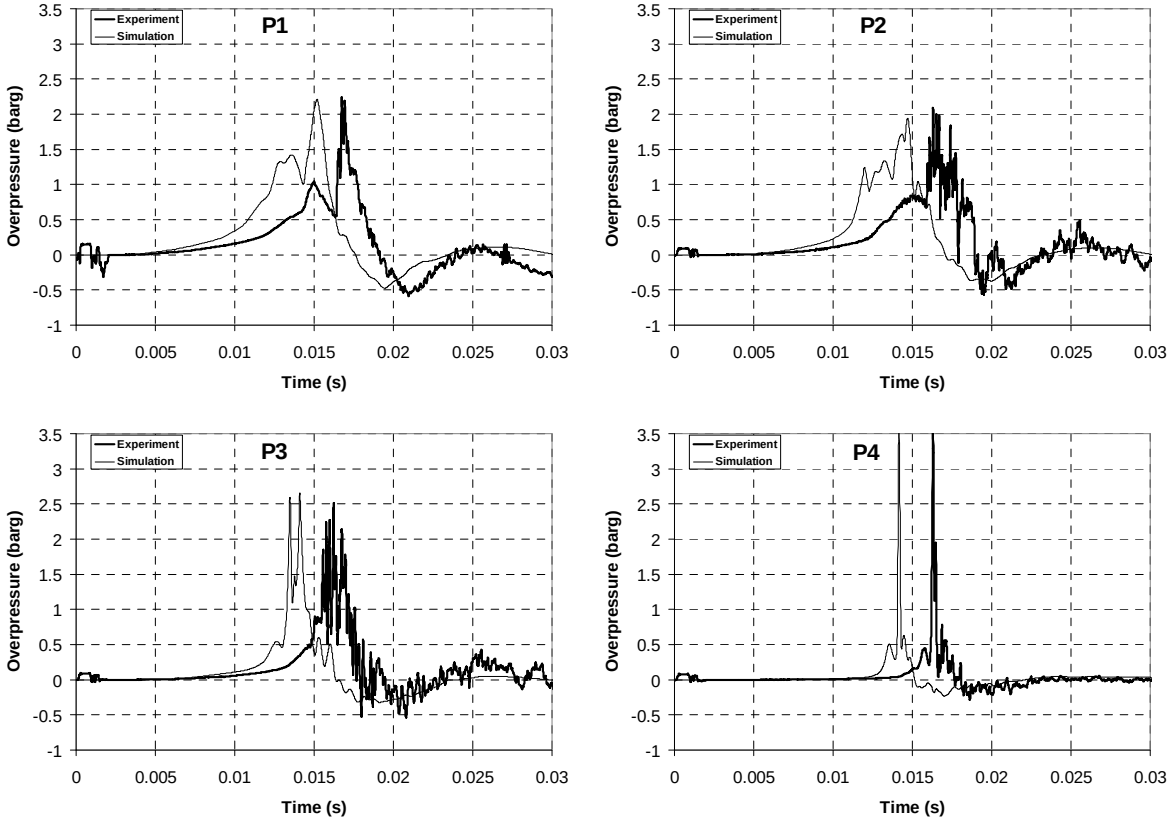

Figure 2.3 – Experimental measurements and FLACS simulation results in the GexCon 1.4 m channel with 4 baffles (BR = 0.17) and ignition in closed end for 24 % H_2-air mixture. Pressure monitors are located in inner end (P1), middle (P2), outer end (P3) and outside channel (P4).

The main missing elements in the generated test matrix were large-scale tests to investigate how well scaling and explosions at large-scale are handled. Some large-scale tests were simulated before the start of this doctoral study, but the effort was limited. A 20 m diameter hemispherical deflagration tests from Fraunhofer-ICT (Becker & Ebert, 1985) was one of the tests simulated. For the experiment, the balloon (total volume 2094 m^3) was placed on the ground and filled with a homogeneous stoichiometric hydrogen-air mixture. The mixture was ignited at the centre of the hemisphere basement, and the flame was seen to be propagating in almost hemispherical form. Pressure dynamics was recorded using 11 transducers installed on the ground level in a radial direction of the hemisphere basement at several different distances. Flame speeds were also estimated based on video recordings. Based on the comparison of simulation and experimental results (Hansen & Storvik, 2005; Gallego et al., 2005), it can be concluded that the experimentally measured flame velocity was reproduced by the simulations. The pressure dynamics obtained numerically were found to be in good agreement with the experiments for the positive values. The agreement in the negative pressures is somewhat worse but they are generally more sensitive to the far-field boundary conditions and the size of the computational domain. Nevertheless, the agreement is reasonable considering the possible errors in some measured pressures.

Another test series that has been simulated is the large-scale hydrogen explosion tests in the FLAME facility performed by Sandia National Laboratories in the 1980s (Sherman, Tieszen & Benedick, 1985). The geometry is a 30.5 m × 1.83 m × 2.44 m channel with closed or partly open ceiling (13 % or 50 %), and varying congestion (with or without baffles blocking 33 % of the channel cross-section). Tests were performed with H_2 concentrations from 7–30 %. The main motivation behind the tests was to study a potential hazard in nuclear plants. However, the tests are relevant for a range of other situations (in particular hydrogen release and explosion scenarios in tunnels). As a part of this study, 29 large-scale experiments were carried out. Removing tests where problems were experienced as well as some tests with (almost) repeated gas concentrations, a total of 23 scenarios in 5 categories remain. These 5 categories are closed ceiling with (2 scenarios) and without baffles (6 scenarios), 13 % open ceiling without baffles (5 scenarios), and 50 % open ceiling with (5 scenarios) and without (5 scenarios) baffles. All of these have been simulated (Hansen, Renoult, Sherman & Tieszen, 2001). Overall, it can be concluded that with a few exceptions simulations reflected the observed explosion characteristics reasonably well. Further description of the comparisons between simulations and observations can be found in Hansen, Renoult, Sherman & Tieszen (2001).

In the end, it can be reiterated that the validation carried out before the start of the study is missing several key elements, notably dispersion scenarios, situations involving combined dispersion and explosion phenomena, etc. These and several other scenarios are considered as a part of the current work (details are given in chapters 4–6). FLACS has been thoroughly validated for natural gas and such a validation exercise is carried out for hydrogen applications to some extent to raise the confidence level in carrying out predictions with FLACS-HYDROGEN.

3 Overview of the work in this thesis

This chapter provides an overview of the work that has been performed as a part of this dissertation study. The next three chapters describe the modelling and validation work that has been undertaken by the author for FLACS-HYDROGEN. This involves simulations of problems that are relevant to hydrogen safety. The motivation behind the above studies has been to improve the reliability, efficiency, and the applicability of FLACS for hydrogen safety problems. A well-validated CFD tool is a pre-requisite for its use in risk and safety assessments. Once a CFD tool has been validated (by comparison with benchmarks), it is possible to:

- Simulate additional scenarios and assess risk
- Study the effects of various parameters, such as confinement, congestion, etc.
- Suggest mitigation techniques for a particular situation
- Simulate scenario variations to challenge standards and validate conclusions from experiments

Many of the simulations have been carried blind, without prior knowledge of experimental results. A "blind" simulation study represents the best way of validating a CFD tool because:

- There exists no possibility of tuning predictions to available results
- It puts the robustness and stability of a tool to test
- It is a good estimate of time required by a tool to obtain reliable results

A summary of recent blind simulations carried out using FLACS is given in Middha & Hansen (2008).

Chapters 4–6 focus on the validation of FLACS for problems relevant to hydrogen safety. Very extensive work has been carried out in this area. The validation work carried out in this thesis is divided into 3 parts. Chapter 4 presents the validation work for hydrogen dispersion, chapter 5 handles explosion problems, and chapter 6 focuses on combined dispersion and explosion scenarios.

The dispersion work described in Chapter 4 includes both gaseous hydrogen (GH_2) releases (subsonic and supersonic) and liquid hydrogen (LH_2) releases. Some of the simulations have also been carried out blind without any prior knowledge of experimental data. This work is important as there has not been much work done previously in order to illustrate the validity of CFD simulations for hydrogen release and dispersion. A summary of the validation effort for hydrogen dispersion is provided in **Paper 1**. There has been some early work done by Venetsanos and coworkers (Venetsanos, Huld, Adams & Bartzis, 2003) but this did not involve actual validation and was in fact an attempt to represent an accident. Newer simulations in a mock-up refuelling station (Baraldi, Venetsanos, Papanikolaou, Heitsch & Dallas, 2009), residential fuel cell systems (Kim, Nam, Shin, Chung & Kim, 2009) and automotive scenarios (Venetsanos, Baraldi, Adams, Heggem & Wilkening, 2008) have been presented but again this has not included any comparison against experimental data. The work by Baraldi et al. (2009) has described numerical analysis of release, dispersion (and combustion) of LH_2 in a mock-up refuelling station. Details of validation of FLACS against large-scale LH_2 experiments are presented in **Paper 2** (similar studies for the ADREA-HF tool are also described in Stathras, Venetsanos, Bartzis, Würtz & Schmidtchen (2000) and Venetsanos & Bartzis (2007)). Further, a lot of relevant work has been carried out as a part of the Network of Excellence HySafe including inter-comparison between various CFD models. An example of this work is given in **Paper 3** for the INERIS garage release experiments (subsonic releases).

FLACS uses a utility program in order to model releases from high-pressure reservoirs. This sonic release model is based on one-dimensional representation of the isentropic flow through a nozzle followed by a normal shock. It provides the release rate and the leak diameter (expanded

to the atmosphere) as a function of time. However, prior to this dissertation, only the ideal gas models have been available that may be a severe limitation for hydrogen systems where storage at pressures as high as 700 bars is common. Work has been carried out in order to extend the models in the utility program in order to include real gas effects. These have been implemented in FLACS. Validation against three different experimental studies for sonic jets has been described. Special attention has been paid to evaluate the performance of FLACS against experimental measurements.

The work described in Chapter 5 involves a review of the laminar burning velocity and flammability limits of hydrogen-air mixtures as a function of concentration, temperature, pressure, oxygen concentration in air, presence of inerts, etc. Experiments were carried out in a 20-litre standard vessel by the author in order to determine the laminar burning velocity of hydrogen-air mixtures. This work is presented in **Paper 4**. A summary of other model improvements carried out as a part of this study specific to hydrogen is also given. A review of the turbulent burning velocity correlations in FLACS is also performed. The second part describes an extensive validation against available experimental data (some work is also described in Chapter 7). A summary of this work is given in **Paper 5**. Details of the extensive work performed in connection with the SRI confined tube experiments (Groethe, Colton & Chiba, 2002) have been described separately in **Paper 6**. Again, most of the CFD validation work has been done as a part of the Network of Excellence HySafe. This has included inter-comparison of various models for simulations in e.g. refuelling station geometry (**Paper 7)** and tunnels (Baraldi, Kotchourko, Lelyakin, Yanez, Middha, Hansen, et al., 2009). Other work has primarily included simulations and methodology development (e.g. Kikukawa, 2008; Wilkening & Baraldi, 2007). There has been significant attention from the nuclear industry for simulating hydrogen combustion and a benchmarking activity is currently ongoing (ISP-49 problem). However, most of the recent work (e.g. Heitsch, et al., 2010) again has not included any validation component that in the view of the author is very important to qualify a CFD tool.

As seen above, most of the validation data available is for basic situations, like free jet releases for dispersion, or pre-mixed homogeneous gas mixtures for explosions. The typical accident scenario is usually more complicated, possibly involving time varying releases impinging on equipment, with delayed ignition of a non-homogenous and possibly turbulent mixture. When aiming for increased precision in risk assessment methods there is a need to validate consequence tools for this added complexity. A very important cause of this gap in "real" validation of CFD tools is that it is challenging to perform good experiments with such a complexity. Good experimental data involving scenarios reminiscent of those seen in real situations are few and far between, especially at large scales (one exception is probably the experiments carried out by Shell/HSL in refueling station geometry (Shirvill, Royle & Roberts, 2007)). The author is not aware of any validation work done against such experimental dataset. Chapter 6 describes validation work carried out by the author against recent combined release and ignition experiments that have been carried out by FZK (Friedrich, Grune, Kotchourko, Kotchourko, Sempert, Stern & Kuznetsov, 2007). These involved vertically upwards hydrogen releases with different release rates and velocities impinging on a plate in two different geometrical configurations. The dispersed cloud was subsequently ignited and pressures recorded. In the weeks prior to the planned experiments, several blind CFD simulations were performed to predict the outcome of the proposed experiments, and if possible, to help the planning. After the experiments were reported, the quality of the blind predictions was evaluated. This work is described in **Paper 8**. These experiments are important for corroborating the underlying physics of any large-scale safety study. This type of experiments also provides a possibility to validate important assumptions used in probabilistic quantitative risk assessments, which are necessary to limit number of scenarios studied (e.g. equivalent stoichiometric cloud size methods).

It is well-known that deflagration to detonation transition (DDT) may be a significant threat for hydrogen explosions. Due to the high reactivity of hydrogen, DDT is likely in a variety of scenarios involving H_2-air mixtures and result in large-scale damage. The situation is exacerbated in the presence of obstacles, which induce turbulence that accelerates flames to a high speed. With the advance in scientific computing, research on DDT has been shifted toward the use of computational approaches. Before the beginning of this work, the standard versions of FLACS could only handle the deflagration mode of combustion. In this work, the use of FLACS to simulate hydrogen explosions in different geometries and get indications about the likelihood of DDT is described. Chapter 7 presents efforts connected to models that are used to describe DDT in FLACS. In this connection, both model development as well as validation has been carried out. **Paper 9** describes the initial methodology and validation work using four practical systems. Further study in terms of the role of flame thickness, geometry, and process parameters on the magnitudes of these gradients and the impact on actual DDT likelihood is described in **Paper 10**. Work has also been carried out to simulate the propagation of a fully-developed detonation front in FLACS.

The likelihood of DDT in FLACS is illustrated in terms of a parameter proportional to the spatial pressure gradient across the flame front (Tegnér & Sjögreen, 2002; Lee & Moen, 1980). This parameter is able to visualize when the flame front captures the pressure front, which is the case in situations when fast deflagrations transition to detonation. It is proposed that the presence of these spatial pressure gradients represents the indication of a possibility of the deflagration front transiting to detonation. Further justification for this is presented in Chapter 7. Other researchers have tried to use the maximum turbulent burning velocity in a given mixture as a criterion of whether DDT is possible (Bradley, Lawes & Liu, 2008). However, the maximum turbulent burning velocity is somewhat difficult to determine beforehand, especially in complicated process geometries. Researchers at Ulster and Telemark have also attempted to establish and use Large eddy simulation (LES) models to characterize DDT and detonations (Zbikowski, Makarov & Molkov, 2008; Vaagsaether, Knudsen & Bjerketvedt, 2007) but this approach is beyond the scope of this dissertation (it is furthermore questionable how useful this can be for complicated geometries such as those found in a typical process facility).

However, the current DDT work must be put into perspective: The description of DDT by FLACS can only be characterized as an "average" description. Some authors criticize this approach. Ng and Lee (2008) have the following comment: "Unfortunately, the current directions of numerical studies tend to reproduce the effects in a so-called realistic accidental scenario. As a result, too many unknown constants have to be adjusted to permit these codes to produce data to match with often-crude ill-defined large-scale test data. Such resulting models can sometimes provide the right answers even if the correct mechanisms are not in the model." It is correct that the exact mechanisms of DDT are not accounted for but the study focuses on the possibility of the shock and flame front travelling together. However, it must be remembered that high-speed turbulent deflagration and DDT are extremely complex phenomena involving a multitude of physical mechanisms which are strongly coupled in a non-linear manner. Exact representation of DDT in a typical hazardous industrial scenario involves scales that can differ by up to 10 orders of magnitude (Ciccarelli & Dorofeev, 2008). An exact simulation for such a 3*D* system will take a very long time using current computational power. At a minimum, there is a need to use parallel computing and/or supercomputers (Rehm, Gerndt, Jahn, Semler & Jones, 1998; Rehm, Nae, Jahn, Vogelsang & Wang, 2002). There are tools that aim to simulate the transition to detonation directly (a review is given in Oran & Gamezo (2007)) but these are mostly confined to small, 2*D* systems and require special, multidimensional numerical simulations that cannot be carried out for risk analyses. If we are to proceed further in understanding and avoiding this phenomenon in realistic process geometries, the approach developed here is very valuable. It is believed that useful results can be obtained using this approach and this represents

an important first step to be able to bridge the gap between CFD simulations and realistic process safety studies involving the possibility of a transition to detonation. As the validation work described showed, the results obtained are remarkably consistent with experimental observations in terms of overpressures and location/time of the occurrence of DDT. Nevertheless, experiments on determining the critical conditions for the onset of detonation (performed by Dorofeev and coworkers) can provide important physics to model the possibility of DDT. This work needs to be done in the future.

The last part of the thesis (Chapter 8) focuses on practical applications of the FLACS tool for hydrogen safety studies. As described in Chapter 1 and illustrated further in **Paper 11**, a CFD tool needs to be well-validated against a range of relevant experiments before it can be used for carrying out consequence and risk analyses for realistic systems. Such a validation exercise has been carried out and described above and in Chapters 4-6. The first part of the work described in Chapter 8 involves the development of CFD-based risk assessment methods for hydrogen applications based on the NORSOK criteria. The importance of establishing methods for carrying out Quantitative Risk Assessment (QRA) for installations involving the use of hydrogen has increased by a large extent in recent years, primarily because of the expected large-scale use of hydrogen as an energy carrier in the future (LaChance, Tchouvelev & Ohi, 2007). Furthermore, as described in Chapter 1, simpler methods can have a questionable validity and it is important to use CFD in order to perform accurate consequence assessment. This work is described in **Paper 11**. In this paper a 3-step approach is proposed, in which the CFD-tool FLACS is used to estimate the risk. A simulation study has been performed by the author (based on the methods described in **Paper 11)** to examine what, if any, is the explosion risk associated with hydrogen vehicles in tunnels. This work is described in **Paper 12**. Its aim was to further our understanding of the phenomena surrounding hydrogen releases and combustion inside road tunnels, and furthermore to demonstrate how a risk assessment methodology developed above could be applied to the current task. There have been other studies involving CFD modelling of release from hydrogen vehicles and subsequent explosion (e.g. Venetsanos, et al., 2008). The study described in this article is more detailed and makes an attempt to estimate the overall risk. The tunnel study has been further extended in order to address some of the questions left unanswered by the work described in **Paper 12.** These have primarily considered wide bridge scenarios where "realistic" ceilings have been used instead of the smooth ceiling assumption used in the previous work. A part of this work has also been carried out by other modellers and an inter-comparison of simulation results (no experiments were available in this case) is described in Venetsanos, Papanikolaou, Middha, Hansen, Garcia, Heitsch, et al., 2010).

One of the main benefits sought by including hydrogen in the alternative fuels mix is emissions reduction – eventually by 100 %. However, in the near term, there is a very significant cost differential between fossil fuels and hydrogen. Hythane (a blend of hydrogen and natural gas) can act as a viable next step on the path to an ultimate hydrogen economy as a fuel blend consisting of 8–30 % hydrogen in methane by volume can reduce emissions of pollutants such as NO_x (and greenhouse gases such as CO_2) while not requiring significant changes in existing infrastructure (more information is available on http://www.hythane.com). Due to this and other advantages, there is a significant focus to introduce hythane in public transport infrastructure worldwide. However, the author has not been able to find many relevant safety studies on the use of hythane in literature. With this purpose, a computational study has been carried out. This work is described in Middha, Engel & Hansen (2009)**.** This work seeks to evaluate whether hythane may be safer than both hydrogen and methane under certain conditions but also presents a general comparison between the relative safety risk between methane, hythane, and hydrogen.

Thus, this dissertation presents the extensive work that has been carried out to develop and validate FLACS-Hydrogen to pave the way to use the tool for applications related to hydrogen safety. Several validation studies have been carried out dealing with cases involving just

dispersion, just explosion, and combined dispersion and explosion. Significant work has been performed to extend the FLACS tool to indicate the possibility of a transition to detonation. The dissertation also includes practical studies including description of a risk assessment framework and the use of this framework for relevant problems. All the conclusions and final remarks are presented in Chapter 9.

4 Dispersion Simulations: Modelling and Validation

This chapter presents validation exercises that have been carried out by the author for hydrogen dispersion. Some of these have also been carried out blind without any prior knowledge of experimental data. Both gaseous hydrogen (GH_2) releases (subsonic and supersonic) and liquid hydrogen (LH_2) releases are considered in this work. A review of the validation work is described in:

Paper 1: Validation of CFD-model for hydrogen dispersion

This paper is published in the Journal of Loss Prevention in the Process Industries (Middha, Hansen & Storvik, 2009). **Paper 1** includes a summary of all the work, including impinging jet releases. The validation exercises summarized in this article include:

LH_2 releases

1. NASA experiments (Witcofski, 1981; Witcofski & Chirivella, 1984)

GH_2 releases: Subsonic Jets

1. INERIS Garage Experiments (Dagba, Perette & Venetsanos, 2005; Lacome, Dagba, Jamois, Perette & Proust, 2007)
2. CEA Garage Experiments (Helium) (Gupta, Brinster, Studer & Tkatschenko, 2007)
3. Subsonic horizontal jet release in a multi-compartment room (Hansen, Storvik & Renoult, 2005)
4. Subsonic, unconfined, horizontal jet release (Swain, Filoso & Swain, 2007)

GH_2 releases: Sonic Jets

1. INERIS unconfined, horizontal jet release (Chaineaux, 1999)
2. HSL unconfined, horizontal jet release (Roberts, Shirvill, Roberts, Butler & Royle, 2006)
3. FZK unconfined, horizontal jet release (Friedrich, Grune, Kotchourko, Kotchourko, Sempert, Stern & Kuznetsov, 2007)

GH_2 releases: Impinging Jets (see chapter 7)

1. FZK Ignited Impinging Jet Experiments (Friedrich, Grune, Kotchourko, Kotchourko, Sempert, Stern & Kuznetsov, 2007)

Modelling results are compared to experimental data, and in general, reasonable agreement is seen for many different kinds of release conditions.

Details of the work performed for liquid hydrogen releases have been described separately in:

Paper 2: Validation of CFD modelling of LH_2 spread and evaporation against large-scale spill experiments

This paper is presented in the 3rd International Conference on Hydrogen Safety and in press in the International Journal of Hydrogen Energy (Middha, Ichard & Arntzen, 2009). A new pool model handling the spread and the evaporation of liquid spills on different surfaces has recently been implemented in FLACS (Melheim, Ichard & Pontigia, 2009). As the influence of geometry on the liquid spread is taken into account in the new pool model, realistic industrial scenarios can be investigated. The model has been extensively validated for Liquefied Natural Gas (LNG) spills (Hansen, Melheim & Storvik, 2008; Davis, Hansen & Ichard, 2009). The model was tested for LH_2 release where experiments carried out by BAM were modelled. In the large scale BAM experiments (Marinescu-Pasoi & Sturm, 1994; Statharas, Venetsanos, Bartzis, Würtz & Schmidtchen, 2000), 280 kg of liquid hydrogen was spilled in 6 tests adjacent to buildings. In these tests, the pool spreading, the evaporation, and the cloud formation were investigated. Liquid hydrogen spill experiments carried out by NASA are also simulated with the new pool

model. The large scale NASA experiments (Witcofski, 1981; Witcofski & Chirivella, 1984) consisted of 7 releases of liquefied hydrogen at White Sand, New Mexico. The release test 6 is used. During these experiments, cloud concentrations were measured at several distances downwind of the spill point. No information about the atmospheric stability classes was available. Simulations have therefore been performed by using the stable and neutral stability classes. Simulations of these tests are found to compare reasonably well with the experimental results.

As **Paper 1** only included a very brief summary of several of the GH_2 release simulations and did not include all the studies that have been carried out, additional details are given below.

4.1 Subsonic GH_2 Releases: Validation against experimental data

4.1.1 Release Experiments in "Garage" geometry

Blind simulations of gas dispersion experiments performed by INERIS in their gallery facility (Lacome, Dagba, Jamois, Perette & Proust, 2007) were carried out as a part of this work. One of the main objectives of the experiments was to help understand the conditions under which small to medium hydrogen releases in confined spaces can become dangerous. The experiment was a hydrogen release scenario (1 g/s for 240 s) through a 2 cm orifice on top of a release chamber with a 5160 s dispersion time thereafter in a room shaped as a rectangular box. Other modellers have also participated in this activity. These include partners in the HySafe Network of Excellence sponsored by the European Union. An inter-comparison of results between CFD simulations and experiments for the INERIS hydrogen release experiments has been published in the 2nd International Conference of Hydrogen Safety and is also published in a special issue of the International Journal of Hydrogen Energy (Venetsanos, et al., 2009). This is described in:

Paper 3: An inter-comparison exercise on the capabilities of CFD models to predict the short and long term distribution and mixing of hydrogen in a garage

A summary of the experiment, including dimensions, release parameters, and sensor locations, is given in **Paper 3**.

Some of the results of the simulations are presented below. In general, high concentrations along the jet in the release phase and a very slow build-up of concentrations at sensors offset from the jet axis are observed. Figure 4.1 consists of plots showing gas volumetric concentrations in a vertical cut plane (Y = 0) for a couple times during the simulations, including the end of the release phase (240 s) and a significant time after the leak has stopped (500 s). The concentration stratification and slow downward movement is clearly observed.

A comparison between FLACS blind predictions and observations is presented in **Paper 1** and **Paper 3**. An example is presented below in Figure 4.2. It can be seen that excellent agreement between simulations and experiments was achieved. It was reported that the geometry used in the experiments was not "tight" i.e. there was a leakage of hydrogen out of the room that led to a loss of about 20 % of the gas. If this is taken into account, the results of the simulations could be changed somewhat but since the simulations over-predict the long-term concentrations somewhat, this is not expected to alter the conclusions too much.

Releases in garages were studied further by carrying out simulations of helium release experiments carried out by CEA (Gupta, Brinster, Studer & Tkatschenko, 2007). The main objectives of the experiments at CEA were the characterization of different scenarios that may arise in a real situation from hydrogen-fuelled vehicle parked inside a garage and the investigation of an optimal ventilation rate for hydrogen risk mitigation. Due to safety reasons, helium gas was used to simulate the hydrogen dispersion characteristics (Swain, Filoso, Grilliot & Swain, 2003).

Since helium is not available as a gas in FLACS, a mix of 7.65 % CO and 92.31 % hydrogen was used to represent a gas with the same molecular weight as helium.

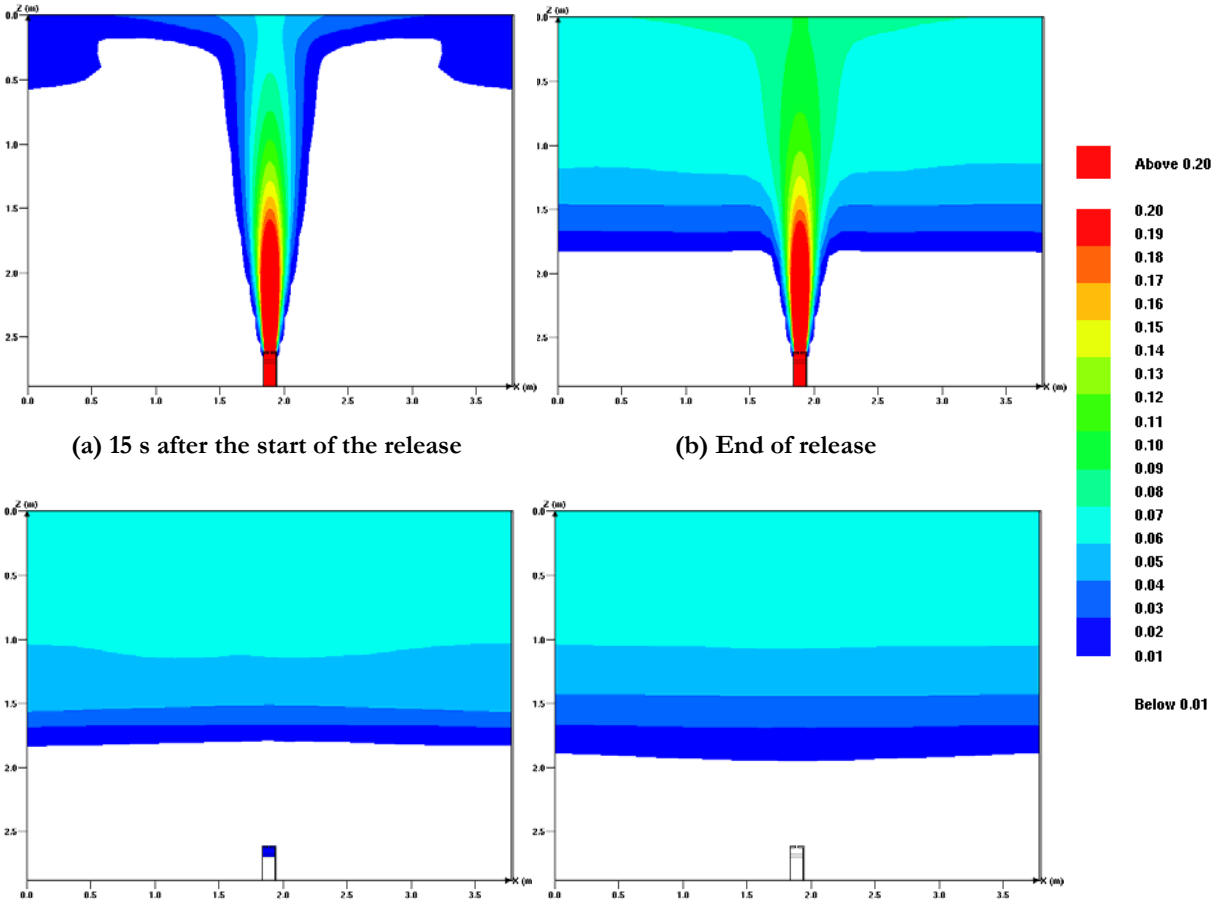

(a) 15 s after the start of the release **(b) End of release**

(c) 60 s after the end of the release **(d) 200 s after the end of the release**

Figure 4.1 – Simulated hydrogen volume concentrations in the INERIS garage geometry in the plane Y = 0 (middle of garage).

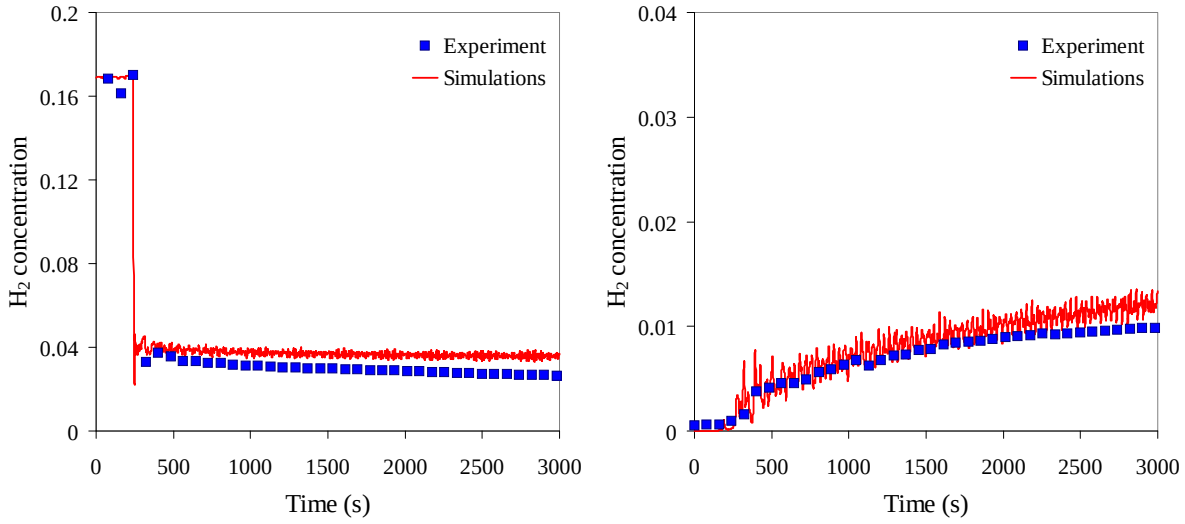

Figure 4.2 – Comparison between FLACS blind predictions and experimental measurements for the INERIS garage tests (Lacome, et al., 2007) for sensor 16 (left) and sensor 12 (right).

In general, behaviour similar to that seen for the INERIS garage simulations is observed with high concentrations along the jet in the release phase and a very slow build-up of concentrations at sensors offset from the jet axis. The stratification of helium concentration in the geometry was evident, both during the release as well as the dispersion phases. The comparison of simulated and observed concentrations for one sensor rod for the entire simulation duration is presented next. Figure 4.3 (top) presents the comparisons for the sensor rod above the release for time up to 300 s (a summary is also given in **Paper 1**). It can be seen that the results agree reasonably well in general. The maximum concentration is somewhat under-predicted by about 1 % and the same discrepancy is also seen after the release is over. The bottom figure compares the calculated and observed concentrations for another sensor rod that is offset from the jet axis in the dispersion phase (time 300–20000 s). The simulated results in this case are also seen to correspond quite well with observations. It should be noted that the simulations are only performed up to 14000 s.

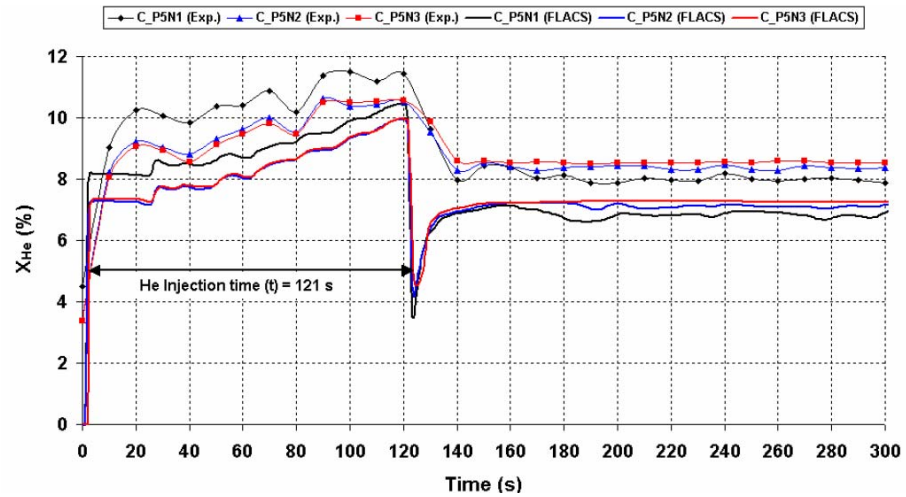

(a) 0 – 300 s

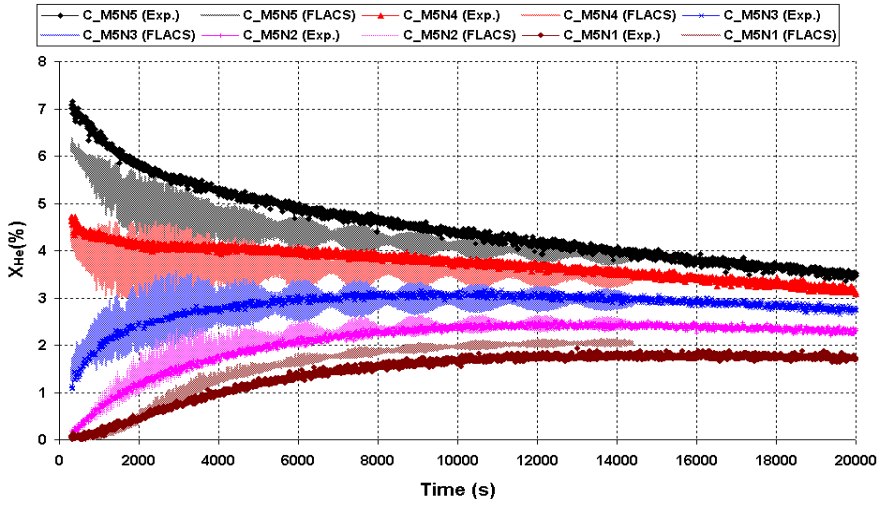

(b) 300 – 20000 s

Figure 4.3 – Comparison between predicted and observed helium volume concentrations in the CEA garage geometry (test 1) one sensor rod directly above the release.

However, it can be seen that the concentrations predicted by the simulations oscillate a lot more compared to those observed in the experiments. A major reason for this deviation is likely the response time for the sensors (which could be sometimes 10 s or more) compared to simulations

which report instantaneous concentrations. At the start of scenario, the simulations predict almost instantaneous increase from 0 to 8 percent above the leak, whereas it takes about 10 s for experiment to get up to this concentration level. Similarly as the leak ends, the sensors need 10 s to adjust to the new concentration level, and thus easily lose an undershoot (seen in the top figure) which may be real. The same explanation can be the reason for more high frequency oscillations in the simulations than in the experiments.

Additional validation work has been carried out involving releases in a vented private garage based on the experiments reported by Swain, Grilliot & Swain (1998). Again, these experiments were carried out involving Helium (and no hydrogen was used). The geometry was a single car garage with dimensions of 6.42 × 3.71 × 2.81 m. Helium concentration sensors were located at all four corners of the garage 0.38 m from each wall. A Clopay model 84A, steel segmented, (closed) garage door is used in the experiments which had dimensions 2.74 m × 2.31 m. A full-scale model vehicle was located inside the garage. This vehicle had dimensions of 4.98 m in length, 1.63 m in width, and 1.34 m in height. The wheels were represented by rectangular boxes with 0.20 m ground clearance. The helium leak location was at the bottom of the vehicle and centred at its width. Schematics of the geometry showing the location of the sensors, leak and the vehicle are shown in Figure 4.4. Two vents were present in the garage, one near the floor and the other at a height of about 1.96 m from the floor. Three different vertical sizes of the vents were used in the experiments: 6 cm, 24 cm, and 50 cm. The release duration was 2 hours (7200 seconds) and release rate was 2 Nl/s from a release area of 0.02 m^2.

The simulations for all three cases were carried out with FLACS. The geometry was relatively easy to build. A 10 cm grid was used in all three cases in order to properly resolve the garage and the vehicle. The grid was adapted near the vent openings in order to resolve them properly. The grid was also refined to 5 cm in the vertical direction down from the leak position to the floor of the garage. The number of grid cells was of the order of 100.000 in each case.

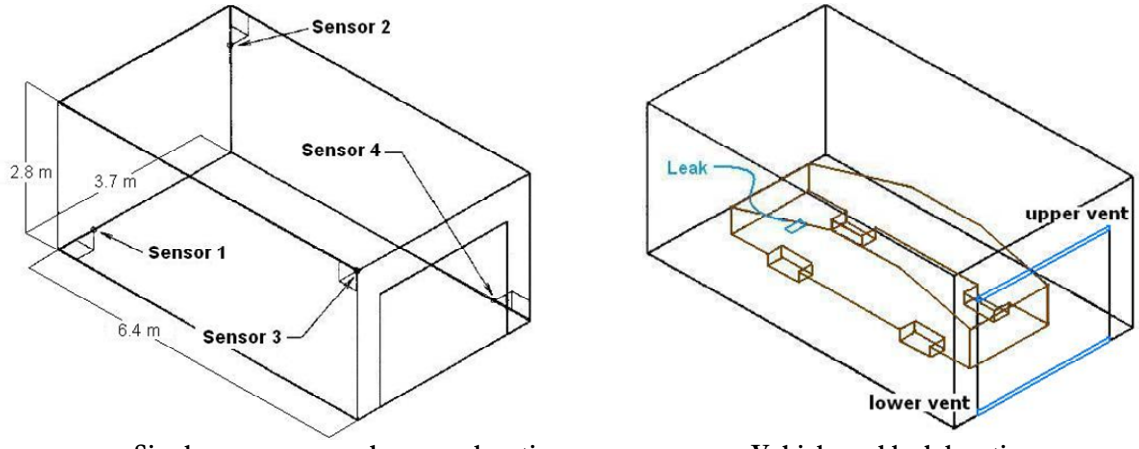

Single car garage and sensors location **Vehicle and leak location**

Figure 4.4 – Schematics of the vented garage geometry showing the location of sensors, the vehicle and the release.

A jet leak was defined in the downward direction with the specified area and velocity. Since the area of the leak was comparable to the grid area, the leak was split into five total leaks so that the leak area was smaller than the grid area. The leaks were defined in a "plus" pattern in order to ensure symmetry. The simulations were carried out for 7200 s. A large time step was chosen by increasing the value of CFLC number to 200 in order to ensure faster simulation times (a sensitivity study revealed that the results are not sensitive to the choice of the time step size or CFLC number). Nonetheless, the simulations on a single CPU machine (with a speed of the

order of 3 GHz took a rather long time (of the order of 20 days) for the entire simulation time of 7200 seconds (2 hours). This is one of the motivations for the planned work on increasing the efficiency of FLACS for dispersion calculations (incompressible solver, parallel capabilities, embedded grid, etc.).

The concentration contours through the garage are in principle similar to the ones presented above for an "empty" garage except the effect of the car. These are therefore not repeated here. What is more important is to estimate whether the simulations are able to capture the effect of the vent area on the concentrations measured at the sensors. Sensors 1 and 4 are near the floor and sensors 2 and 3 are near the ceiling. Thus, sensors 2 and 3 are expected to report high helium concentrations and sensors 1 and 4 are expected to report low helium concentrations (due to buoyancy). The comparison of the simulated and experimental concentrations for all four sensors for all three vent sizes is presented in Figure 4.5. In the case of the smallest vent size (2.5 inches), sensors 2 and 3 report concentrations between 2–2.5 vol. % that is reproduced very well in the simulations. The experiments report a concentration of 0.2–0.3 vol. % at sensors 1 and 4. The values at sensor 1 are reproduced very well in the simulations while those at sensor 4 are somewhat over-predicted. In the case of the medium vent size (9.5 inches), sensors 2 and 3 report a concentration of 1.2–1.5 vol. % which is reproduced reasonably well in the simulations. Sensors 1 and 4 report a concentration between 0.1–0.2 vol. % (even though some measurements report a value of close to zero for sensor 4). The concentration at sensor 1 is again predicted very well while there is again an over-prediction for sensor 4. The results for the largest vent size (19.5 inches) show that sensors 2 and 3 report a slightly lower concentration of 1.1–1.3 vol. % which is reproduced very well in the simulations. Sensors 1 and 4 report a concentration between 0–0.2 vol. % which is also predicted reasonably well. Simulations done by other modellers for the same experiment are reported by Papanikolaou, et al. (2009).

Therefore, it can be concluded that the extensive work done for simulations of subsonic releases of hydrogen (and helium) in realistic garage geometries shows that FLACS is able to capture the observed concentrations quite well in both the release and the dispersion phases. The effect of forced ventilation was also studied based on the recommended ventilation rates available in literature. Further simulations were performed in order to "challenge" the ventilation recommendation. Details of these calculations can be found elsewhere (Venetsanos, et al., 2006).

It can be mentioned that FLACS simulations the only predictions to agree well with experimental results in both phases for the INERIS experiments. Blind simulations for the CEA experiments were only carried out using FLACS. Therefore, FLACS can be used to carry out the design of garages to protect against the release of highly buoyant gases such as hydrogen.

4.1.2 Subsonic horizontal jet release in a multi-compartment room

This section reports simulations of subsonic horizontal hydrogen release (low momentum) and subsequent dispersion in a small-scale, multi-compartment room. Key results from the work presented in this section are published in the proceedings of the 2nd International Conference on Hydrogen Safety, San Sebastian, Spain, September 11-13, 2007 (Jordan, Xiao, Middha, et al., 2007). The experiments were carried out at GexCon in cooperation with Statoil and Norsk Hydro (now merged into Statoil). For the purpose of validation, test D27 was used. The test D27 is characterized by a comparatively small geometrical scale. A photograph of the experimental geometry is shown in Figure 4.6. The experimental rig consists of a 1.2 × 0.2 × 0.9 m vessel, divided into compartments by use of four baffle plates with dimensions 0.2 × 0.3 m. There is one vent opening at the wall opposite the release location centrally located about 1 cm above the floor with dimensions 0.1 × 0.2 m.

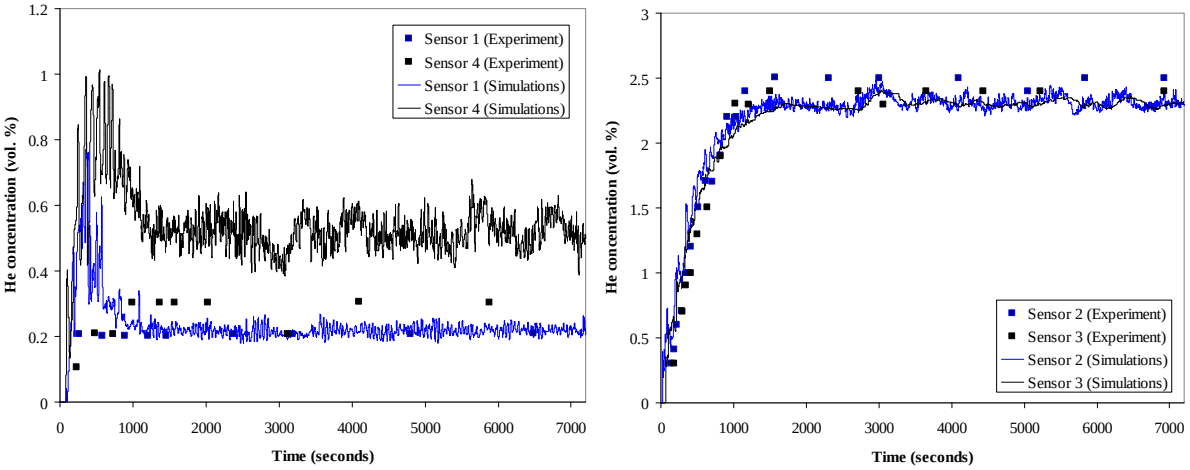

2.5 inches vent

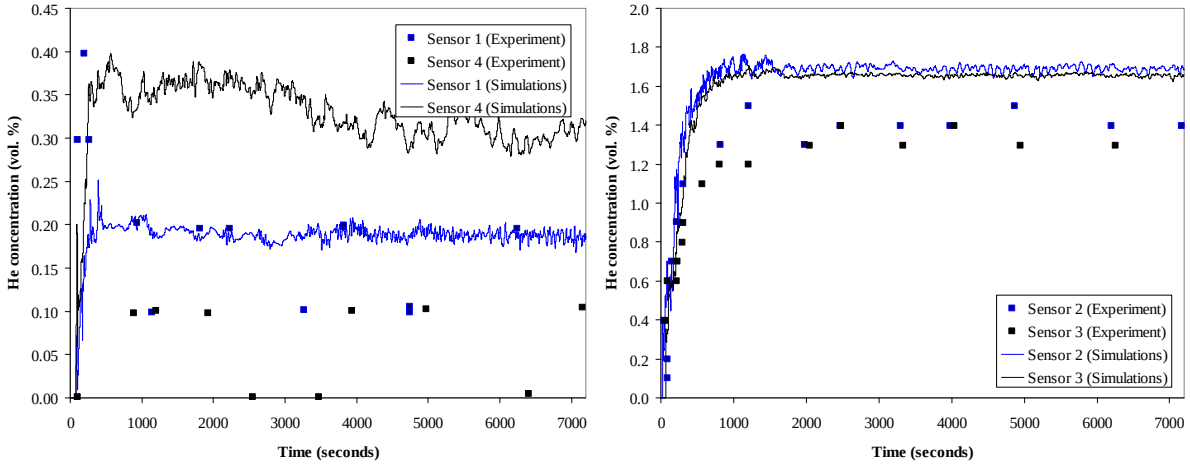

9.5 inches vent

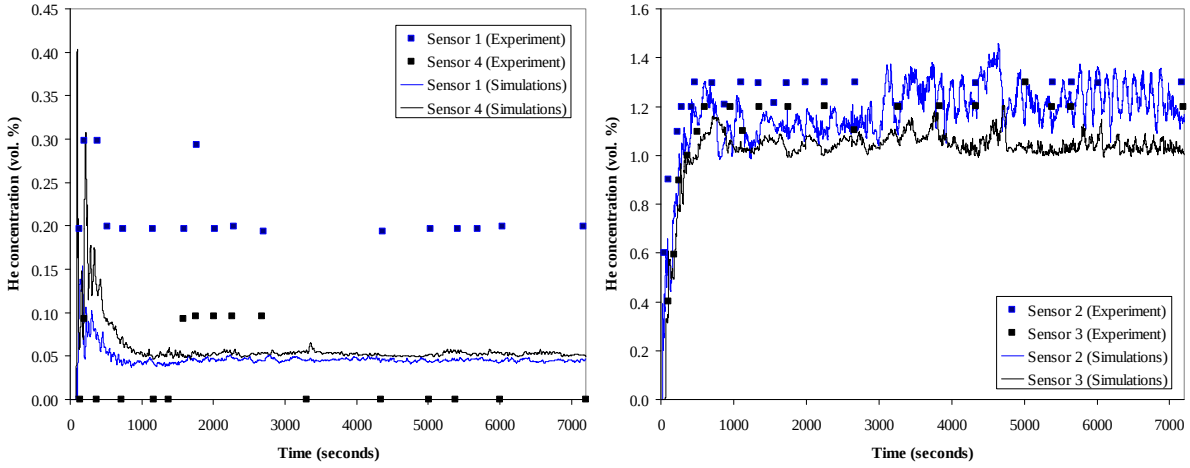

19.5 inches vent

Figure 4.5 – Comparison between FLACS simulation and experimental measurements for all four sensor locations in the Swain garage geometry with a full-scale vehicle and two vents: Sensors 1 and 4 (left) and sensors 2 and 3 (right).

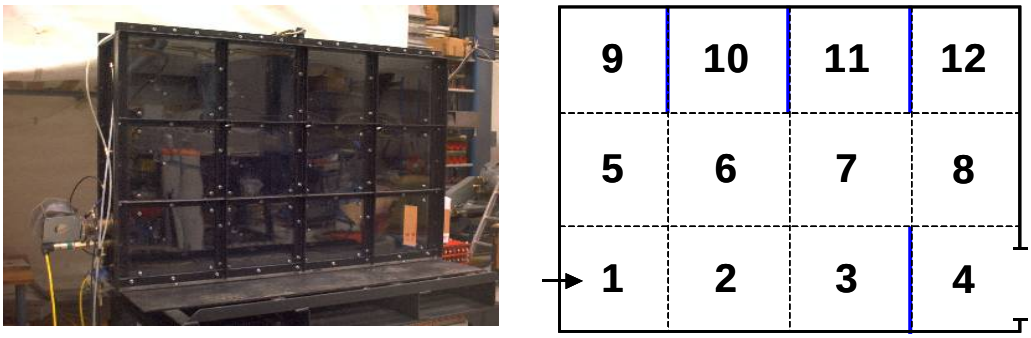

Figure 4.6 – (left) Picture of the experimental geometry (right) Geometric configuration for GexCon test D27 along with sensor locations. The release position is indicated by the arrow.

The baffle plates could be moved to create different geometric configurations in the experiments. The geometric configuration used for the test D27 is also shown in Figure 4.6. The actual release was a nominally constant flow of 1.15 Nl/s for 60 seconds. With a 12 mm nozzle diameter this corresponds to an average exit velocity of 10.17 m/s. Hydrogen concentrations were recorded at 12 locations in the rear wall (see Figure 4.6), using Oldham sensors type OLCT20D. The sensors are of the chatarometric type, which means that they are based on the measurement of the thermal conductivity of hydrogen compared to air. According to their specification they provide an accuracy of 1 vol. % H_2 over the full range of 0–100 vol. %. The sensors were located flush on the wall in the centre of the indicated sections. Through the test series some problems with the gas concentration measurements were experienced for certain sensors (3, 6, 11). A negative concentration was often seen for a short period before sensors "recovered" and seemed to give good results. Sensor 4 frequently became unstable, and is suspected to give consistently poor results. Some tests were carried out by swapping sensors, and these confirmed poor behaviour of the mentioned sensors. Further details on the experiments can be found in Wilkins & Renoult (2003).

Normally, it is recommended to refine the grid only around the jet, and not along it. This implies that if the leak direction is +X, the grid only needs to be refined in Y and Z direction. But in this case, the grid was also refined in X direction, owing to the high buoyancy of hydrogen and the fact that this was a low-momentum leak. The grid should be refined in a 3–5 CV region around the leak, and then gradually smoothed. Poor results are seen without this refinement. The total number of grid cells was around 40 000 and the simulation time was of the order of 2.5 days.

Figure 4.7 shows the snapshot of the H_2 concentration field in a XZ section of the geometry in the plane of the leak at different times during the leak, and after the leak has ended. The effect of the baffles on the stratification is clearly seen. Following the experiments, concentration values were recorded at various sensors. However, as reported in the experimental description, some sensors did not perform properly. Therefore, it was recommended to only compare results from sensors 1, 2, 5, 7, 8, 9, 10, and 12.

The simulation results are compared to the experimental data for these sensors in Figure 4.8. The steady state concentrations for sensors 5, 7, 8, 9, 10, and 12 are only slightly lower than those reported in the experiments. The concentrations in the locations 9 and 10 reach a steady state which is satisfactorily modelled. As the baffle plate between these two compartments lies right in the rising jet release the concentrations in these locations are a sensitive indicator for a good

buoyant jet modelling. For these sensors, it is important to realize that the concentration for sensor 12 begins to increase much later compared to sensors 9 and 10. The explanation is simply that the domain where sensor 12 is located has the largest distance from the release point and that the domains 9 and 10 have to be filled first before hydrogen might flow into this area. It is most interesting to compare predicted "arrival time" of hydrogen gas at sensors 9 and 10 with the observations. It can be seen from Figure 4.8 that this time of arrival compares with the observations very well. The time to reach a concentration of 15 % at the same locations is predicted between 16–19 s for sensor 9 and 17–20 s for sensor 10 after release start. Also, the "arrival time" of the concentration rise for sensor 12 is indeed much larger than those for sensors 9 and 10. The maximum concentration for sensors 1 and 2 also corresponds well to the experiments. However, some discrepancies can be seen. Due to the position of sensors 1 and 2 in the jet direction, a delay of nearly 40 seconds in the rise of concentrations is observed. The H_2 concentration is seen to rise too quickly in the simulations for these sensors, and it also falls much less than seen in the experiments. The concentration rise is also somewhat quicker for sensors 5, 7, 9, and 10. Some of these discrepancies may be attributed to experimental uncertainties, especially the response time of the various sensors. Thus, it may be concluded that overall, the simulation results compare reasonably well with experimental data.

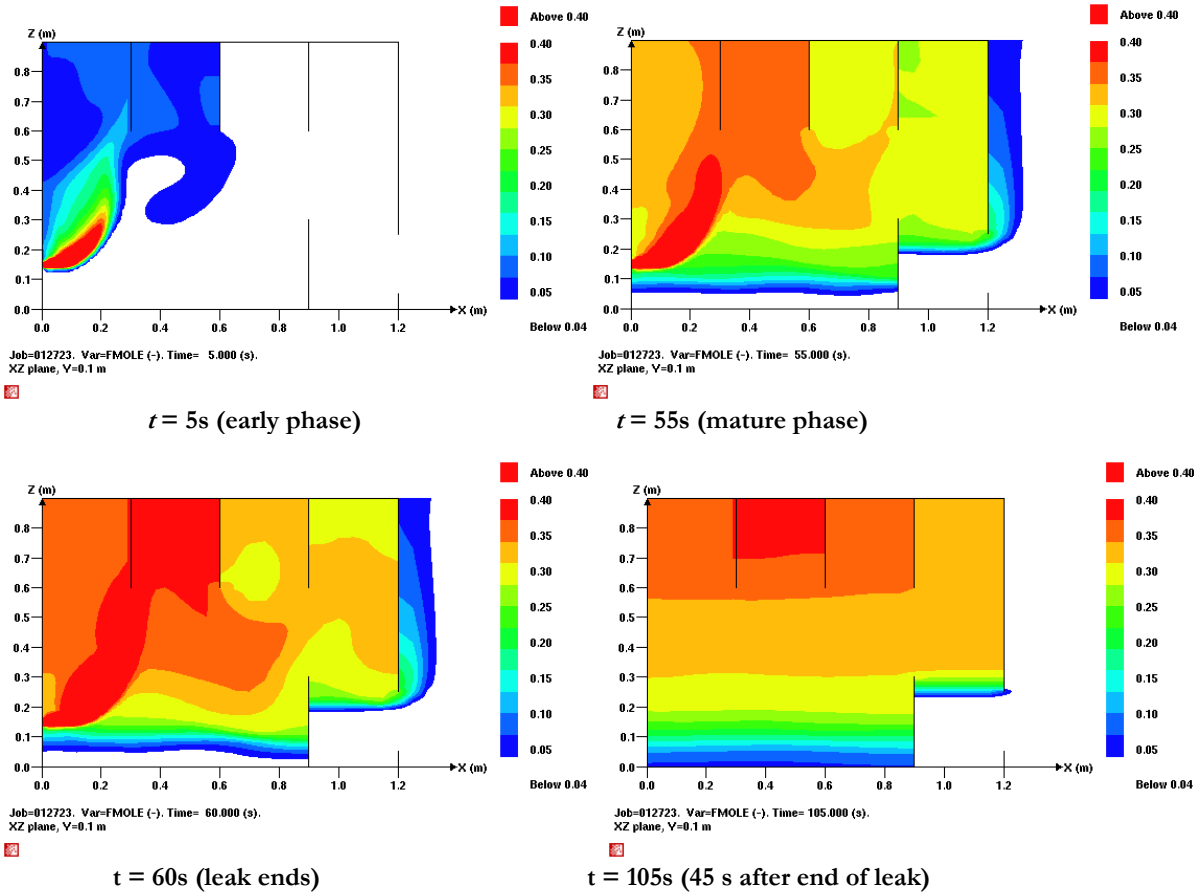

t = 5s (early phase) | *t* = 55s (mature phase)

t = 60s (leak ends) | t = 105s (45 s after end of leak)

Figure 4.7 – H_2 concentration field in a XZ section of the geometry in the plane of the leak for GexCon D27 experiments at various times

Similar results were also seen for the agreement between predicted and observed concentration fields for experiments carried out by Swain, Filoso & Swain (2007) in order to determine the maximum distance of an ignition source to a hydrogen leak to ignite the leak successfully (see **Paper 1**). This experiment and GexCon test D27 (described above) has further led to

modification of FLACS user guidelines for low momentum releases of buoyant gases as better grid refinement along the jet was needed to model the buoyancy accurately.

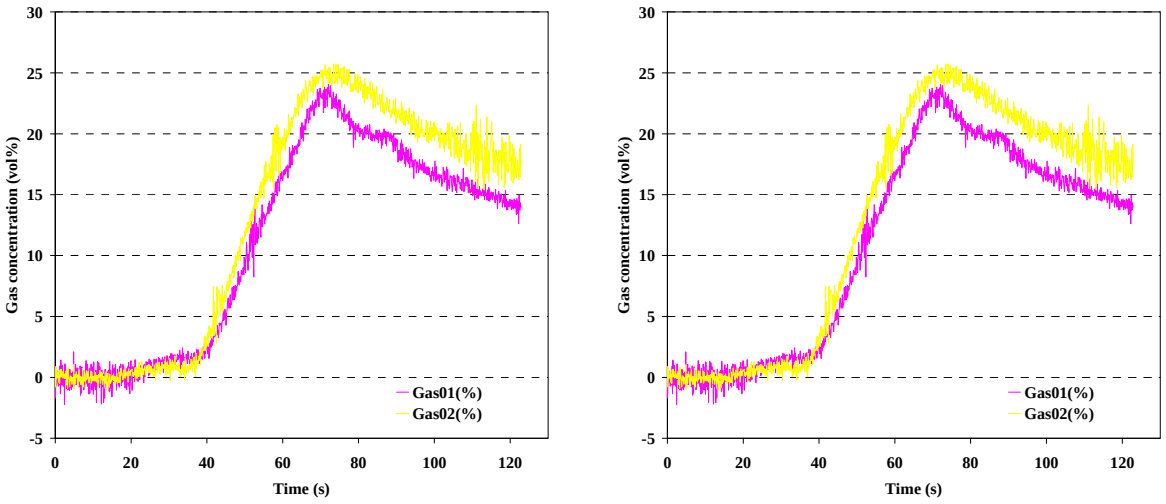

a. Sensors 1 and 2

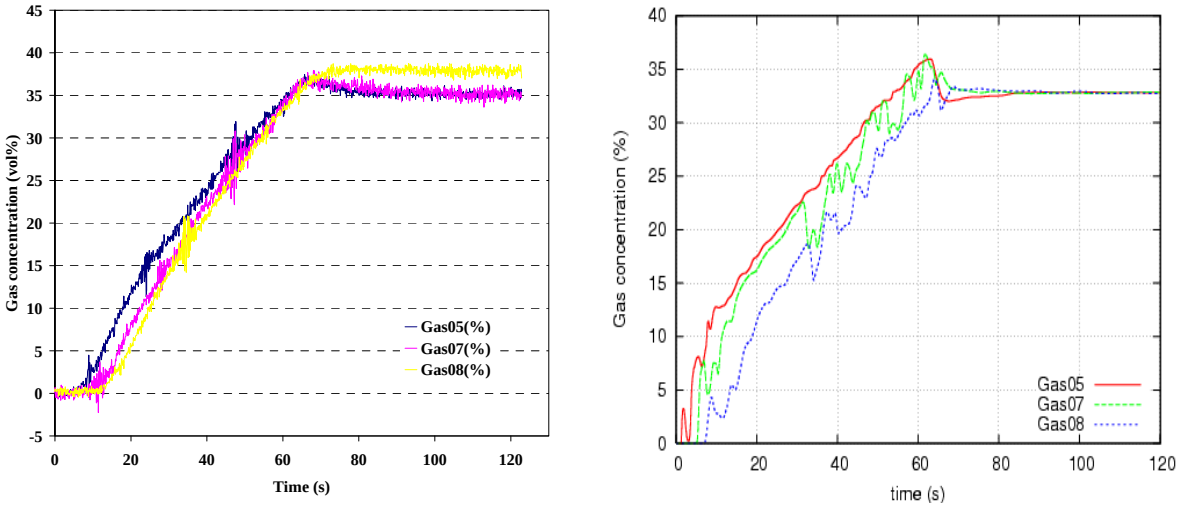

b. Sensors 5, 7, and 8

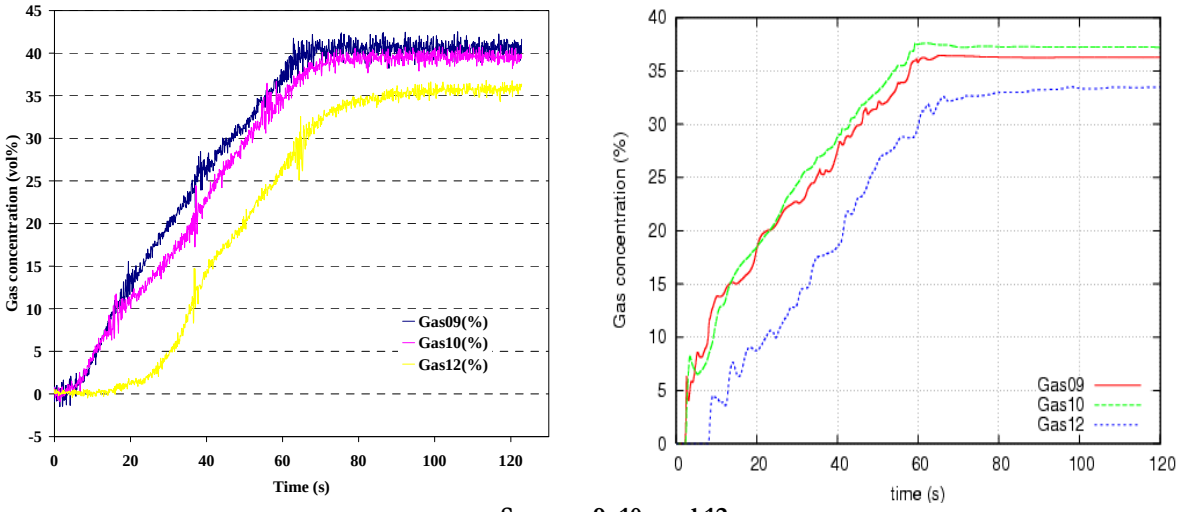

c. Sensors 9, 10, and 12

Figure 4.8 – The variation of H_2 concentration with time: Experiment (left) and Simulations (right)

4.1.3 Subsonic gaseous release in a vented hallway

Swain, Grillot & Swain (1998) have performed hydrogen dispersion experiments in simple vented enclosures (with corresponding CFD validation using the FLUENT code). In the vented hallway experiment (see Figure 4.9), the geometry used is a half-scale hallway. The hydrogen leaked from the floor at the left end of the hallway with the dimensions of 2.9 m × 0.74 m × 1.22 m. At the right end of the hallway, there is a roof vent and a lower door vent for the purpose of ventilation. The hydrogen leak rate is 2 SCFM (Standard Cubic Feet per Minute) for a period of 20 minutes. Four sensors are placed in the domain to record the local hydrogen volumetric concentration variations with time. More experimental details can be found in Figure 4.9 below. FLACS has been used to simulate the concentration profiles for the experiments described above, which have then been compared to observations. A large time step was chosen to ensure fast simulation times (a sensitivity study revealed that the results are not sensitive to the choice of the time step size).

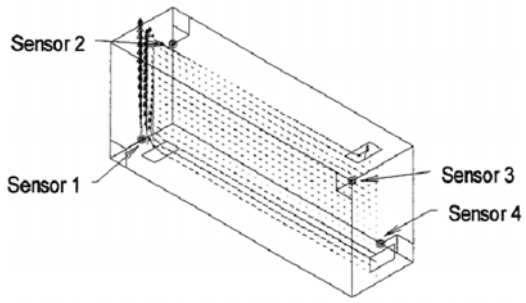

	X (m)	Y (m)	Z (m)
Hallway size	2.90	0.74	1.22
Sensor 1 location	0.1524	0.144	0.1524
Sensor 2 location	0.1524	0.5208	1.0088
Sensor 3 location	2.6762	0.144	1.0088
Sensor 4 location	2.6762	0.5208	0.1524
Roof vent size	0.1524	0.3048	0.00
Roof vent location	2.6	0.2176	1.22
Door vent size	0.0	0.3048	0.1524
Door vent location	2.9	0.2176	0.1524
H_2 inlet size (leak)	0.1524	0.3048	0.00
H_2 inlet location (leak)	0.1524	0.2176	0.00
H_2 (leak)	Leak rate: 2 SCFM (standard cubic feet per minute); leak duration: 20 minutes		

Figure 4.9 – (left) The schematic of the geometry with velocity vectors during the leak phase plotted (right) Experimental parameters for the Swain hallway experiments

A "diffuse" leak was defined in the upward direction with the specified area and velocity. Two different grids were used in the simulations in order to estimate the sensitivity of the results to grid resolution. The coarse grid (but still according to the grid guidelines) had a grid resolution ranging from 0.11–0.15 m (1610 cells) and the fine grid had a grid resolution ranging from 0.05–0.08 m (12880 cells). A comparison of the results for the two different grid resolutions showed that the results are almost insensitive to grid size. Figure 4.10 presents a comparison of simulated and observed hydrogen concentrations in the hallway geometry for all four sensor locations.

It can be seen that the simulations generally agree reasonably well with the experimental observations. The concentrations at sensors 2 and 3 that are located near the roof are slightly under-predicted (by around 20 %) while the agreement for sensors 1 and 4 is much better. Thus, it may be concluded that FLACS is able to represent these experiments in a reasonable manner.

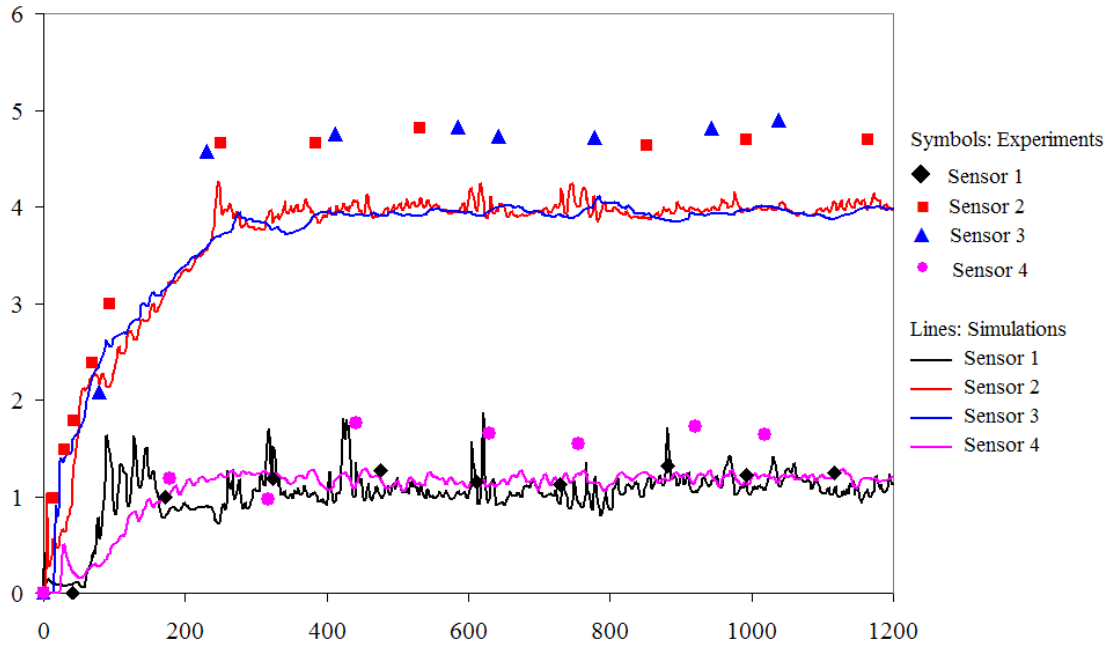

Figure 4.10 – Comparison between FLACS simulation and experimental measurements for all four sensor locations in the hallway geometry.

4.2 Sonic Releases

It is expected that a large part of hydrogen storage will be as a compressed gas stored in reservoirs under pressure. This is due to the fact that liquefying hydrogen (in order to reduce its volume) needs extremely low temperatures (of the order of 20 K). Further, compression to very high pressures is required. This is due to the fact that the energy density of hydrogen is significantly smaller than e.g. gasoline. The energy density of hydrogen at N.T.P is of the order of 10,000 KJ/m^3 while that of gasoline and diesel at the same conditions is of the order of 31 million KJ/m^3. Hydrogen compressed to 690 barg has an energy density of approximately 4.5 million KJ/m^3 that is still about 6-7 times smaller than that of gasoline but it is sufficient to get a reasonable travel range for a H_2 vehicle (for comparison, the energy density of LH_2 is around 9 million KJ/m^3).

If a hole or breach appears in the wall of such a tank, a jet is created which may develop into an explosive cloud. The intensity of the explosion likely to take place in this cloud depends on the cloud characteristics, such as the concentration of combustible material, the velocity field and turbulence. The cloud characteristics in turn depend on the hole size, position, and the direction of the release. Confinement and congestion in the surrounding area also play a significant role. Therefore, it is important to characterize releases from high-pressure reservoirs. The following can be indicated about high-momentum hydrogen jets that are created as a result of any release from a high-pressure source:

- Hydrogen mixes rapidly with ambient air, generating a concentration field because of the turbulence of the jet.
- The concentration field can be divided into 3 zones: Zone 1 including the outlet, where the hydrogen concentration is higher than the upper flammability limit (UFL = 75 vol. %), zone 2 where the hydrogen concentration is lower than the lower flammability limit (LFL = 4 vol. %) and zone 3 in which the hydrogen concentration is between LFL and UFL. In zone 3,

- The volume of zone 3 depends primarily on the diameter of the outlet and on the instantaneous hydrogen pressure at the source,
- This volume decreases continuously as the hydrogen pressure decreases.

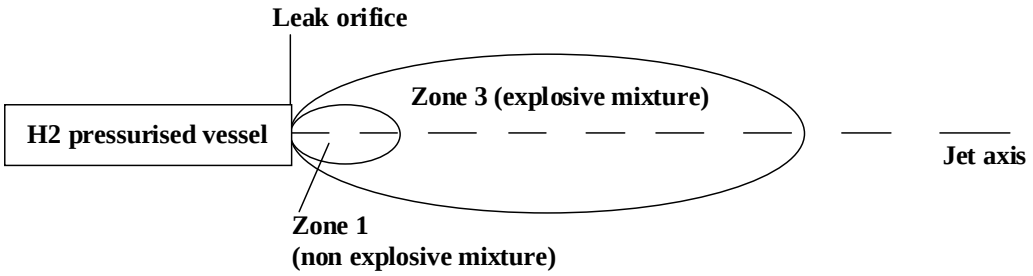

Figure 4.11 – A schematic view of the various concentration "zones" created upon discharge of hydrogen from a high-pressure source as a turbulent high speed jet.

4.3 Release Modelling

4.3.1 Existing Model: Jet Utility Program

In FLACS, a utility program known as the Jet Program has been developed previously in order to calculate the source term for such a release that can be used to model the resulting concentration field. The jet program has the following basis:

From a high-pressure reservoir (stagnation point), there is isentropic flow through the nozzle (heat in/out can be specified but the heat transfer coefficients are normally not considered). This is followed by a single normal shock (where Rankine Hugoniot relations are utilized) which is subsequently followed by expansion into ambient air. No air entrainment is considered. The area that is reported in FLACS is the area of the expanded jet and the velocity that is reported is subsonic velocity after shock. This is based on the notional nozzle approach proposed by Birch (Birch, Brown, Dodson & Swaffield, 1984; Birch, Hughes & Swaffield, 1987).

The jet program provides the boundary condition for the modelling of releases and the detailed shock structure, etc. is not modelled in FLACS. This has been found to give reasonably accurate results when compared to "exact" calculations which can take up to several months. A schematic of the jet model is shown below in Figure 4.12. A large reservoir of high pressure gas at stagnant conditions with pressure P_o and temperature T_o is assumed to be present upstream of what is shown in Figure 4.12. The gas flows from the reservoir into the inlet tube with mass flow rate $\dot{m}$ and exits the tube at sonic conditions at station 1. The conditions at the jet exit are determined assuming an isentropic expansion from the reservoir conditions to the jet exit:

$$\frac{P_1}{P_o} = \left(\frac{2}{\gamma + 1} \right)^{\frac{\gamma}{\gamma - 1}} \tag{4.1}$$

$$\frac{T_1}{T_o} = \frac{2}{\gamma + 1} \tag{4.2}$$

$$\rho_1 = \frac{P_1 M}{\bar{R} T_1} \tag{4.3}$$

$$v_1 = c_1 = \sqrt{\gamma R T_1} \tag{4.4}$$

$$\dot{m} = \rho_1 v_1 A_1 \tag{4.5}$$

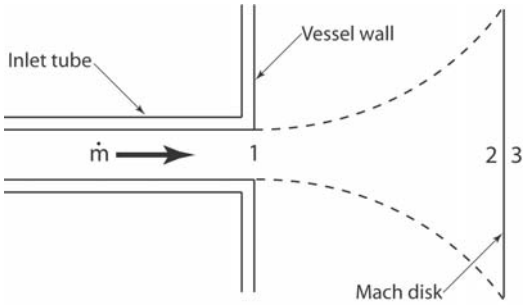

Figure 4.12 – Schematic of under-expanded jet model showing stations where analytical models are applied; sonic conditions assumed at jet exit (station 1); normal shock located at stations 2-3 interface; subsonic flow at station 3.

Note that P_o, T_o, A_1, and the gas (hence M and γ) are assumed to be given. Assuming adiabatic expansion between stations 1 and 2, a 1D momentum balance (ignoring entrainment and viscosity) is applied to the control volume shown in Figure 4.13.

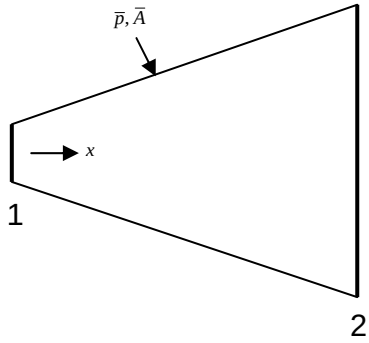

Figure 4.13 – Schematic of control volume for Jet model momentum equation.

The momentum balance can be written as:

$$\rho_2 u_2^2 A_2 - \rho_1 u_1^2 A_1 = P_1 A_1 - P_2 A_2 + \overline{P} \overline{A}_x \tag{4.6}$$

Let $\overline{P} = \alpha P_1 + (1-\alpha) P_2$ and let $\overline{A}_x = \Delta A = A_2 - A_1$. Equation (4.6) can then be written as:

$$\rho_2 u_2^2 A_2 - \rho_1 u_1^2 A_1 = (P_1 - P_2)\left[\alpha A_2 + (1-\alpha) A_1\right] \tag{4.7}$$

and with the aid of the continuity equation solving (4.7) for u_2 gives

$$u_2 = u_1 \left\{ 1 + \frac{(P_1 - P_2)}{\rho_1 u_1^2} \left[\alpha \frac{A_2}{A_1} + (1-\alpha) \right] \right\} \tag{4.8}$$

Setting $\alpha = 0$ in equation (4.8) yields the expression in the Jet utility program for the velocity at station 2.

Normal shock relations, conservation of mass, ideal gas equation of state, and equality of A_2 and A_3 are used to relate conditions at stations 2 and 3:

$$M_3^2 = \frac{M_2^2 + \frac{2}{\gamma - 1}}{\frac{2\gamma}{\gamma - 1} M_2^2 - 1} = \frac{v_3^2}{c_3^2} = \frac{v_3^2}{\gamma R T_3} \tag{4.9}$$

$$P_3 = P_2 \left(\frac{2\gamma}{\gamma + 1} M_2^2 - \frac{\gamma - 1}{\gamma + 1} \right) \tag{4.10}$$

$$T_3 = T_2 \frac{\left(1 + \frac{\gamma - 1}{2} M_2^2 \right)}{\left(1 + \frac{\gamma - 1}{2} M_3^2 \right)} \tag{4.11}$$

The adiabatic energy equation between stations 1 and 2 gives

$$T_2 = T_1 + \frac{\left(v_1^2 - v_2^2 \right)}{2 C_p} \tag{4.12}$$

From the equation of state and conservation of mass A_2 can be determined, giving the Mach disk diameter for the Jet model.

4.3.2 Development of a Real Gas Model

The model described above is based on the ideal gas law that only describes an ideal gas, that is, a gas consisting of molecules occupying negligible space and without attraction for each other. In reality, gas molecules do occupy space, although very little, and they do attract one another, although very weakly. The space that the molecules occupy slightly reduces the volume available to hold more gas, and the molecules attraction for each other slightly increases the pressure.

The ideal gas relationship can be used accurately to describe the behaviour of real gases at pressures up to approximately 100-150 barg at normal ambient temperatures. At higher pressures, the results become increasingly inaccurate as illustrated in Figure 4.14. It is clear that the deviation in the density of hydrogen is very significant at pressures that are expected to be used in hydrogen vehicles (350 barg or 700 barg). Therefore, work was undertaken by the author in order to develop a version of the jet program based on the real gas law. For this purpose, the Abel-Noble equation of state (EOS) was chosen. The reason for this choice was that the Abel-Noble EOS is simple and is till able to predict the density at higher pressures to a reasonable accuracy.

The Abel-Noble EOS is given by:

$$Z = \frac{P}{\rho RT} = \frac{1}{1 - \frac{\rho}{a}} = 1 + \frac{P}{aRT} \tag{4.13}$$

where Z is the compressibility, R is the gas constant that has the value of 4124 J/kg.K for hydrogen and a is a model constant with a value of 129 kg/m^3 for hydrogen.

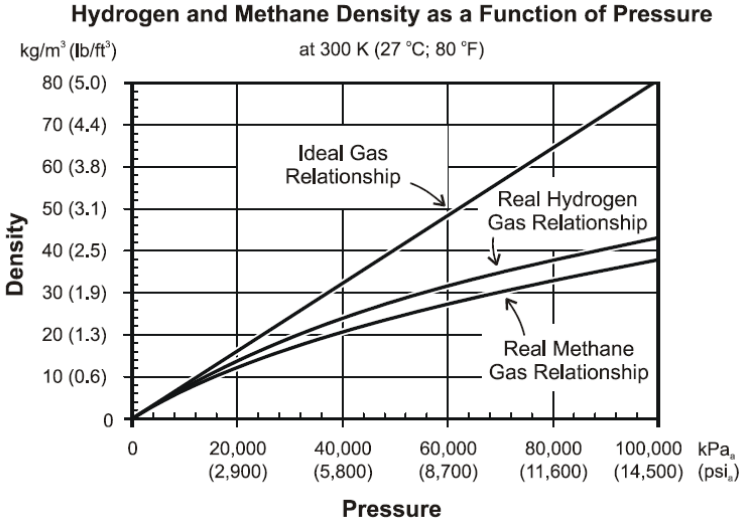

Figure 4.14 – Hydrogen density as a function of pressure (taken from Dempsey, 2001)

The first step in the development of a real gas model for modelling hydrogen releases from high pressure sources is to modify the thermodynamic equations. This has been carried out as a part of this study and is described below:

Denoting the "effective" isentropic exponent as n ($n = \gamma$ for ideal gas where $\gamma = C_p / C_v$), we have (Cornelius & Srinivas, 2004):

$$n = \frac{\gamma\left[Z + T\left(\frac{\partial Z}{\partial T}\right)_\rho\right]}{Z + T\left(\frac{\partial Z}{\partial T}\right)_p} \tag{4.14}$$

For the Abel-Noble EOS,

$$Z = 1 + \frac{P}{aRT} \Rightarrow \left(\frac{\partial Z}{\partial T}\right)_p = -\frac{P}{aRT^2}$$

Also,

$$Z = \frac{a}{a - \rho} \Rightarrow \left(\frac{\partial Z}{\partial T}\right)_\rho = 0$$

Therefore,

$$n = \frac{\gamma\left[Z + 0\right]}{Z - T\dfrac{P}{aRT^2}} = \frac{\gamma Z}{1} = \gamma Z \tag{4.15}$$

The velocity of sound for a real gas is given by:

$$c = \sqrt{ZnRT} = Z\sqrt{\gamma RT} = Zc_{ideal} \tag{4.16}$$

The velocity of the flow through a nozzle (throat) is given as a function of the pressure p as:

$$v = c_{ideal}\left[\frac{2}{\gamma - 1}\left(1 - \frac{P}{P_0}\right)^{\frac{\gamma-1}{\gamma}}\right]^{\frac{1}{2}} \tag{4.17}$$

Here, P_0 is the pressure inside the reservoir. The corresponding equation for a real gas is:

$$v = c_{real}\left[\frac{2}{n - 1}\left(1 - \frac{P}{P_0}\right)^{\frac{n-1}{n}}\right]^{\frac{1}{2}} \tag{4.18}$$

The enthalpy change is given by

$$dh = C_p dT + \left[\underline{V} - T\left(\frac{\partial \underline{V}}{\partial T}\right)_p\right]dP \tag{4.19}$$

Here $\underline{V} = 1/\rho$ is the specific volume. For a real gas,

$$\left(\frac{\partial \underline{V}}{\partial T}\right)_P = \left(\frac{\partial\left(\dfrac{ZRT}{P}\right)}{\partial T}\right)_P = \frac{RT}{P}\left(\frac{\partial Z}{\partial T}\right)_P + \frac{ZR}{P} = \frac{\underline{V}}{Z}\left(\frac{\partial Z}{\partial T}\right)_P + \frac{\underline{V}}{T}$$

$$\Rightarrow dh = C_p dT - \left[\frac{T\underline{V}}{Z}\left(\frac{\partial Z}{\partial T}\right)_P\right]dP$$

The Gibb's free energy is given by $g = h - Ts$. Therefore, $dg = dh - Tds - sdT$. Also, $dg = \underline{V}dP - sdT \Rightarrow Tds = dh - \underline{V}dP = dh - \dfrac{dP}{\rho}$

For isentropic flow, $ds = 0$. Therefore, using the relation above and Equation (4.19) we get:

$$0 = C_p dT - \frac{dP}{\rho}\left[\frac{T}{Z}\left(\frac{\partial Z}{\partial T}\right)_P + 1\right]$$

$$= C_p dT - \frac{dP}{P}\underbrace{\frac{P}{\rho}}_{ZRT}\left[\frac{T}{Z}\left(\frac{\partial Z}{\partial T}\right)_P + 1\right]$$

$$\Rightarrow \frac{dT}{T} = \frac{dP}{P}\frac{\mathrm{R}}{C_p}\left[T\left(\frac{\partial Z}{\partial T}\right)_p + Z\right] \tag{4.20}$$

Also,

$$du = Tds - Pd\underline{V} = C_v dT + \left[T\left(\frac{\partial P}{\partial T}\right)_{\underline{V}} - P\right]d\underline{V}$$

Using the isentropic condition ($ds = 0$) again, we have

$$C_v dT = -T\left(\frac{\partial P}{\partial T}\right)_{\underline{V}} d\underline{V} = \frac{T}{\rho^2}\left(\frac{\partial P}{\partial T}\right)_\rho d\rho$$

For a real gas, $\left(\frac{\partial P}{\partial T}\right)_\rho = \rho ZR + \rho RT\left(\frac{\partial Z}{\partial T}\right)_\rho$. Using this and the relationship above, we can obtain:

$$\frac{dT}{T} = \frac{\mathrm{R}}{C_v}\frac{d\rho}{\rho}\left[Z + T\left(\frac{\partial Z}{\partial T}\right)_\rho\right] \tag{4.21}$$

From Equations (4.20) and (4.21) we have:

$$\frac{d\rho}{\rho}\frac{\mathrm{R}}{C_v}\left[Z + T\left(\frac{\partial Z}{\partial T}\right)_\rho\right] = \frac{dP}{P}\frac{\mathrm{R}}{C_p}\left[T\left(\frac{\partial Z}{\partial T}\right)_P + Z\right]$$

$$\Rightarrow \frac{d\rho}{\rho} = \frac{dP}{P}\underbrace{\frac{C_v}{C_p}}_{1/\gamma}\left[\frac{Z + T\left(\frac{\partial Z}{\partial T}\right)_P}{Z + T\left(\frac{\partial Z}{\partial T}\right)_\rho}\right]$$

Using Equation (4.15) and the relation above, we obtain:

$$\frac{d\rho}{\rho} = \frac{1}{n}\frac{dP}{P} \tag{4.22}$$

The above equation can be used to determine how the change of pressure and density are related under isentropic conditions. For an ideal gas, the well-known relationship states that

$\frac{\rho}{\rho_0} = \left(\frac{P}{P_0}\right)^{1/\gamma}$. Using the definitions connected with the Abel-Noble EOS given in Equations (4.13) and (4.15), we have for the real gas case:

$$\frac{d\rho}{\rho} = \frac{1}{\gamma Z}\frac{dP}{P} = \frac{a-\rho}{\gamma a}\frac{dP}{P}$$

$$\Rightarrow \frac{d\rho}{\rho(a-\rho)} = \frac{1}{\gamma a}\frac{dP}{P}$$

Integrating, we get:

$$\frac{\rho}{\rho_0}\frac{a-\rho_0}{a-\rho} = \left(\frac{P}{P_0}\right)^{1/\gamma} \tag{4.23}$$

Other relevant thermodynamic quantities also need to be evaluated for the chosen EOS. One of them is the difference in the constant pressure and constant volume heat capacities. It is given by

$$C_p - C_v = \frac{-T\left(\frac{\partial P}{\partial T}\right)_{\underline{V}}^2}{\left(\frac{\partial P}{\partial \underline{V}}\right)_T}.$$

Since $P = \frac{ZRT}{\underline{V}}$, we have $\left(\frac{\partial P}{\partial T}\right)_{\underline{V}} = \frac{ZR}{\underline{V}} + \frac{RT}{\underline{V}}\left(\frac{\partial Z}{\partial T}\right)_{\underline{V}}$. For the Abel-Noble EOS,

$$Z = \frac{\underline{V}a}{\underline{V}a - 1} \Rightarrow \left(\frac{\partial Z}{\partial T}\right)_{\underline{V}} = 0.$$

Therefore, $\left(\frac{\partial P}{\partial T}\right)_{\underline{V}} = \frac{ZR}{\underline{V}}$. On the other hand,

$$\left(\frac{\partial P}{\partial \underline{V}}\right)_T = -\frac{ZRT}{\underline{V}^2} + \frac{RT}{\underline{V}}\left(\frac{\partial Z}{\partial \underline{V}}\right)_T$$

$$= -\frac{ZRT}{\underline{V}^2} + \frac{RT}{\underline{V}}\left[-\frac{a}{(\underline{V}a-1)^2}\right]$$

$$= -\frac{RTa}{\underline{V}}\frac{\underline{V}a}{(\underline{V}a-1)^2}$$

$$= -\frac{RT}{\underline{V}}Z^2$$

Hence,

$$C_p - C_v = +T\frac{Z^2R^2}{\underline{V}^2}\frac{\underline{V}^2}{RTZ^2} = R \tag{4.24}$$

Therefore, the result is the same as that for an ideal gas. It can also be shown that similar to ideal gases, C_p does not change with change of pressure (at a given temperature) and C_v does not change with change of volume (at a given temperature). The details are not presented here for brevity.

Next, the energy conservation law is considered. This is given by:

$$\frac{dv^2}{2} + \frac{dP}{\rho} + \underbrace{Tds}_{0} = 0$$

Integrating and using the fact that in the reservoir (state 0), the velocity is zero, it can be obtained:

$$\frac{v^2}{2} = -\int_{P_0}^{P}\frac{dP}{\rho} \tag{4.25}$$

From (4.23), we have $\frac{\rho}{\rho_0}\frac{a-\rho_0}{a-\rho} = \left(\frac{P}{P_0}\right)^{1/\gamma}$. Setting $\frac{\rho_0}{a-\rho_0} = B$, we get $\frac{\rho}{a-\rho} = B\left(\frac{P}{P_0}\right)^{1/\gamma}$. From this, the density can be calculated explicitly as:

$$\rho = \frac{aB\left(\frac{P}{P_0}\right)^{1/\gamma}}{1+B\left(\frac{P}{P_0}\right)^{1/\gamma}} \Rightarrow \frac{1}{\rho} = \frac{1}{a}\left(1+\frac{1}{B}\left(\frac{P}{P_0}\right)^{-1/\gamma}\right) \tag{4.26}$$

Using the above relation in Equation (4.25), we have:

$$\begin{aligned}\frac{v^2}{2} &= -\frac{P_0}{a}\int_1^{P/P_0}\left[1+\frac{1}{B}\left(\frac{P}{P_0}\right)^{-1/\gamma}\right]d\left(\frac{P}{P_0}\right) \\ &= \frac{P_0}{a}\left[\left(1-\frac{P}{P_0}\right)+\frac{1}{B}\frac{\gamma}{\gamma-1}\left(1-\left(\frac{P}{P_0}\right)^{(\gamma-1)/\gamma}\right)\right]\end{aligned} \tag{4.27}$$

At the throat, the Mach number $M = 1$. Using Equations (4.15) and (4.16):

$$v^2 = c_{real}^2 = \gamma Z^2 RT = \gamma\frac{P}{\rho}\frac{a}{a-\rho}.$$

Using Equation (4.26), we can express the above expression in terms of only pressure because the terms involving density can be expressed as:

$$\frac{1}{\rho}\frac{a}{a-\rho}=\frac{1}{a}\left[2+B\left(\frac{P}{P_0}\right)^{\frac{1}{\gamma}}+\frac{1}{B}\left(\frac{P}{P_0}\right)^{-\frac{1}{\gamma}}\right]$$

Combining this with Equation (4.27), we obtain a relation that needs to be solved for (p/p_0) in order to obtain the pressure at the throat (and hence the other properties):

$$\frac{\gamma}{2}\frac{P}{P_0}\left[2+B\left(\frac{P}{P_0}\right)^{\frac{1}{\gamma}}+\frac{1}{B}\left(\frac{P}{P_0}\right)^{-\frac{1}{\gamma}}\right]=\left(1-\frac{P}{P_0}\right)+\frac{1}{B}\frac{\gamma}{\gamma-1}\left(1-\left(\frac{P}{P_0}\right)^{(\gamma-1)/\gamma}\right) \tag{4.28}$$

Next, we need to represent the normal shock equations for the real gas model. The normal shock equations are generally given as:

Mass Conservation: $\rho_1 v_1 = \rho_2 v_2$

Momentum Conservation: $P_1 + \rho_1 v_1^2 = P_2 + \rho_2 v_2^2$

Energy Conservation: $h_1 + \frac{v_1^2}{2} = h_2 + \frac{v_2^2}{2}$

For a real gas, $\rho v^2 = \frac{P}{ZRT}\underbrace{\frac{v^2}{\gamma RTZ^2}}_{M^2}\gamma RTZ^2 = \gamma ZPM^2$

Therefore, the momentum conservation equation can be written as: $P_1(1+\gamma Z_1 M_1^2) = P_2(1+\gamma Z_2 M_2^2)$, or

$$\frac{P_2}{P_1}=\frac{1+\gamma Z_1 M_1^2}{1+\gamma Z_2 M_2^2} \tag{4.29}$$

Similarly, the continuity equation can be expressed as:

$\rho_1 v_1 = \rho_2 v_2 \Rightarrow \rho_1^2 v_1^2 = \rho_2^2 v_2^2 \Rightarrow \frac{P_1^2}{Z_1^2 R T_1^2 \gamma} = \frac{P_2^2}{Z_2^2 R T_2^2 \gamma} \Rightarrow \frac{P_1^2}{T_1} M_1^2 = \frac{P_2^2}{T_2} M_2^2$. Hence,

$$\frac{T_2}{T_1}=\left(\frac{P_2}{P_1}\right)^2\left(\frac{M_2}{M_1}\right)^2 \tag{4.30}$$

Before representing the energy conservation equation in terms of the Abel-Noble EOS, we need to express equation (26) for the change in enthalpy for the chosen EOS. We have

$$\left(\frac{\partial Z}{\partial T}\right)_P=\frac{-P}{aRT^2}\Rightarrow\frac{T\cancel{V}}{Z}\left(\frac{\partial Z}{\partial T}\right)_P=\frac{P\cancel{V}}{ZRT}\frac{1}{a}=\frac{1}{a}$$

Therefore,

$$dh = C_p dT - \frac{1}{a}dP \tag{4.31}$$

Hence, the energy conservation equation can be written as

$$C_p T_1 - \frac{1}{a} P_1 + \frac{v_1^2}{2} = C_p T_2 - \frac{1}{a} P_2 + \frac{v_2^2}{2}$$

$$\Rightarrow C_p T_1 - \frac{1}{a} P_1 + M_1^2 \frac{\gamma R Z_1^2 T_1}{2} = C_p T_2 - \frac{1}{a} P_2 + M_2^2 \frac{\gamma R Z_2^2 T_2}{2}$$

Combining and simplifying, we get:

$$T_1\left(1+\frac{\gamma-1}{2}M_1^2 Z_1^2\right)+\frac{\gamma-1}{a\gamma \mathrm{R}}(P_2-P_1)=T_2\left(1+\frac{\gamma-1}{2}M_2^2 Z_2^2\right) \tag{4.32}$$

Equations (4.29), (4.30) and (4.32) represent the normal shock equations for the current EOS. These equations were solved numerically using the Newton-Raphson technique to arrive at the Mach number after the shock and hence the values of all other parameters.

Comparisons to existing tools and experimental data have revealed that the model works well. This is now implemented in FLACS and is an important addition to since the design pressures of hydrogen storage systems can be up to 700 bar where real gas effects are extremely important. A comparison between the release rates for the ideal gas and real gas models for releases occurring from a 4 mm orifice from a 350 bar and 700 bar reservoir are shown in Figure 4.15. Analyses of an accidental release from such systems can provide an incorrect result if an ideal gas model is used to estimate the release rate.

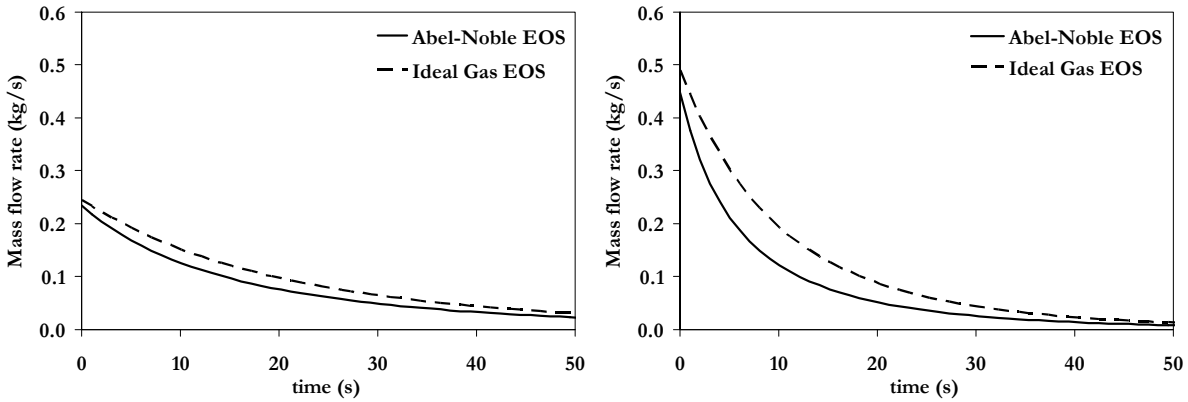

Figure 4.15 – Comparison between the release rates for the ideal gas and real gas models for releases occurring from a 4 mm orifice from a 350 bar (left) and 700 bar (right) reservoir

4.4 Validation against experimental data

The validation work for sonic releases is summarized in the following subsections.

4.4.1 Unconfined, horizontal jet release (INERIS)

This experimental study was performed at INERIS and sought to characterize the clouds formed by supercritical jets of hydrogen released in the open through an orifice in a storage vessel. The volume of the source was 19-litres. The internal diameter of the tube between the vessel and the orifice (diameter 0.5 mm) was 1.6 mm and the orifice was fixed in such a way that the jet was horizontal. The gas storage pressure was 200 bars. The vessel was filled with hydrogen at the desired pressure and the discharge of hydrogen was triggered by opening a control valve. The pressure and the temperature of hydrogen were also measured during the discharge. The

concentration of hydrogen was measured by four catalytic sensors placed on the jet axis at a distance of 0.5, 0.6, 0.7 and 0.8 m from the release location.

The Jet utility program was used to estimate the release rate and the expanded diameter. The release rate was found to be 2.1 g/s occurring through an effective area of 34.2 mm^2. Based on this, a grid of 6.7 mm was used to resolve the release (the default prevailing grid resolution was 2.5 cm). A plot presenting the full flammable plume predicted by FLACS, in addition to velocities is shown in Figure 4.16.

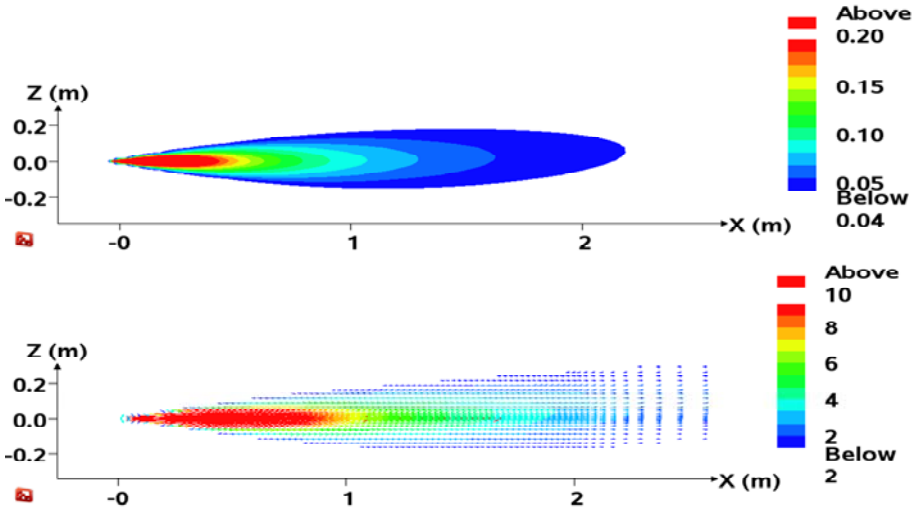

Figure 4.16 – Predicted plume shape (top) and velocities in the plume (bottom) for the 200 bar hydrogen release through a 0.5 mm orifice. Red colour is shown for concentrations above 20 %, blue colour stops at LFL of 4 %.

The simulated hydrogen concentrations as a function of time for all four sensors are shown in Figure 4.17. The figure also shows the variation of concentration as a function of time as measured in the experiments for a release from a 200 bar source. The four curves represent the four different sensor locations, with the highest concentrations reported at X = 0.5 m and the lowest concentrations reported at X = 0.8 m. Each curve shows a sharp increase of the concentration at a certain time (this time is directly proportional to the distance of the sensor from the release). Then, the concentration values fluctuate around a mean value which slowly decreases, as the pressure in the vessel decreases. However, the decrease of the pressure is not significant since the diameter of the orifice is quite small and the duration of the release is less than 10 s. The concentrations decrease sharply to zero at the end of the release. These general trends seen in the observed concentration field are captured in the simulations. However, it can be seen that the simulations over-predict the concentration levels significantly. An error of almost 100 % is seen, i.e. the observed concentrations are about half those seen in the simulations at all four sensor locations.

Further analysis was undertaken in order to understand this significant over-prediction of results. Simulations with different grids revealed that the results were almost independent of grid resolution. No effect of the size of time steps was seen. The difference between actual density and that calculated by the ideal gas law is expected to be only 10 % at 200 bar pressure and is thus insufficient to explain the discrepancy (the real gas models reported above were not used in this study). The sensitivity of the results to the turbulence parameters used for defining the initial release was also studied (as an input to the jet utility program that is used to determine the boundary conditions, including expanded area and release rate, for the dispersion simulations). This revealed that the turbulence length scale (TLS) had a strong impact on the final concentration field. However, in order to match the observed concentrations well, a TLS value

10 times larger than expected had to be used. Even then, an error of 10–20 % was seen. The results for the sensor placed at a distance of 0.5 m from the release location are shown in Figure 4.18 where both the relative turbulence intensity (RTI) and TLS are varied proportionately. Therefore, it is not believed that this is the reason for the discrepancies that are seen.

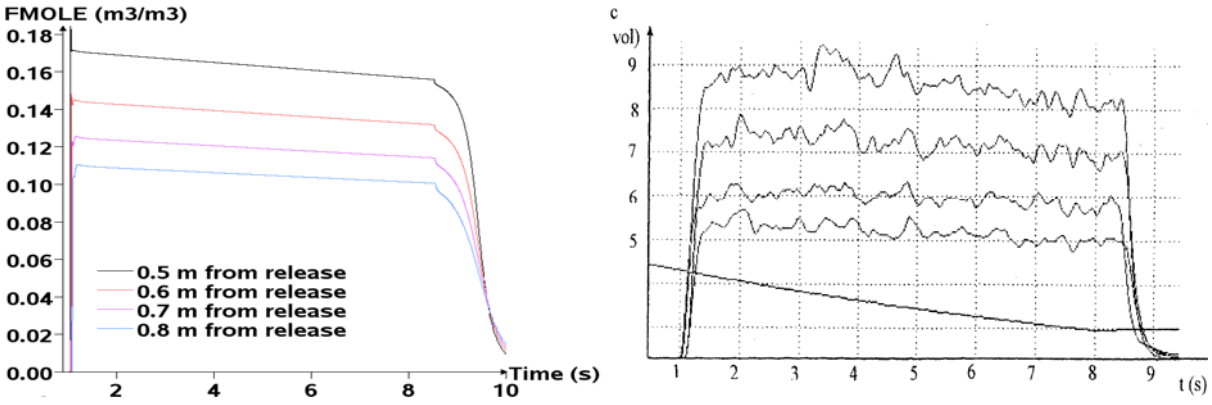

Figure 4.17 – Simulated (left) and observed (right) hydrogen concentrations as a function of time in the INERIS tests (Chaineaux et al.) for a release from a 19 litre vessel at 200 bar (orifice size 0.5 mm) at four different locations on the jet axis: 0.5, 0.6, 0.7 and 0.8 m from the release.

The results were also plotted as inverse concentration as a function of normalized distance (the normalization factor was the notional diameter). This is expected to yield a linear relationship. It can be seen from Figure 4.19 that the simulated concentrations also result in a linear profile. However, the slope is significantly different (by a factor of 2 or so that is similar to the order of over-prediction).

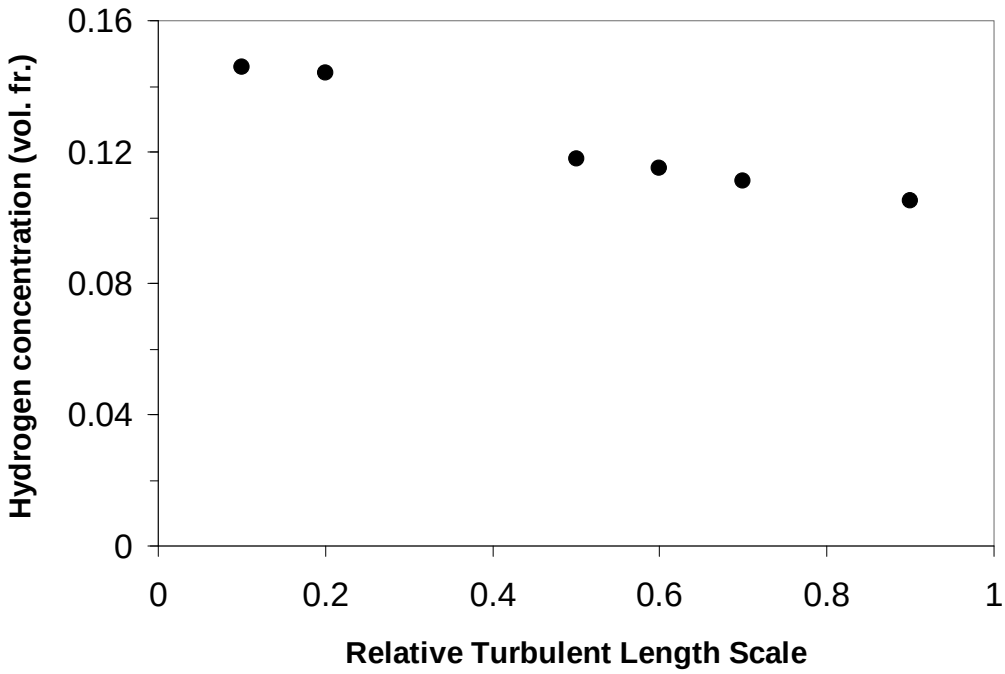

Figure 4.18 – Simulated hydrogen concentration at a distance of 0.5 m from the release as a function of relative turbulence length scale in the INERIS tests (Chaineaux et al.) when both the RTI and TLS are changed proportionally.

Since this analysis did not identify any critical issues with the simulations, further efforts were directed to identify whether the measurement techniques could have had an influence on the experimental results. This was based on previous experience from the Phase 3B project (Hansen, Bergonnier, Renoult & van Wingerden, 2001). The discussion below may also apply for other experiments described later in this chapter.

Oxygen sensors of catalytic type have been used to measure hydrogen concentrations in the INERIS experiments. However, these sensors may have a significant weakness. Normally, the output of the sensors is calibrated prior to the experiment, so that 20.95 % oxygen is reported. This calibration is normally carried out at calm conditions, with limited or no flow velocities. In experiments involving high-speed jets, the jet not only leads to higher hydrogen concentration, but also increases the flow velocity across the sensors. So, even though the presence of hydrogen reduces the reported oxygen concentration (which is translated into the hydrogen concentration), the increase of flow velocity leads more oxygen molecules into the catalytic sensor, and the reported oxygen concentration is higher than it should. The result of this is that the sensors report a too low gas (hydrogen) concentration (Hansen, et al., 2001).

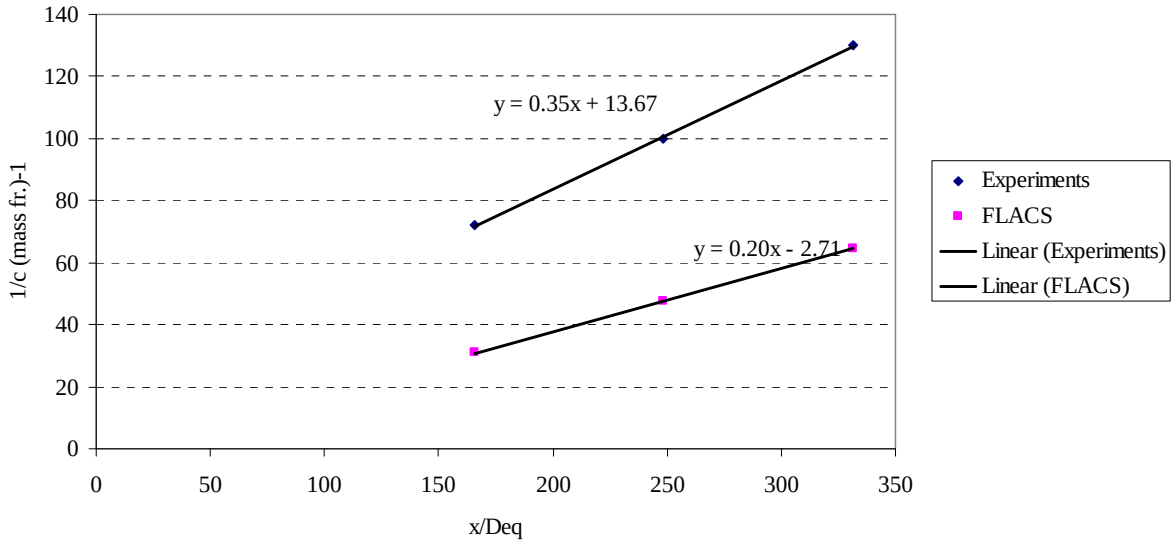

Figure 4.19 – Simulated and experimentally observed inverse hydrogen concentration as a function of reduced distance in the INERIS tests (Chaineaux et al.) for a release from a 19 litre reservoir at 200 bar (orifice size 0.5 mm).

The problem was first seen when studying large-scale experiments performed by Advantica at the Spadeadam test site in the UK from 1999–2001 under a JIP that was studying large gas releases and subsequent explosion. It was seen that the simulated concentrations are very different from those observed for sensors placed directly on the jet axis. Attempts have previously been made by Hansen and coworkers (Os, 2002; Hansen, et al., 2001) to explain this serious discrepancy. A very clear trend was found in which the "simulated error" correlated well with the flow velocity change due to the onset of the jet. The work indicated that for each 1 m/s change in flow velocity from the jets, there is a underreporting of gas concentration of the order 0.2–0.5 vol. % (Hansen, et al., 2001). Thus, it was concluded that catalytic oxygen sensors are strongly influenced by changes in flow pattern. A general quantification of the effect was difficult as this could depend of both how the sensor is physically protected (e.g. rain cover or similar), but evidence was seen that the effect was stronger for small velocity changes than for large velocity changes (this could probably be explained by the fact that the oxygen absorption should be

expected to get less efficient with increasing velocity). Therefore, all measurements inside a jet were likely to be too low with regard to gas concentration (Hansen et al., 2001, Os, 2002).

The above analysis was applied to the simulations of the INERIS jet as a part of the work in this thesis. The difference between the simulated and the reported concentrations is shown in Table 4.1. The simulated velocity change due to the jet is also presented. It can be seen how the jet increases the flow velocity to 16 m/s at 0.5 m and 10 m/s at 0.8 m distance. The observed concentrations are adjusted based on the hypothesis presented above and it is shown what it would mean to the observed concentration if a systematic measurement error of 0.5 vol. % per m/s change of flow velocity would apply. It can be seen that very good agreement between the observed and simulated concentrations is then achieved.

Table 4.1 – Comparison INERIS test versus FLACS. In the last column, 0.5 vol. % is added to the reported concentration by INERIS for each m/s flow in the jet.

Distance	FLACS H_2 (vol. %)	FLACS velocity	INERIS H_2 (vol. %)	Observed concentration adjusted for error (e.g. 0.5 % / ms^{-1})
0.5 m	17.0 %	16.3 m/s	9.0 %	17.2 %
0.6 m	14.5 %	13.5 m/s	7.5 %	14.3 %
0.7 m	12.5 %	11.5 m/s	6.0 %	11.8 %
0.8 m	11.0 %	10.0 m/s	5.4 %	10.4 %
1.0 m	9.0 %	8.0 m/s		
1.5 m	6.0 %	5.0 m/s		
2.0 m	4.4 %	3.7 m/s		

4.4.2 Sonic, unconfined, horizontal jet release (HSL)

The experiments were performed by Health and Safety Laboratories (HSL) on behalf of Shell Global Solutions. The details of the experiments are given in Roberts, Shirvill, Roberts, Butler & Royle (2006). The concentration of hydrogen in the un-ignited plume was derived from measurements of the oxygen concentration within the cloud using "AO2 Oxygen CiTicel" sensors. The measurement principle of these sensors (as described in the previous section) is that any decrease in the concentration of oxygen is caused by displacement of oxygen by hydrogen gas.

The concentration signals comprised a rapid rise to a plateau, a "constant" period and then a fall. A large effect of wind was seen in several of the tests where the concentrations during the release period were very variable due the jet being blown off line. The results for test 7 (10 MPa release through a 3 mm orifice) are illustrated in Figure 4.20 (Roberts, et al., 2006). This test had relatively steady concentration measurements and the wind speed and direction was satisfactory. The results from test 13 (7.4 MPa release pressure through a 3 mm orifice) are also illustrated in the same figure, indicating the effect of a more variable wind speed and direction on the concentration measurements. For this reason, test 7 was used for CFD validation.

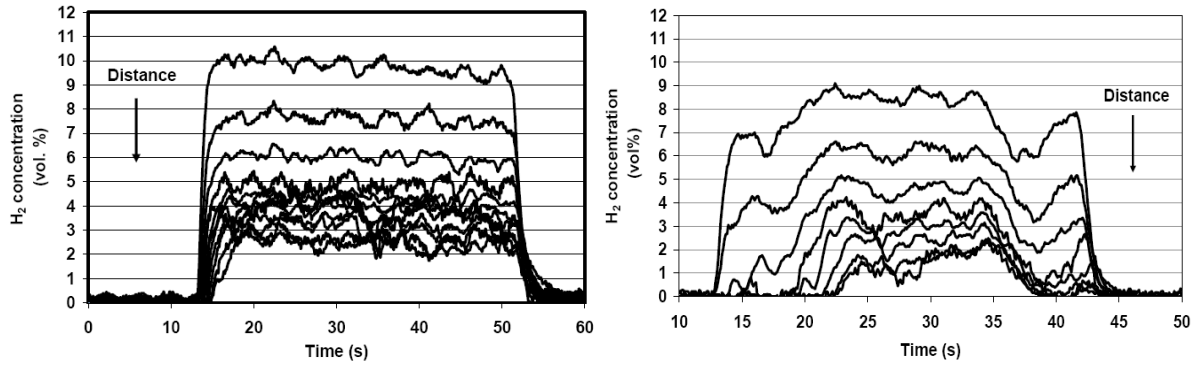

Figure 4.20 – H_2 concentration as a function of time for HSL unconfined releases (Top) Test 7 (pressure 10 MPa, 3 mm orifice). (Bottom) Test 13 (pressure 7.4 MPa, 3 mm orifice).

As shown in **Paper 1**, the experimental and simulation results agree quite well with each other. The experiments also reported distance to LFL concentration at two different heights, 1.5 m and 2.0 m (corresponding to the positions of the monitor points). It was measured to be 8 m in both cases. The simulations predicted a distance to LFL of 7.7 m at a height of 1.5 m that agrees well with experimental observations. However, the distance to LFL increased to 8.6 m at a height of 2.0 m as the buoyancy of hydrogen contributed to increased concentrations at higher elevations (see Figure 4.21). The experimental plume was found to be less buoyant.

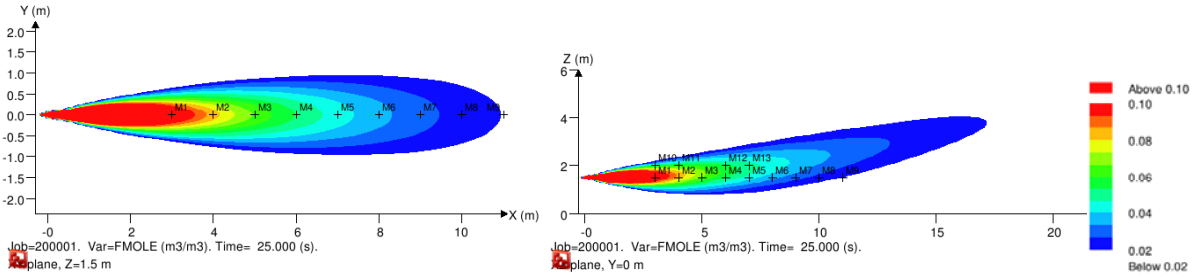

Figure 4.21 – Hydrogen concentrations in the plane Z = 1.5 m (top) and Y = 0 m (bottom) for the HSL sonic horizontal hydrogen release. The monitor points are also shown.

The good agreement seen here is different from the conclusions obtained from the simulations of the INERIS experiments reported in the previous section (even if the experimentalists have also reported using oxygen sensors for the HSL experiments). Based on our work and discussions with other researchers involved in similar work, it may be concluded that the pseudo source approach used has limitations for the case of very small nozzles (e.g. 0.5 mm) used in the case of INERIS tests. Similar conclusions were also seen for the simulations of the FZK release experiments (reported in the next section). More work is thus required in this area.

4.4.3 Sonic, unconfined, horizontal jet release (FZK)

The experimental facility consisted of a high-pressure gas system to provide hydrogen release at pressures in the range 20–260 bar through the nozzle. A picture of the experimental setup is shown in Figure 4.22. Hydrogen concentration profile and flow velocity were simultaneously measured in three different cross-sections at distances 0.75, 1.5, and 2.25 m from the nozzle. The experiments were carried out in order to evaluate amount of burnable hydrogen–air mixture (above the lower flammability limit) in free turbulent jet at different pressures. The experimental details are reported in Friedrich, Grune, Kotchourko, Kotchourko, Sempert, Stern & Kuznetsov (2007). All calculations have been performed blind without prior knowledge about experimental

results when submitting the predictions. Simulation time was around 2-3 days. Four sets of experiments were recommended to be simulated. They are also summarized in Figure 4.22 below. The experiments were modelled as free jets. No geometrical details were represented. The jet utility program was used to calculate the release rates and other characteristics of leaks from a high-pressure reservoir. A nozzle discharge coefficient of 0.85 was used and heat loss was ignored. The mass flow rates calculated by the jet program were found to agree very well with those given along with the experimental description.

The grid size across the leak is chosen so that the expanded leak area (to ambient pressure) fills roughly 90 % of the grid cell. Minimum grid cell areas are 0.9 cm (100 bar, 1 mm), 1 cm (208 bar, 0.75 mm), 1.25 cm (196 bar, 1 mm) and 0.3 cm (160 bar, 0.25 mm). Reasonable results could also have been obtained with a coarser grid resolution and faster simulation times. Some test simulations with a coarser grid and longer time steps (with a few hours simulation time) were performed. These simulations gave very similar results to the submitted ones.

Test No.	Pressure (bar)	Orifice dia. (mm)	Mass flow rate (g/s)
HD 31-34	100	1	4.45
HDH3	208	0.75	5.28
HD22-24	160	0.25	0.45
HDH13	196	1	8.85

As mentioned earlier, the simulations were carried out before the experiments were performed. After the experimental results were collected, it was quickly realized that several of the datasets could not be used for comparison with simulations. These included HD31-HD34 and HDH13 (unreliable measurements) and HDH03 (only one radial profile available and only 2 s injection time). Therefore, it was decided to carry out comparisons with only one dataset, i.e. HD22-HD24. This dataset consists of the results for a release from a 160 bar source from a 0.25 mm orifice that is actually even smaller than the one used for the INERIS experiments.

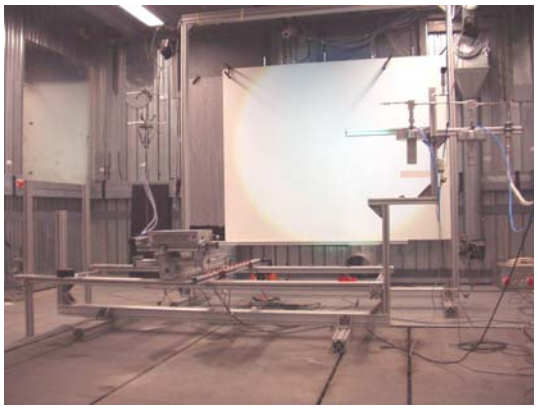

Figure 4.22 – Side view of the experimental set-up for the FZK release experiments along with a summary of all four experiments simulated with FLACS.

The simulations of a similar high pressure jet from experiments done at INERIS have been presented in Section 4.4.1. As described there, FLACS over-predicted the concentrations measured in these experiments significantly (+50 % or more). One analysis presented there considered the possible problem with oxygen sensors (section 4.4.1). However, as presented in Section 4.4.2, FLACS predictions are very consistent with other test series (e.g. HSL/SHELL experiments presented at Hazards conference 2006). Shell/HSL reported that even moderate crosswind will strongly influence (reduce) axial concentrations measured in this type of experiments (Figure 4.20). Therefore, it is possible that the INERIS results may have been influenced by some crosswind, wrong orientation of the jet or measurement problems. Since the

FZK experiments were performed indoor with no wind influence, it can be very interesting to compare FLACS predictions with these experiments.

However, if the hypothesis propounded at the end of last section (regarding the suitability of the pseudo-source approach for very small nozzles) is correct, the simulations should again over-predict the concentrations. The comparison of the experimental data for the only suitable dataset with the simulations is presented next. Figure 4.23 presents the radial concentration distribution at three different axial distances from the release location for both experiments and FLACS simulations. An over-prediction of the centreline concentration is evident for the position 0.75 m from the release location while the agreement is much better for locations further from the release. Similar observations can be made from the comparison of axial velocities as expected (shown in Figure 4.24). The width of the simulated curves is larger in all three cases.

Therefore, it can be concluded that jet concentrations seem to be over-predicted sometimes (for small nozzles / flow rates). Possible explanations for this deviation could be the fact that the internal details of the nozzle (not described in simulations) are much more important for smaller nozzles. Also, for small jets, there are more fluctuations in the resulting plume, which implies lower averaged measurements. Differences in measurement methods for releases from a small and large nozzle can also contribute to the discrepancy. Therefore, this issue still needs to be understood in greater detail.

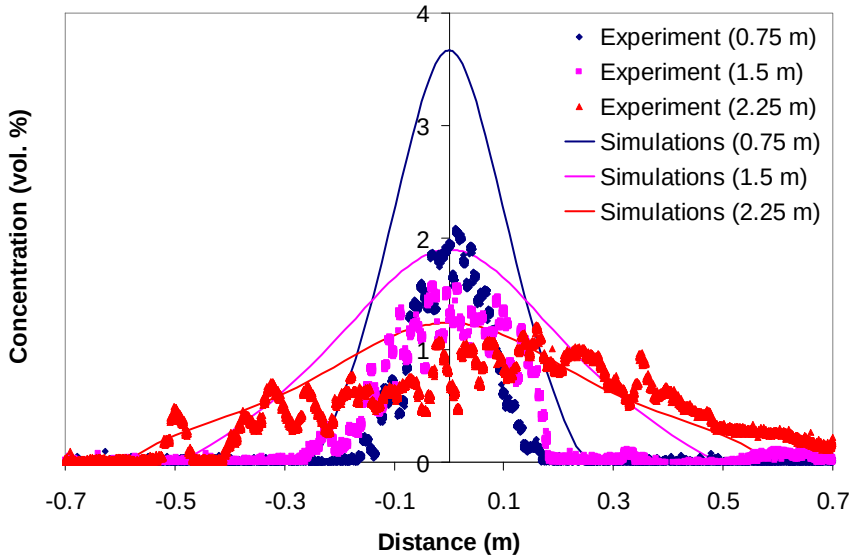

Figure 4.23 – Comparison of experimental and simulated radial concentration distribution at three different axial distances for test HD22-24 (FZK release experiments).

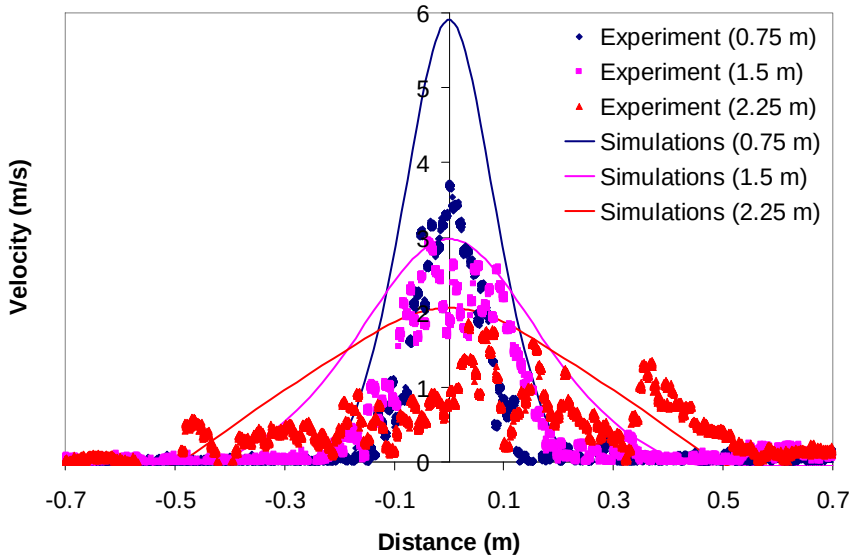

Figure 4.24 – Comparison of experimental and simulated radial velocity distribution at three different axial distances for test HD22-24 (FZK release experiments).

4.5 Final Remarks

The development and use of FLACS as a dispersion tool has mainly been focused on modelling the spreading of natural gas on offshore platforms until late 1990s. In 2003, a model development and validation exercise with simulations of 100 s of onshore large-scale experiments was carried out (Hanna, Hansen & Dharmavaram, 2004). This was motivated by the importance of reliable dispersion predictions in QRA studies. An accurate description of ventilation characteristics also plays a very important role in the correct estimation of the shape, size, and location of the flammable gas cloud. Through the 1990s several ventilation validation studies were performed on real offshore oil installations and large-scale tests sites, including Oseberg-C (Norsk Hydro), Beryl-B (Mobil), Nelson (Enterprise Oil), Spadeadam test site, etc. The current chapter has discussed the extensive validation activity in the area of dispersion of hydrogen and presented some relevant results. Modelling results are compared to experimental data, and in general, reasonable agreement is seen for many different kinds of release conditions. Examples of subsonic and sonic gas releases (free space and impinging) as well as liquid hydrogen releases are presented. A range of different experiments is simulated, including low momentum releases in a garage, sub-sonic jets in a garage with stratification effects and subsequent slow diffusion, low momentum and subsonic horizontal jets influenced by buoyancy, and free jets from high-pressure vessels. LH_2 releases are also considered. Several of the simulations are performed as blind predictions.

In general, reasonably good agreement is seen between simulations and experiments. The agreement is especially good for e.g. hydrogen release in garages. The prediction capability is somewhat mixed for high-pressure releases in the open and this is a topic that needs to be studied further. Overall, it may be concluded that FLACS can be a useful tool for predicting hydrogen dispersion problems. It can also be used for designing ventilation and other mitigation systems. This is important as reliable tools are needed for modelling indoor releases of hydrogen if the dream of a possible hydrogen economy is to be realized.

5 Explosion Simulations: Modelling and Validation

5.1 Introduction

Several different flame propagation mechanisms are possible following the ignition of a hydrogen-air mixture, ranging from a laminar flame that does not lead to any significant overpressures to deflagration (subsonic propagation mode) to detonation (supersonic propagation mode) that has very severe consequences (15–20 barg overpressure).

The dominant mechanism in hydrogen explosions is turbulent combustion. This is by nature highly complex, especially because of the fact that the interaction between turbulence and combustion is "bidirectional". Turbulence has an obvious effect on combustion that is confirmed by much higher burning rates and thus much more severe consequences (this is even more dramatic for hydrogen due to a very large laminar burning velocity). Several processes may be responsible for the increased burning rate in turbulent fuel-air mixtures. Turbulent flow structures may distort the flame front and increase the surface area of the flame. Turbulence also increases the transport of heat and mass, and leads to enhances mixing of reactants and products. However, combustion also affects turbulence in many ways by means of production of density variations, buoyancy, dilatation due to heat release in chemical reactions, variation in molecular transport properties, etc. (Williams, 1986; Kuo, 2005).

For flame propagation inside tubes with obstacles, the final flame speed depends on several parameters, among others; dimension and shape of tube, size and distance between repeated obstacles, composition of fuel-air mixture. Different propagation regimes have been seen for explosions of hydrogen-air in tubes with repeated obstacles, depending on both the geometry and the mixture (Breitung, et al., 2000). For a weak ignition source, a hydrogen-air explosion will in general start in a laminar flame propagation regime, where the mechanisms are fairly well understood. However, fluid dynamic instabilities and other instabilities will in general soon lead to a wrinkled flame front and then to turbulent flame propagation.

In general a wrinkled or quasi-laminar flame will soon become a turbulent flame. Turbulence is easily generated for flow in confined or obstructed geometries. Some of the turbulence generating mechanisms are the Rayleigh-Taylor instability (e.g. when cold gas is accelerated into hot gas), the Kelvin-Helmholtz instability (fluids moving with different speeds) and other shear generated production of turbulence, cf. Arntzen (1998). Turbulence may on the one hand enhance flame propagation, but may on the other hand also contribute to local or global quenching. This phenomenon is governed by the magnitude of the Karlovitz number. The Karlovitz number is a dimensionless quantity, where a characteristic time for the burning velocity of the flame is divided by a characteristic time scale for the smallest turbulent eddies of the flow. For small Karlovitz number less than one and a flamelet regime, turbulence may lead to strong stretching of the laminar flamelets and local quenching. For higher Karlovitz number and a turbulent reaction zone, turbulence may mix cold unburned gas into the reaction zone so much that it leads to quenching.

For the case of hydrogen-air mixtures, buoyancy effects can be especially important. Buoyancy has the effect that the flammability range is larger for upward flame propagation than for downward propagation. Thus it may happen that a flame being able to propagate upward is quenched due to buoyancy for downward flame propagation. Buoyancy will exert an upward force on the hot combustion products, and this may change the flow pattern and possibly give cooling effects (e.g. contact with cold wall). On the other hand, cold gas accelerated into hot gas due to buoyancy can lead to Rayleigh-Taylor instabilities and enhanced flame acceleration.

5.2 Burning velocity of hydrogen-air mixtures

Since the laminar burning velocity plays a critical role in determining the reactivity and subsequent overpressure generation for a particular mixture, a thorough review of the values used in FLACS has been carried out. The laminar burning velocity (S_L) of premixed hydrogen-air flames is a key parameter that has both fundamental and practical significance. It can be used for characterizing the consequences of a hydrogen explosion, and a high S_L value is one of the primary reasons that hydrogen-air deflagrations can be so destructive. Another fundamental parameter is the laminar flame thickness (δ_L) that is generally estimated as (e.g. Turns, 2000):

$$\delta_L = \frac{\alpha}{S_L} \xrightarrow{\Pr=1} \delta_L \approx \frac{\upsilon}{S_L} \tag{5.1}$$

where α is the thermal diffusivity, υ is the dynamic viscosity, and a Prandtl number (Pr) of unity has been assumed. This is generally a good assumption for combustion systems.

Laminar burning velocities for hydrogen-air mixtures have been determined by several researchers. Figure 5.1 presents data taken from several older measurements from 1937 to 1993 (this figure is taken from Aung, Hassan & Faeth, 1997). Results that are not corrected for stretch are indicated by open symbols (the detailed references are not provided here for brevity). It can be concluded that even if a certain scattering is seen in the experimental results, the measurements that correct for flame stretch agree with each other within the bounds of experimental uncertainties over the available test range (Aung, Hassan & Faeth, 1997).

It can be seen that most of the measured values of unstretched laminar burning velocities that have not been corrected for stretch are significantly larger than the stretch-corrected results. This behaviour is even more obvious at fuel-rich conditions where discrepancies can be as large as a factor of 2. This is due to much higher flame stretch (represented by large Markstein numbers) at these conditions. An explanation is given below:

Flame stretch collectively describes the "deformation" of flame due to effects of aerodynamic straining, flame curvature and flame/flow instabilities and unsteady behaviour. For sufficiently small values of stretch, the stretched laminar burning velocity $S_{L,str}$ is related to the "unstretched" laminar burning velocity by a linear relation. This linear relation is characterized by the Markstein length, L_M and can be represented as (e.g. Hu, Huang, He, et al., 2009):

$$S_{L,str} = S_L - L_M K_u \tag{5.2}$$

where K_u is the stretch rate of a flame surface element A_f defined as $A_f^{-1}\frac{dA_f}{dt}$ and S_L is the one-dimensional unstretched flame speed relative to the unburned mixture. The nondimensional Markstein number, Ma is often used instead of the Markstein length. This is defined as $Ma = L_M / \delta_L$ where δ is a characteristic flame thickness that is given in Equation (3.1). Therefore, a larger value of Markstein number leads to larger deviation from the unstretched flame speeds. The above equation can be further non-dimensionalized by using the Karlovitz number $Ka = K_u \alpha / S_L^2$. Using this, equation (3.2) can be expressed as:

$$\frac{S_{L,str}}{S_L} = 1 - KaMa \tag{5.3}$$

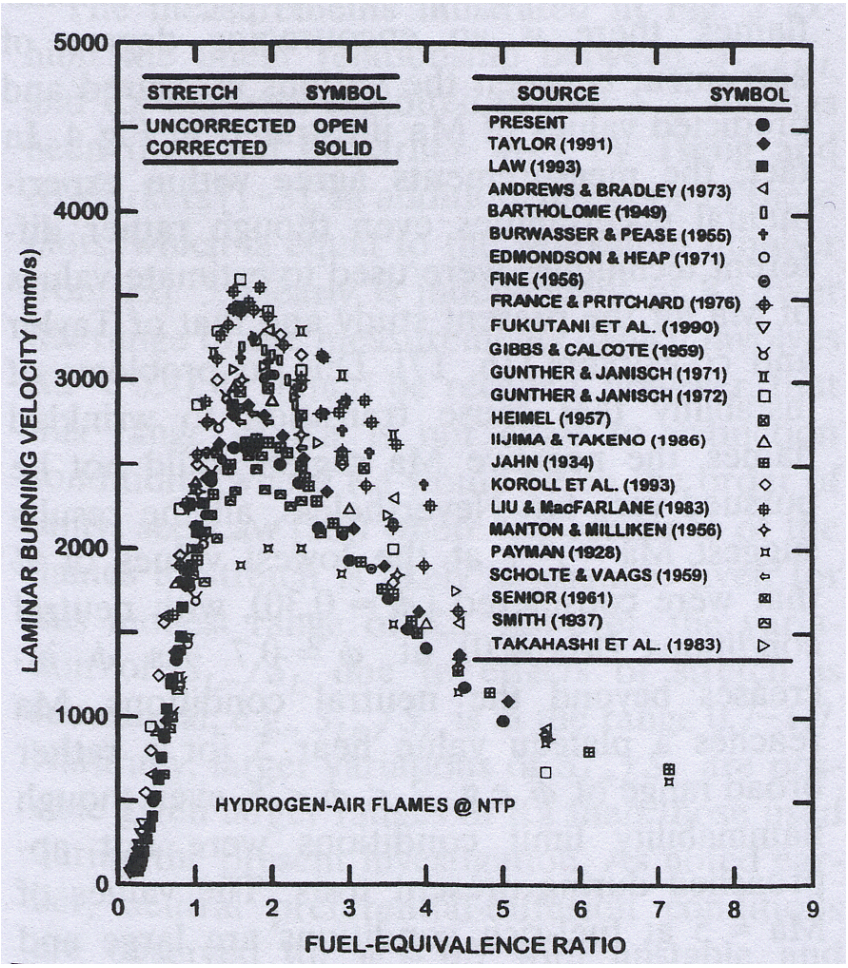

Figure 5.1 – Laminar burning velocities for hydrogen/air mixtures from several experiments (Aung, Hassan & Faeth, 1997).

The laminar burning velocities used in FLACS have been based on the work of Taylor and coworkers (Dowdy, Smith, Taylor & Williams, 1990; Taylor, 1991). This work included the study of freely (outwardly) propagating spherical hydrogen/air laminar premixed flames in order to find both unstretched laminar burning velocities and the sensitivity of the flames to stretch. This approach sought to minimize uncertainties about effects of finite flame thickness, curvature, and unsteadiness when reducing measurements to find unstretched laminar burning velocities and Markstein lengths. Taylor and co-workers also developed a chemical rate mechanism for hydrogen combustion that was used to perform detailed numerical simulations of the outwardly propagating spherical hydrogen/air flames and obtained good estimates of their measurements of both unstretched laminar burning velocities and Markstein lengths (Dowdy, Smith, Taylor & Williams, 1990; Taylor, 1991).

The current study has also included the evaluation of some newer measurements made in this decade with respect to the values reported by Taylor and coworkers that have been adapted in FLACS. In general, these use similar techniques as described above by Taylor and coworkers and Faeth and coworkers. Davis & Searby (2002) used counterflow flames for the determination of laminar burning velocities and developed a procedure for the proper evaluation of Markstein numbers in order to correct for stretch effects. Kwon & Faeth (2001) used freely outward propagating spherical laminar premixed flames at several different concentrations (ER = 0.6–4.5) and pressures up to 3 bar. All these conditions were seen to satisfy the linear correlation given above in Equation (5.3). Tse, Zhu & Law (2000) developed a novel experimental apparatus for the study of constant-pressure, outwardly propagating spherical flames that could be used for

ambient pressures up to 60 bar. Their results can be used to study the prevailing flame propagation mechanisms at high pressures that are more commonly seen in e.g. internal combustion engines. The results are shown in Figure 5.2. It can be seen that the values are very consistent with each other even though Davis & Searby (2002) report somewhat higher maximum values of the laminar burning velocities.

Experiments have also been carried out by the author in a standard 20-litre sphere to determine laminar burning velocities of hydrogen-air mixtures. This work has been carried out in order to further evaluate the laminar burning velocities for hydrogen-air mixtures and further to gain experience in the experimental techniques used in the determination of laminar burning velocities. This is described in:

Paper 4: Turbulent and Laminar Burning Velocities of Hydrogen-Air Mixtures from Constant Volume Explosions in a 20-litre Vessel

This paper is presented in the 31st International Symposium of Combustion in Heidelberg, Germany (Middha, Skjold & Dahoe, 2006). In this work, a thin-flame model is used to estimate turbulent and laminar burning velocities of hydrogen–air mixtures from pressure-time (p-t) data obtained in a constant volume explosion vessel. The results are used to explore correlations for the decay of turbulence in such vessels, and the applicability of traditional correlations between laminar and turbulent burning velocity for hydrogen-air mixtures.

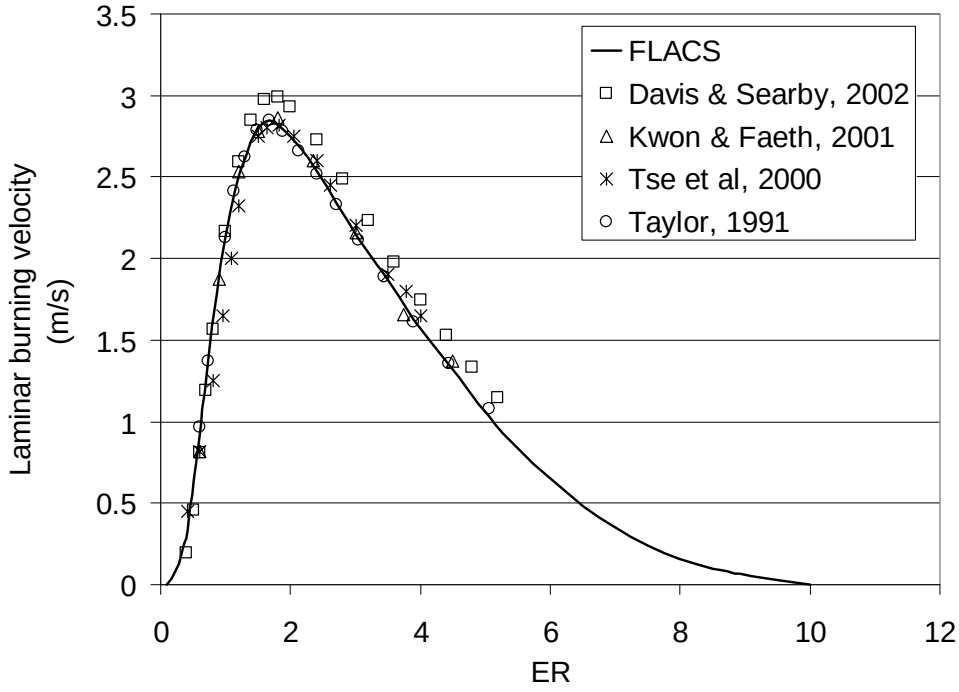

Figure 5.2 – Laminar burning velocities for hydrogen/air mixtures in FLACS compared to several recent experiments.

Based on the results described above, no corrections were made to the default values of laminar burning velocity in FLACS. An evaluation of the models to calculate turbulent burning velocity was also carried out. Herein, three recent experimental studies on the measurement of turbulent burning velocities for hydrogen-air mixtures were analyzed. This included studies on (a) Turbulent burning rates of methane-hydrogen mixtures in a fan-stirred bomb (Fairweather, Ormsby, Sheppard & Woolley, 2009), (b) Turbulent burning velocity of hydrogen-air flames at elevated pressures in a fan-stirred near-spherical combustion chamber (Kitagawa, Nakahara, Maruyama, Kado, Hayakawa & Kobayashi, 2008), and (c) Turbulent burning velocity of two-

component fuel mixtures of hydrogen, methane and propane in a constant-volume near spherical chamber (Muppala, Nakahara, Aluri, Kido, Wen & Papalexandris, 2009). The results for these studies were compared to model predictions of turbulent burning velocities for hydrogen (and methane)-air mixtures. However, no conclusions could be drawn since two of the studies indicated that the Bray models over-predicted the turbulent burning velocity for hydrogen (but also methane)-air mixtures and one of the studies were in reasonably good agreement with FLACS model predictions for both hydrogen and methane. Therefore, no further work on the turbulent burning velocity models was carried out and they were used as is.

However, there are several corrections and improvements that have been made as a part of the current work. The UFL for hydrogen-air mixtures has been somewhat arbitrarily set earlier to a value of ER = 10. This has been corrected to correspond to the experimentally determined value of 75 vol. % or ER = 7.25. In order to do this, the value of the laminar burning velocity at a concentration of ER = 5.5 has been maintained (equal to 0.84 m/s) and then a linear trend has been assumed to a value of 0 m/s at ER = 7.25.

The dependence of the lower and upper flammability limits on temperature and pressure were also corrected. These have been based on older formulations that are generally used for hydrocarbons and their validity for hydrogen has not been tested. The experimental data was taken from recent experiments carried out under the EU-sponsored project SAFEKINEX: SAFe and Efficient hydrocarbon oxidation processes by KINetics and Explosion eXpertise. This work was led by Federal Institute for Materials Research and Testing (BAM) in Germany. Measurements of flammability limits of hydrogen-air mixtures were also carried out. Experimental data produced as a part of this project is reported in public reports (Holtappels, 2005). The default formulation in FLACS assumed a too slow fall in LFL but a too quick rise of UFL (in addition to a higher starting value) as the temperature is increased. However, the trend for the increase of UFL is almost similar to that seen in the experiments. This is shown in Figure 5.3. The pressure dependence of the flammability limits is shown to be completely incorrect (Figure 5.4). The UFL values are seen to rise very quickly to 100 % while the experiments reveal that the UFL is only weakly dependent on pressure. The LFL values also show an opposite trend as compared to that seen in the experiments. The newer values have been included in the improved version of FLACS.

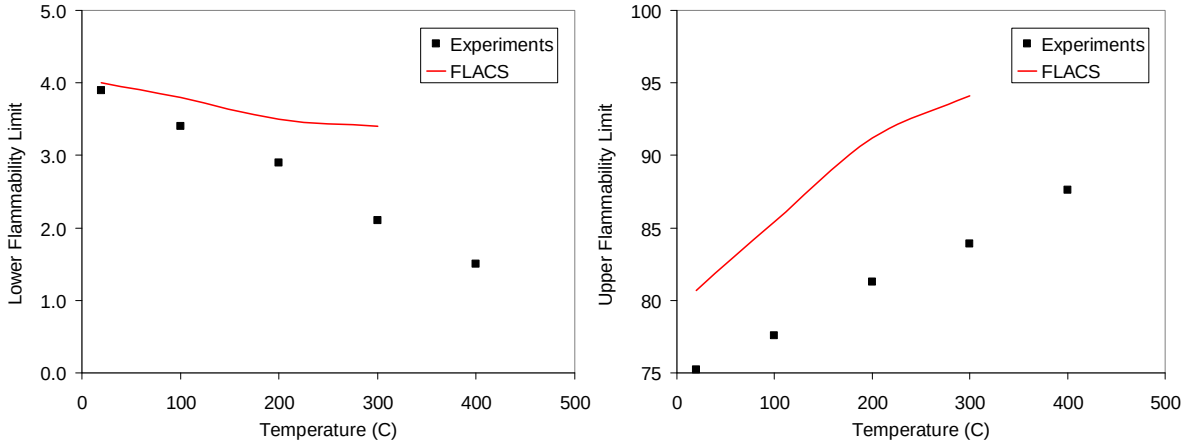

Figure 5.3 – Flammability limits for hydrogen/air mixtures as a function of temperature in FLACS (default) as compared to experimental data.

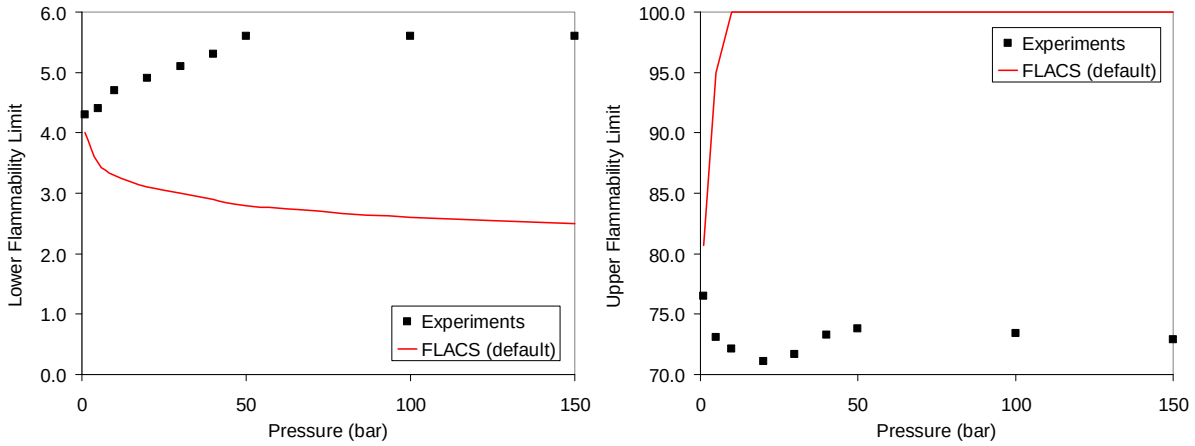

Figure 5.4 – Flammability limits for hydrogen/air mixtures as a function of pressure in FLACS (default) as compared to experimental data.

The models for properly implementing hydrogen explosions in reduced oxygen environments have been implemented in FLACS using experimental data on effect of added nitrogen on flammability and laminar burning velocity of hydrogen-air mixtures. In particular, the flammability data have been taken from Zabetakis (1965). The data for laminar burning velocity has been taken from the work done by Faeth and coworkers (Qiao, Kim & Faeth, 2005). This data has been fitted to a mathematical function that has been directly implemented in FLACS. Examples for H_2-N_2 and H_2-CO_2 mixtures are shown in Figure 5.5.

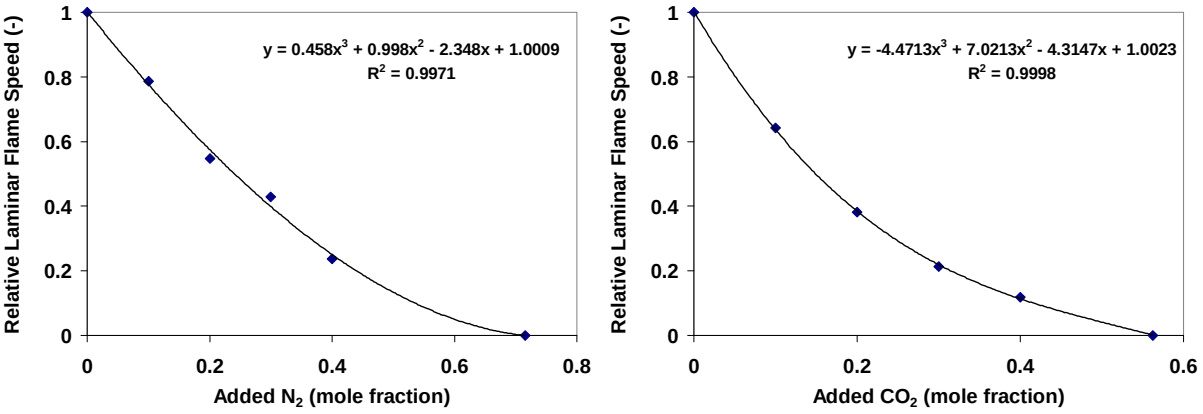

Figure 5.5 – Reduction in laminar flame speed for H_2/air mixtures as a function of added diluents N_2 (left) and CO_2 (right). The polynomial fits implemented in FLACS are also given.

5.3 Validation of FLACS against available experimental data

This section presents validation exercises that have been carried out by the author for hydrogen explosions. Some of these have also been carried out blind without any prior knowledge of experimental data. It must also been mentioned that several of the validation exercises are carried out in work described in Chapter 7 (and not here) as they involved a transition to detonation that is the subject of that chapter. A review of the validation work is described in:

Paper 5: Using computational fluid dynamics as a tool for hydrogen safety studies

This paper is published in the Journal of Loss Prevention in the Process Industries (Middha & Hansen, 2009a). Several validation exercises are summarized in this article. These include:

1. Vented Tube Experiments (HYCOM Project) (Breitung, et al., 2005)
2. SRI Confined Tube (Groethe, Colton & Chiba, 2002)
3. Shell experiments in a simulated vehicle refuelling environment (Shirvill, Royle & Roberts, 2007)
4. BP/HSL experiments in a congested rig (Royle, Shirvill & Roberts, 2007)
5. SRI Tunnel (Sato, Merilo, Groethe, Colton, Chiba, & Iwabuchi, 2006)

Modelling results are compared to experimental data, and in general, reasonable agreement is seen for many different kinds of geometries and conditions.

Details of the extensive work performed in connection with the SRI confined tube experiments have been described separately in:

Paper 6: Hydrogen Explosion Study in a Confined Tube: FLACS CFD Simulations and Experiments

This paper is published in the proceedings of the 21st ICDERS (Middha, Hansen, Groethe & Arntzen, 2007) and described simulations of FLACS for all 8 scenarios (different blockage ratio, concentration, and number of obstacles) and comparison to experimental data. In general, the simulations compare reasonably well with experimental predictions. Both the values and locations of overpressures and flame are represented with reasonable accuracy.

Experiments # 4 and 5 were only mentioned in **Paper 5.** Therefore, additional details regarding the experiments # 3, 4 and 5 are given below:

5.3.1 Hydrogen explosions in a simulated vehicle refuelling environment

This section describes the simulations of a hydrogen explosion experiment in an environment simulating a vehicle refuelling station. This calculation is significant as safety of refuelling stations, where hydrogen will be handled routinely by general public, is of particular interest in the framework of the emerging hydrogen economy. The range of accidental scenarios, potential hazards and outstanding safety issues related to the hydrogen refuelling stations may be seen through recent publications on the subject (e.g. Markert, Nielsen, Paulsen & Andersen, 2007; Kikukawa, Yamaga & Mitsuhashi, 2008). The experiment in a mock-up of a hydrogen refuelling station was conducted jointly by Shell Global Solutions (UK) and the Health and Safety Laboratory (UK) in order to study the potential hazards and consequences associated with a hydrogen-air mixture explosion. The "worst-case" scenario of a stoichiometric hydrogen-air mixture explosion was offered for this simulation exercise. The calculations have been performed blind and no information about experimental results was available when submitting the predictions.

This work was a part of the benchmarking carried out under the HySafe Network of Excellence. Other modelers have taken part in this study and the work presented in this section is published in International Journal of Hydrogen Energy. This paper includes an inter-comparison of the results between several other tools which took part in the benchmarking exercise (Makarov, et al., 2009). This is included as **Paper 7** in the appendix. A picture of the experimental facility along with the location of the transducers is shown in Figure 5.6. Other experimental details are presented in **Paper 7** and are not repeated here.

Thus, the experimental setup involved different levels of confinement, leading to a wide range of combustion regimes and contributing to a complex pattern of pressure rise in time and space. One may expect that before reaching obstacles (close to the ignition point) and in unobstructed space (upper direction of flame propagation) the flame will propagate in a quasi-laminar regime, accelerating with time due to flame instabilities similar to deflagration in an open atmosphere. All the geometrical entities obstructing flame propagation — the wall, refuelling units, car mock-up

— may be considered as turbulisers causing combustion acceleration and pressure rise. The largest overpressure was recorded in the congested space under the car, where relatively large flame turbulisation occurs, and inside the engine compartment of the mock-up car, where a large portion of the hydrogen-air mixture is stored in a confined space. Further details on experimental observations are given in **Paper 7**.

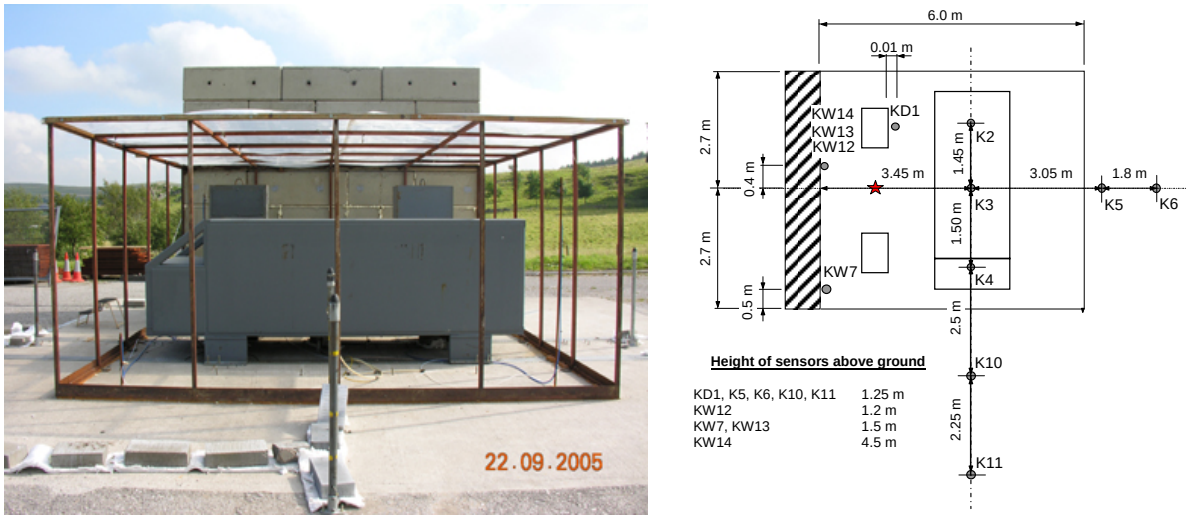

Figure 5.6 – (left) A photo from the test site. (right) Location of pressure transducers relative to the experimental rig.

The frames holding the plastic have been modelled in FLACS. It is expected that the frames can have a significant impact on the explosion development. Guidelines described previously have been followed while defining the computational grid and boundary condition. The minimum grid resolution according to guidelines is that the cloud shall be resolved by at least 10 grid cells in the smallest direction. This requires a maximum grid cell size of 25 cm. It is generally recommended to use an even finer resolution for hydrogen due to higher reactivity and expected sharper gradients. If the space below the car shall be resolved properly (0.3 m) this will require a finer grid resolution. Based on this we used two different grid resolutions with 10 cm and 5 cm grids. For a practical situation, the coarser grid (10 cm) would typically be used. In this case, the 5 cm grid is slightly more optimal because some of the geometry objects can not be properly resolved with a 10 cm grid, and it is more optimal with 6 grid cells below the car then with 3 grid cells. Simulation time was 5 h for coarse grid calculation and 45 h for fine grid calculation.

In Figure 5.7, the maximum pressure reported at ground level during the simulation at different locations is shown. Due to turbulence behind and flame fingering around obstructions like dispensers the car, and the support structure for the polyethylene sheets containing the gas, very strong flame acceleration was seen when the flame propagated out of the original gas filled volume. The flame development during the simulation presented in **Paper 5** wherein the high pressures observed at the end of the simulation correspond with the time when the different parts of the flame meet behind the car.

The predicted overpressure at the pressure sensors was of the order 0.2–0.4 barg inside the volume initially filled with gas. The predicted pressure curves for two sensors inside the gas cloud are shown in Figure 5.8 for both the grids. It can be seen that the results for the two grids agree reasonably well with each other. Average difference between the arrival times of the pressure peak obtained on the coarser grid compared to the fine one was 7.9 % and average difference in overpressure peak values obtained on the coarser grid 2.1 %.

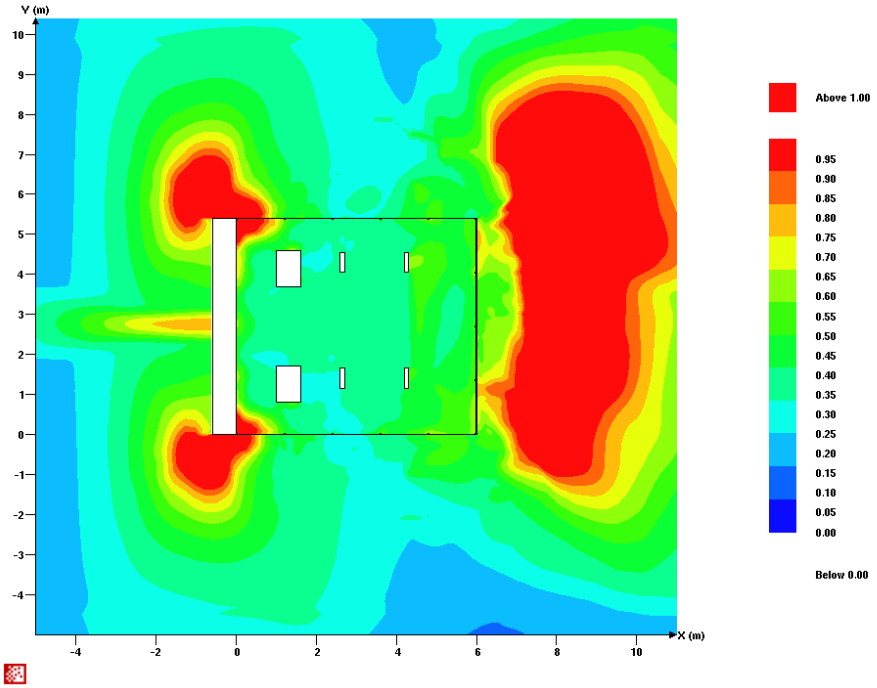

Figure 5.7 – Maximum pressure reported at different locations at ground level during the simulation of hydrogen explosion in refueling station geometry.

The predicted overpressures are compared to the experimental data next. Figure 5.9 presents the simulated and experimental overpressures for six sensors. It can be seen that the simulations are able to predict the experimental data to a reasonable degree of accuracy that is remarkable since these calculations were blind. There is fairly good prediction of the maximum overpressure time, and reasonably moderate overpressure errors for most of the sensors. The results are generally conservative with pressure error between –10 % (in one sensor) and +46 % within the refuelling station. Simulated pressure dynamics clearly reproduce experimental double-peak structure under the car (K2, K3, K4) and further from the car (K5, K10, and K11).

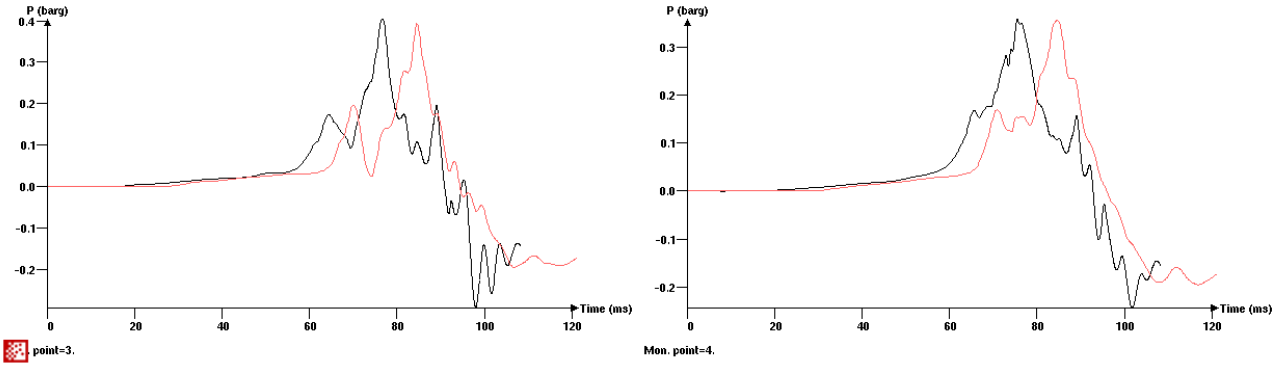

Figure 5.8 – Pressure curves reported at 2 different sensor locations inside the hydrogen-air gas cloud for two different grids: 5 cm (black curves) and 10 cm (red curves).

The same degree of agreement is not seen for some of the sensors e.g. sensors on the wall. A surprisingly large error was observed for the sensor K6 affected by recirculation flow in the wake behind the car. The overpressure peak in the sensor K6 was smaller when simulated on the coarser grid, yet it is larger than the experimental one. It is believed that the high simulated overpressure in this sensor is correct and may be an indication of a possible deflagration-to-detonation transition (DDT), which could take place if the experiment had been repeated.

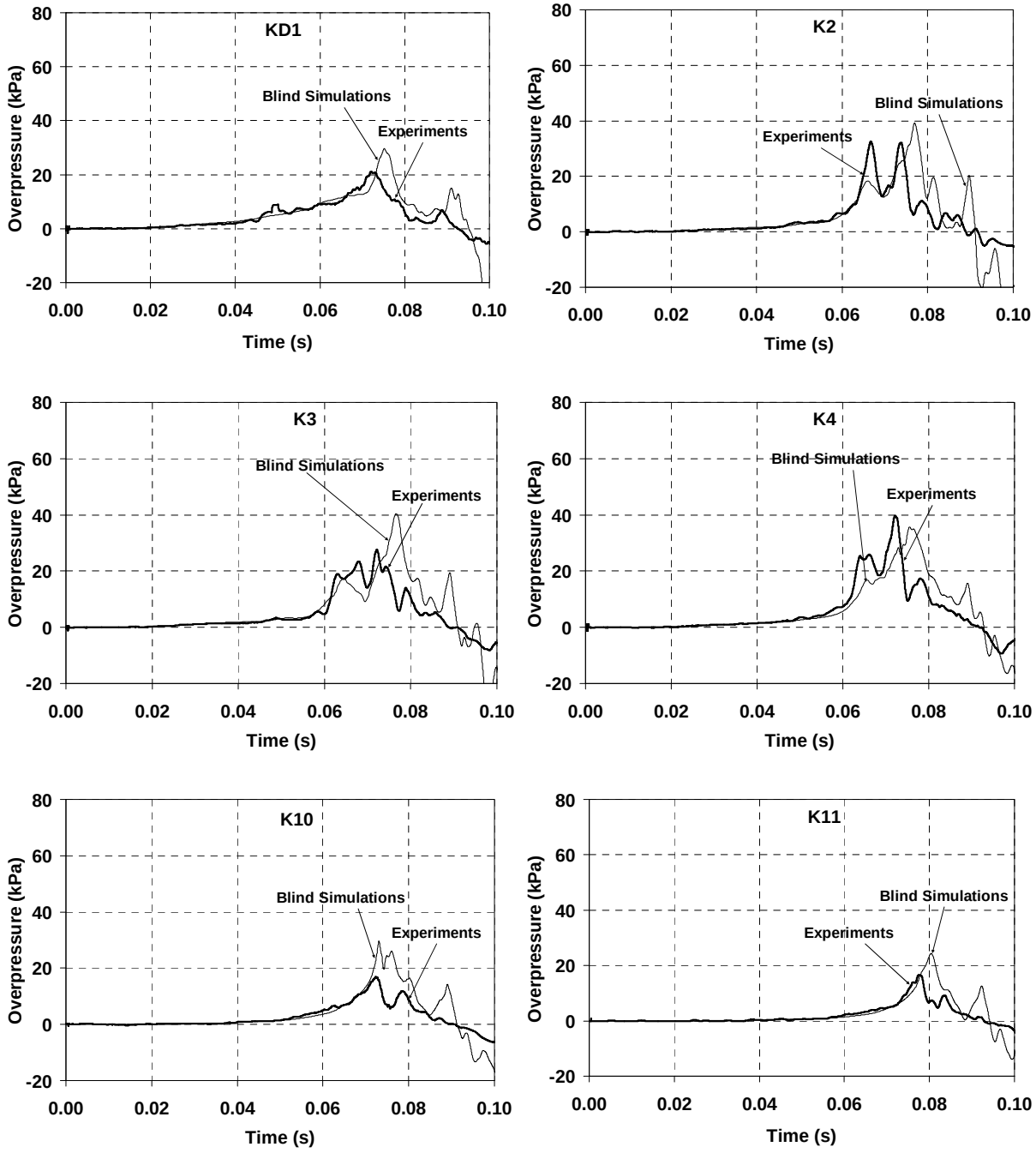

Figure 5.9 – Comparison of experimental and simulated results for various sensors during the simulation of hydrogen explosion in refueling station geometry.

The simulations also indicated that the presence of the gas containment support structure strongly accelerated the flames (Figure 5.7). Sensitivity simulation was performed where this structure was not included, and this gave significantly lower pressures. Similar observations may have been done for balloon experiments (Groethe, Merilo, Colton, et al., 2005) where experiments gave much higher pressure than expected, possibly due to support structure.

In general, the simulations had a reasonable agreement with experimental data. For a blind prediction like this, it was expected that predicted pressure level inside the refueling station (0.2–0.4 barg) would be within ± 30-40 % of the experiment and this was found to be the case. The exact shape of the curves, with multiple peaks and reflections, is difficult to reproduce in

detail because even minor differences in flame path around an object may influence the course of the explosion. However, Figure 5.9 shows a reasonable level of agreement.

For the external pressures, the uncertainty was expected to be larger. In the calculations, it can be seen that a higher overpressure is predicted at sensor 6 (more than 1 barg) than at sensor 5, even if sensor 5 is closer to the explosion. This has to do with possible DDT and that this affected sensor 6 to a greater extent than sensor 5. Since the experiments did not lead to a DDT, over-prediction of blast pressure at sensor 6 as well as sensor 5 was seen. The question however remains open as to whether the predicted high pressures are an indication of physical phenomena (DDT), which may occur in another similar experiment or under slightly modified conditions, or just an artifact of turbulence and/or of turbulent combustion models.

Further, it may be mentioned that blast measurements from other projects has sometimes indicated a significant error in reported experimental blast pressures because pressure waves arrive from an unexpected angle, and get reflected in the sensor. If methods are used that would be vulnerable for pressure waves from other directions, this could lead to errors in the recordings.

Finally it can be mentioned that the scenario with such a large unconfined stoichiometric gas cloud is not considered to be very realistic. However, if turbulence from the jet may influence the initial flame propagation, one can expect very significant flame speeds and overpressures even for much smaller gas clouds.

5.3.2 Explosion Experiments in a congested, repeated pipe grid

In this section, FLACS simulations of H_2 combustion experiments performed by Shell/BP/HSL are described. The experiments were performed at the Dalehead site at the Health and Safety Laboratories at Buxton, England (Royle, Shirvill & Roberts, 2007). The simulations are performed as blind predictions, and no knowledge or indication on the results of the experiments was provided before the simulations were carried out. The experiments also included hydrogen/methane/air mixtures. These have also been used for validation for FLACS for simulating hythane (hydrogen-methane blend) explosions. More details on this are presented in Chapter 8.

The experiment setup is in a highly congested, repeated pipe grid, which is filled with reactive mixtures of either ethylene or hydrogen. The purpose of the simulations was to learn to what extent FLACS can reproduce the type of experiments performed. A total of 16 explosion scenarios have been simulated (8 different gas concentrations and two different congestion levels). Only the results with stoichiometric hydrogen-air mixtures were made available for comparison. The details of the geometry are presented in the next section. Concentrations ranging from an equivalence ratio of 0.8 (lean) to 1.7 (rich) were studied. The details of the geometry and simulation scenarios are described in the following.

The test facility comprised a concrete pad measuring approximately 10 × 10 m inset in a 24 × 18 m tarmac pad. A confining wall was also present to prevent the exposure of the main laboratory to potentially high overpressures. The congestion rig comprises a 3 m (width) × 3 m (depth) × 2 m (height) metal framework, structured so as to consist of eighteen 1 m^3 cubic units. The framework is capable of holding a range of metal grids. For 20 % congestion (area), each grid comprises a number of 26 $\pm$ 1 mm diameter (nominal 1″) bars spaced 125 mm apart. The gates are inserted vertically into the lower layer of cells and horizontally into the upper layer of cells.

In the lower layer, there are seven different lengths of grids. The grids are arranged within the rig so as to form concentric squares around the centre cube. For the experiments, either four or seven concentric squares of grids were used around the central, empty 1 m cube. More details are

available in Royle, Shirvill & Roberts (2007). A snapshot of the geometry is presented in Figure 5.10. The fuel/air mixture in the congestion rig was ignited using an ignition source located at a height of 0.5 m and positioned in the centre of the lower, central cube).

Figure 5.10 – A picture of the congestion rig with plastic film (Royle, Shirvill & Roberts, 2007).

In the top layer of cells, the grids are placed horizontally and are all of the same dimensions. Each grid runs the full length of the frame (3m) and is one cell wide (1 m). Hence three grids are required to fill one complete layer within the upper cells. Either four or seven layers of grids, with alternating layers running North-South and East-West (the bars of the lowest layer) were used for the experiments described in this report. The outside of the metal frame and grid arrangements was covered with a thin plastic film, similar to a cling film. The purpose of the film was to produce a near-airtight cover to the rig to enable it to be filled with a flammable fuel-air mixture. Immediately prior to filling with the flammable mixture, the plastic film was cut with a sharp knife along the corner edges (both side and top). This was done to limit the confinement presented by the film on ignition.

Two types of overpressure sensors were used in the experiments. Brüel & Kjær 8103 hydrophones were used to measure 'lower' overpressures (up to 10 bar) and Kulite ETL-345F-375M Series 40 bara piezo-resistive transducers were used to measure 'higher' overpressures. All the Kulite sensors were positioned at a height of 0.5 m above the ground. Because of the topology, the hydrophone 15 (at 16 m) had to be mounted 1.2 m above the pad and hydrophone 16 (at 32 m) 4.4 m above the pad. The location of the sensors is illustrated in Figure 5.11. Because of the topology, the hydrophone 6 (at 16 m) had to be mounted 1.2 m above the pad and hydrophone 11 (at 32 m) 4.4 m above the pad.

The simulations are done in quiescent conditions with the ambient temperature of 20°C and initial atmospheric pressure of 1 bar. The position of the ignition point was always fixed 0.50 m above ground in the centre of the geometry array. The representation of the geometry in FLACS for both geometrical configurations is presented below. 5 different grid resolutions were considered near the experimental geometry: 2.5 cm, 4 cm, 5 cm, 6.67 cm, and 10 cm. In relation to the cloud size, all these grid sizes should be according to guidelines. In a 1994 FLACS study on grid dependency, recommendations for regular repeated pipe arrays concluded that one should optimally aim for 3–5 grid cells across the pitch between repeated pipes, and grid sizes very similar to the diameter of the repeated objects should be avoided. For a realistic geometry with arbitrary distances between objects, such guidelines are not too relevant, but for the current

case with a very systematic array of pipes they should be followed. Following these guidelines, the 4 cm and 5 cm grids will be the recommended ones.

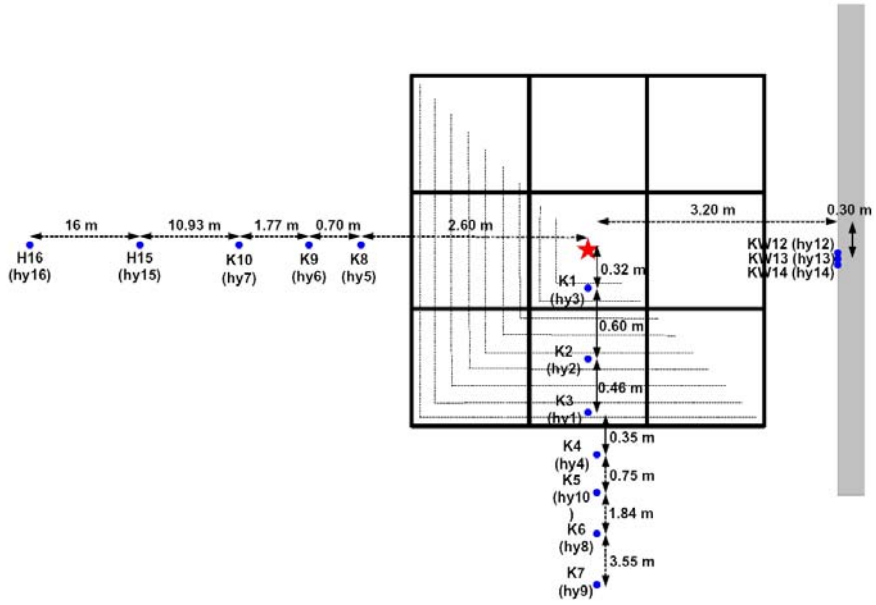

Figure 5.11 – Pressure sensor positions in the congested rig tests (Royle, Shirvill & Roberts, 2007).

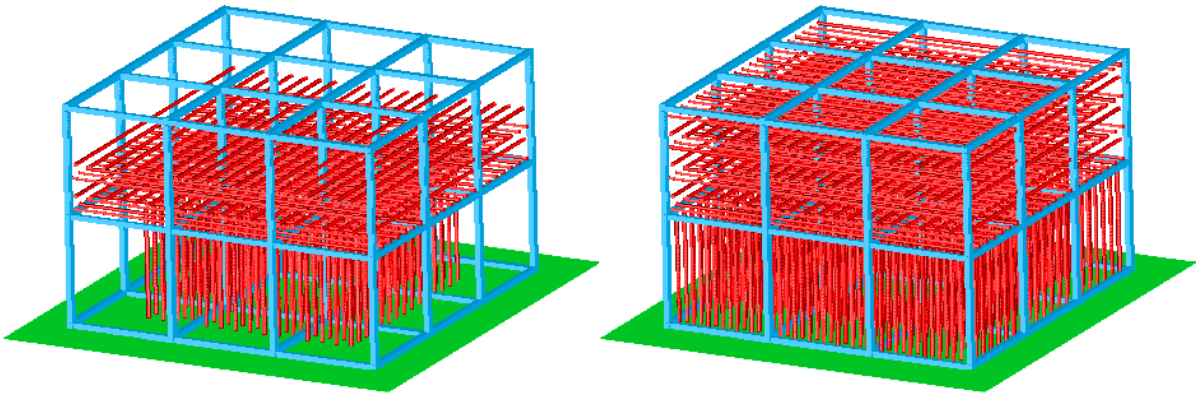

4 pipe rows **7 pipe rows**

Figure 5.12 – 3D views in CASD of the congested grid geometry for the congested grid geometry.

A quick grid sensitivity study revealed that the 4 cm and the 5 cm grid resolution were found to give almost identical results, but the 4 cm grid was computationally more expensive. Hence, all simulations were carried out using a grid resolution of 5 cm. Slightly lower pressures were found using the coarser grids, and for the 2.5 cm grid (same as pipe diameter) a factor of 2 lower pressures were seen (expected due to some problems generating sufficient turbulence behind objects of exactly 1 grid cell size).

The grid was stretched away from the geometry until the boundary to improve computational efficiency except in the –X direction where the uniform grid was maintained. This was due to the fact that most of the external pressure sensors are placed in that direction. In total, the simulation

domain contained a little more than 1 million control volumes. The calculations are carried out on standard 1 CPU PCs (typically 2-3 GHz) with 512-2048 Mb RAM running Linux operating system. Simulation time on single CPUs is a few hours.

The simulation results for the explosion simulations in both geometries are presented next. It was seen that, in general, much higher pressures are observed for the 7-pipe row configuration (as expected). In particular, the maximum pressure recorded for the 4-pipe row geometry is 1.8 barg, while the maximum pressure for the 7-pipe row geometry is 6.0 barg (at or near the corner of the congested rig in both cases). Also, for the sensor closest to the ignition point, the maximum observed pressures are 1.2 and 3.0 barg respectively for the 4-pipe and 7-pipe row geometries. The difference is not that large far away from the ignition point (0.8 and 1.2 barg respectively). Similar results are observed for other concentrations, in the sense that pressures in the 7-pipe row geometry are considerably higher in general. Also, slightly lean concentrations (ER = 0.9) mixtures are found to have the highest pressures for hydrogen. In most cases, it is found to be higher than stoichiometric mixtures as well. In particular, the maximum observed pressure was 2.1 barg for the 4-row geometry (ER 0.9) and 7.1 barg for the 7-row geometry (ER 0.9). The pressures are found to be lower for richer mixtures. The observed pressures for richer mixtures (ER 1.2 to 1.7) are found to be fairly close to each other.

The pressure development through the simulation domain is presented in greater detail in the following figure. Figure 5.13 depicts the maximum pressure at all times inside and outside the experimental geometry for both the geometries at all times at two different vertical locations for the stoichiometric concentration. One of the vertical locations is the ground level while the other is chosen on the upper grid. The overpressures on a vertical plane near the perimeter of the geometry are also shown.

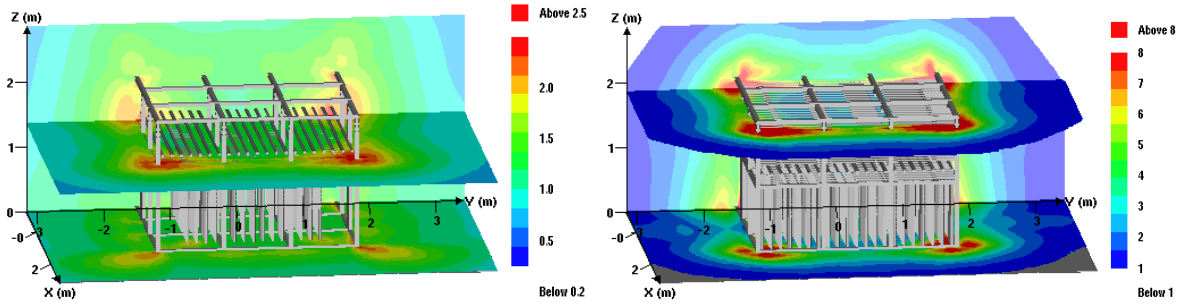

4 pipe rows **7 pipe rows**

Figure 5.13 – The maximum pressure observed in the entire simulation domain for the congested repeated pipe geometry (ER = 1.0) for both geometries.

It can be seen that, in general, the highest pressures are seen near the corners of the cubical grid for both geometrical configurations. This is found to be true for all concentrations. Also, for the 4-pipe row geometry, much higher pressures are seen at the upper level than the ground level. For the 7-pipe row geometry, the pressures at the ground level are somewhat higher. It can be seen that very high pressures are seen in this case near the corners (greater than 8 barg). Also, as seen from the pressure traces, the overpressures are higher for leaner mixtures as compared to the stoichiometric mixture.

Figure 5.14 presents a comparison of the simulation results with the experimental data. Two plots are shown where the pressure levels are plotted on sensors parallel to the wall as a function of the distance from the ignition point in the first plot and on sensors perpendicular to the wall as a function of the distance from the wall in the second one. It can be seen that the pressure levels in the explosion are well reproduced for most sensors. Significant pressures were seen at when the flame exited the pipe array (possibly due to deflagration-to-detonation transition DDT which was

indeed seen in the experiments). Also the simulation gave high pressures at the edge of the pipe-array, but the observed local pressure increase at the sensor array parallel to the wall was not seen. The second plot in Figure 5.14 shows the pressure decay up to 16 m away from the wall. The FLACS simulations predicted somewhat higher pressures than seen in the experiments close to the wall, but the far-field sensors show reasonably good agreement. It may therefore be concluded that the experiments are reproduced reasonably well with FLACS.

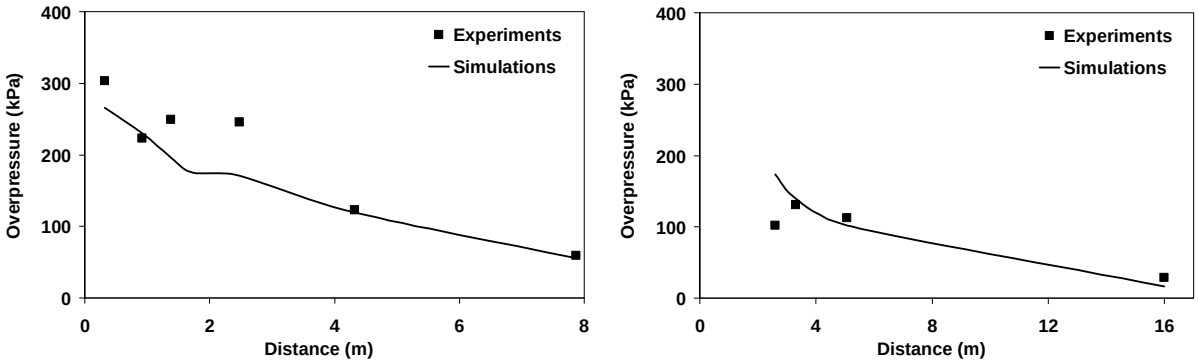

Measurements parallel to wall **Measurements perpendicular to wall**

Figure 5.14 – Comparison of experimental overpressures with simulation results for the congested rig experiments.

5.3.3 Hydrogen explosions in a simulated traffic tunnel

In case of release in a tunnel, hydrogen will be trapped inside the tunnel for a longer time, increasing the probability of ignition. Moreover in case of ignition, the strength of the explosion is enhanced compared to an unconfined case because the magnitude of the overpressure depends strongly on the degree of confinement. As shown in hydrogen explosion experiments, 1 kg of hydrogen at stoichiometric ratio can generate an overpressure peak of about 150 kPa in a tunnel environment (Groethe, Merilo, Colton, et al., 2007) while a maximum overpressure of 10 kPa was recorded in an equivalent experiment with 1 kg of hydrogen in an unconfined set-up (Sato, Iwabuchi, Groethe, et al., 2006). Therefore hydrogen accidents in a tunnel environment can potentially generate critical situations in term of damages. The prediction of the consequences of hydrogen explosions is important in order to ensure the safety of installations where such explosions can occur. The assessment of explosion hazards of the flammable mixture in tunnels is instrumental in order to reach a level of safety/risk that is socially acceptable. This study seeks to assess the prediction capabilities of FLACS for describing gas explosions in tunnels by comparison with the experiments. Other modellers have taken part in this exercise and an inter-comparison between the simulations and experiments is published in International Journal of Hydrogen Energy (Baraldi, Kotchourko, Lelyakin, Yanez, Middha, Hansen, et al., 2009). This study is also valuable as it forms a basis for the very extensive study that is carried out for describing the risk of hydrogen vehicles in tunnels as a part of the HyTunnel project under the network of excellence HySafe. This is described in Chapter 8.

The experimental set-up consisted of a 78.5 m long tunnel with a diameter of 2.4 m and a cross-sectional area of 3.74 m^2. The experimental facility was a one-fifth scale mock-up of a typical tunnel for road transport. The explosive hydrogen-air mixture was located in a 10 m long region between two sheets of high-density polyethylene in the middle of the tunnel, filling a volume equal to 37 m^3. Several experiments were carried out, using different hydrogen concentration. For the purpose of the simulation exercise described in this section, the experiments with 30 % hydrogen volumetric concentration in air have been considered. For the 30 % hydrogen

concentration, two different geometrical set-ups were prepared: a completely empty tunnel and a tunnel with 4 vehicle models on the floor centreline inside the hydrogen-air mixture. The latter experimental configuration is shown in Figure 5.15. The vehicle models measured 0.94 m in length, 0.362 m in width and 0.343 m in height, representing typical real-vehicles at one-fifth scale. The distance between vehicles was 1.52 m. The blockage ratio due to the presence of the vehicles was 0.03. Pressure transducers were mounted on the side wall of the tunnel along its entire length. The ignition position was located in the middle of the tunnel for all experiments.

The overpressures that were generated by the deflagrations were nearly constant along the length of the tunnel. The deflagration in the empty tunnel with 30 % hydrogen concentration generated a peak pressure of about 1.50 bar. The presence of the vehicles/obstacles did not increase significantly the strength of the explosion and the overpressures were only slightly higher compared to the case without vehicles. It must be emphasized that those result are partly expected, since the blockage ratio (0.03) is very small.

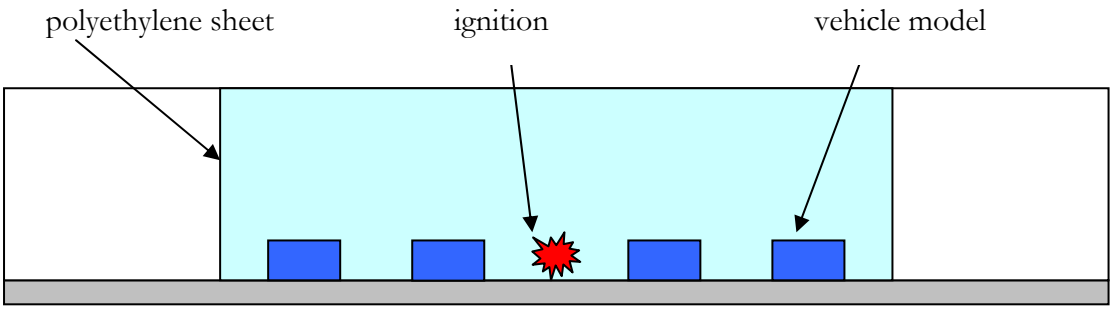

Figure 5.15 – Experimental configuration in the central part of the tunnel where the hydrogen-air mixture (in light blue), the four vehicle models and the ignition position are located.

Four sensors in the experiments have been selected in representative positions for the propagation of the blast wave along the tunnel for the comparison between the experimental data and the simulation results among all the available pressure transducers along the side wall of the tunnel. The first two sensors are located within the hydrogen flammable cloud, being at 1 m and 3.61 m distance from the ignition location. The two other sensors are located outside the flammable cloud at 10.61 m and at 30.4 m from ignition. The last sensor is located at about 9 meters from the exit of the tunnel.

A structured Cartesian grid was used. The grid resolution was 5 cm, and the total number of cells was approximately 375000. The grid was extended outside the tunnel in order to represent the external flow. The simulations were carried out on a 3.0 GHz dual-core Linux PC. The CPU time was about 3 hours.

In Figure 5.16, the comparison of the overpressure history between experiments and simulations is shown for the case with vehicles in the tunnel for a hydrogen concentration of 30 %. The level of agreement for the overpressure peaks is quite satisfactory, with an accuracy that is well within 20 %. The results also agree well with the experimental data in terms of pressure dynamics. Simulations for a 20 % hydrogen cloud were also carried out. In this case, a pressure level of the order of 0.5 barg is predicted. The shape of the pressure traces indicated significantly slower flames. However, the simulated pressure values for the 20 % case are somewhat higher compared to those seen in experiments (the results are presented in Figure 5.17).

The comparison between experimental data and simulation results for the tunnel without cars is similar to the case with obstacles in the tunnel. The errors in all simulation results are within a range of 15 % which is within the range of experimental uncertainty. In this case, the pressure

level is found to be very similar to the obstacle case (this should be expected as the BR is very small and there are only 4 obstacles). These results are not shown here for brevity.

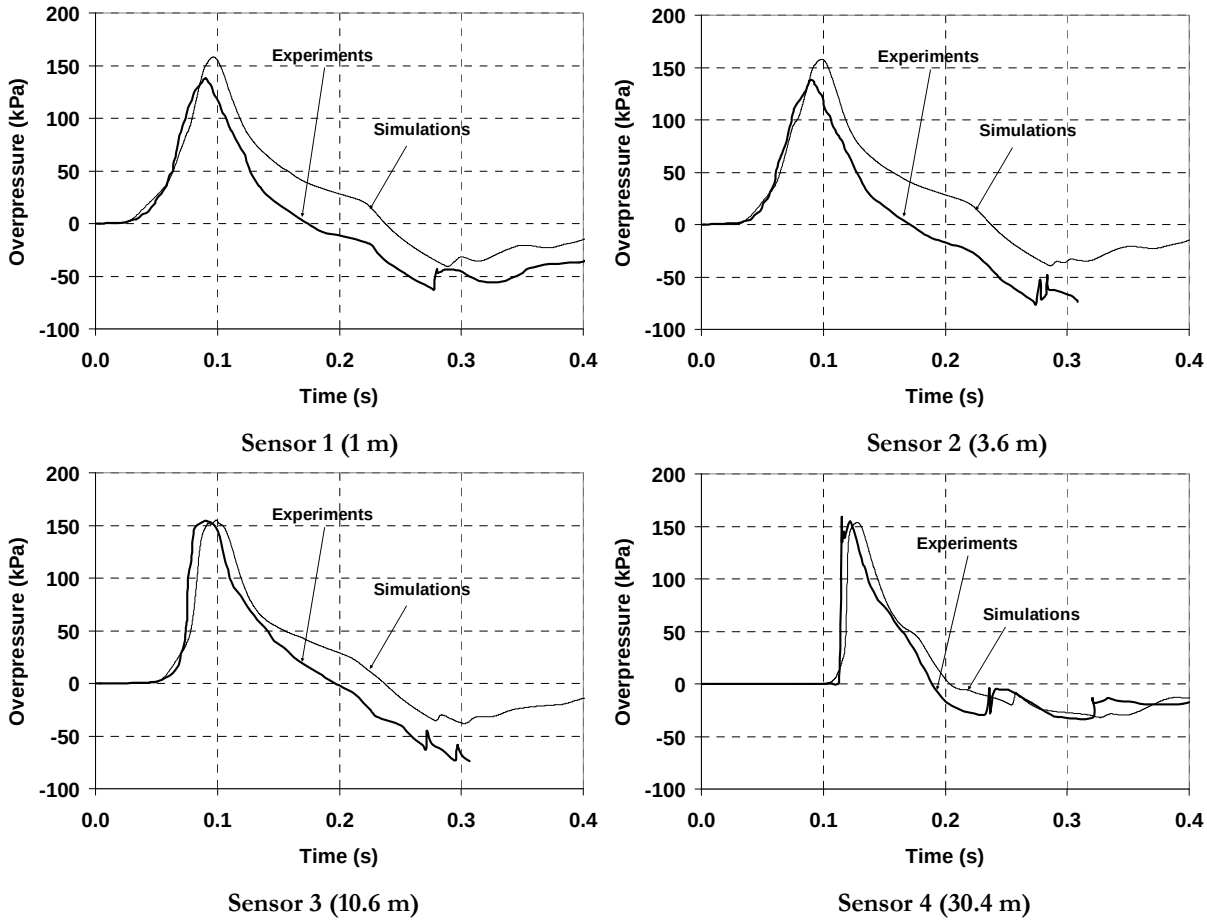

Figure 5.16 – Comparison of simulated and observed overpressure as a function of time for the 30 % hydrogen scenario (tunnel with cars).

Although the geometrical layout is simple, the physical mechanisms involved in the ignition and acceleration of the flame are quite complex. After ignition the flame travels in the laminar regime where the propagation mechanism is based on the molecular diffusive transport of mass and energy. During the initial acceleration stages, the flame enters into the turbulent propagation regime. The polyethylene sheets are broken by the overpressure generated by the explosion. The contact surface between the hydrogen and air that is initially located at 5 m from the central ignition position is moved forward by the gas flow generated by the propagating flame in front of the flame itself. Because of that phenomenon, the flame will carry on burning beyond the initial edge of the flammable hydrogen cloud. Due also to this effect, the flame and the combustion products reach the ends of the tunnel that are located at 39 m from the ignition position and at 34 m from the initial position of the hydrogen-air contact surface. After the early stages of propagation, the strength of the blast wave is almost constant along the whole length of the tunnel while it decays rapidly as soon as the blast wave exits from the tunnel because of the strong expansion.

The simulations are capable of capturing the maximum overpressures. Both in the case without obstacles and in the case with obstacles, the maximum of the blast wave increases with the distance from ignition point in the early stages of propagation. Moreover the shape of blast wave profile changes also with the distance, showing a progressive steepening of the leading edge. Both

those behaviours are well captured by the simulations. Although the quantitative agreement between the experimental data and the simulation results for the overpressure peaks is good, a tendency of a slight over-prediction is recorded for the first three sensor positions, while some slight under-prediction appears for the sensor close to the tunnel exit. Another remarkable point of agreement between the experiments and the simulations is the arrival time of the blast wave that travels with the speed of sound of the medium in which it is propagating. Initially the blast wave travels in the 30 % hydrogen-air mixture and subsequently in air. The simulations are capable of mimicking the propagation of the blast wave with the correct speed. The simulation error for the pressure peaks is within 20 % and this can be considered a quite satisfactory result overall.

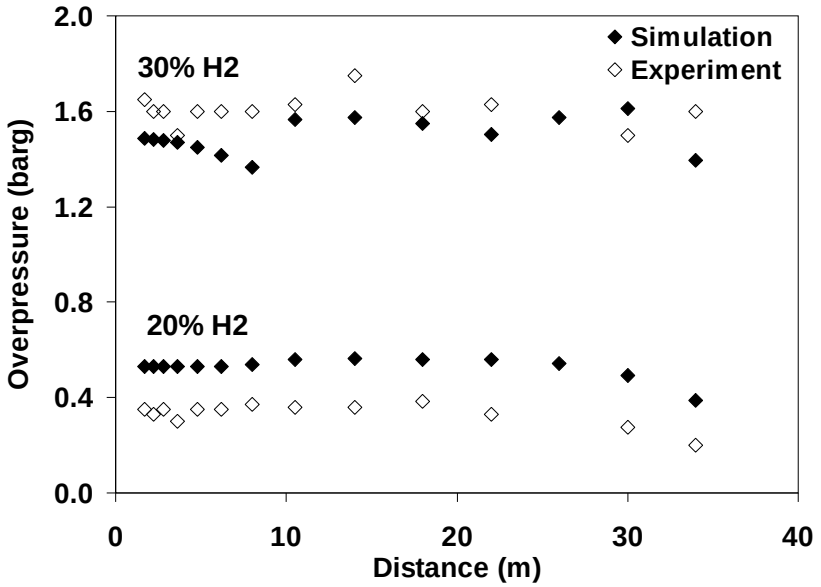

Figure 5.17 – Comparison of simulated and observed overpressure as a function of distance for the tunnel with obstacles for both concentrations.

Although the maximum overpressure is captured with a good level of accuracy at time $t \sim 0.09$ s, after that time the simulation results start to depart progressively from the experimental profile. At time $t = 0.2$ s the pressure difference between the experimental and the calculated value is in the 0.25–0.40 bar range. It is well known that heat losses have the effect of decreasing the overpressures and that this effect increases with time. In order to model very fast phenomena such as detonations, the effect of the heat losses can usually be neglected. For relatively slower phenomena such as deflagrations, their effect becomes more relevant. Since the heat loss models were not included in the simulations, this is a possible explanation for this discrepancy.

Thus, a relevant finding in the analysis of the comparison of simulation results and experimental data is that the simulations are capable of capturing the correct value of the pressure peaks, the correct time of arrival of the blast wave and therefore the correct speed of propagation of the blast wave. However, it must be kept into account that the simulations were performed with full knowledge of experimental results. Nevertheless, the simulation results show that FLACS is capable of describing the hydrogen combustion in a tunnel environment, given similar initial conditions in term of tunnel congestion and mixture composition to those in the experiments. Future validation investigations need to include other typical conditions and features of road tunnel such as a higher level of traffic congestion and a ventilation system. These have been performed to some extent as a part of the HyTunnel project and are described in Chapter 9.

5.4 Final Remarks

Validation of the CFD tool is one of the most critical requirements for its use in QRA studies. The gas explosion modules in FLACS have been evaluated with data from hundreds of gas explosion experiments in the laboratory and in the field (Hansen, Storvik & van Wingerden, 1999). With increasing interest in hydrogen safety in recent years, a strong effort has been made to learn more about hydrogen dispersion and explosions and improve FLACS in that area. This chapter summarizes the extensive validation work that has been carried out for simulation of hydrogen explosions during the course of this study. Such studies have also included "blind" benchmarks where the results of the experiments were unknown before carrying out of simulations of the suggested scenario. Modelling results are compared to experimental data, and in general, reasonable agreement is seen for many different kinds of geometries and conditions. However, it must be kept in mind that modelling hydrogen explosion (and dispersion) is very complex and some discrepancies can be expected in certain cases, even if more and more scenarios are modelled accurately. It is extremely important to represent the geometry and scenario as accurately as possible to get the best possible results.

6 Combined Dispersion/Explosion Simulations: Validation against Experimental Data

Computational Fluid Dynamics (CFD) tools have been increasingly employed for carrying out quantitative risk assessment (QRA) calculations in the process industry. However, these tools must be validated against representative experimental data in order to have a real predictive capability (with studies on variations of various important parameters that may affect explosion loads and hence risk). Nonetheless, when CFD consequence prediction tools are validated, there is a significant focus on basic situations, like free jet releases for dispersion, or pre-mixed homogeneous gas mixtures for explosions. It must be pointed out that the typical accident scenario is usually more complicated, possibly involving time varying releases impinging on equipment, with delayed ignition of a non-homogenous and possibly turbulent mixture. When aiming for increased precision in risk assessment methods there is a need to validate consequence tools for this added complexity. For post-accident simulations, it is obvious that there is a need to reproduce the complex physics of the accident scenario, and validation of tools for the combined release and ignition scenarios is important. For the modelling of such a situation, validation or verification against idealized scenarios is far from sufficient. A very important cause of this gap in "real" validation of CFD tools is that it is challenging to perform good experiments with such a complexity. Good experimental data involving scenarios reminiscent of those seen in real situations are few and far between, especially at large scales. Even for hydrocarbons, there are only a very few such experiments available, the most notable being the Phase3B experiments carried out at Spadeadam test site in north-west England.

For that reason, the recent experiments performed by FZK are important (Friedrich, Grune, Kotchourko, Kotchourko, Sempert, Stern & Kuznetsov, 2007). These involved vertically upwards hydrogen releases with different release rates and velocities impinging on a plate in two different geometrical configurations. The dispersed cloud was subsequently ignited and pressures recorded. These experiments provided the possibility to compare the performance of FLACS against a "realistic" situation. This work is described in:

Paper 8: CFD calculations of gas leak dispersion and subsequent gas explosions: Validation against ignited impinging hydrogen jet experiments

This work is published in the proceedings of the 2nd Intl. Conference of Hydrogen Safety, San Sebastian, Spain, September 11-13, 2007 and published in the Journal of Hazardous Materials (Middha, Hansen, Grune & Kotchourko, 2010). Further details of the work carried out are available elsewhere (Middha & Hansen, 2005; Hansen & Middha, 2007). This work involved blind CFD simulations to predict the outcome of the proposed experiments, and if possible, to help the planning. After the experiments were reported, the quality of the blind predictions was evaluated.

The simulated gas concentrations are found to correlate reasonably well with observations. The overpressures subsequent to ignition obtained in the blind predictions could not be compared directly as the ignition points chosen in the experiments were somewhat different from those used in the blind simulations, but the pressure levels were similar. Simulations carried out subsequently with the same ignition position as those in the experiments compared reasonably well with the observations. These experiments are important for corroborating the underlying physics of any large-scale safety study. This type of experiments also provides a possibility to validate important assumptions used in probabilistic quantitative risk assessments, which are necessary to limit number of scenarios studied (e.g. equivalent stoichiometric cloud size methods). Such calculations are performed and are presented in the chapter on Risk Analysis.

It seems justified to conclude that the results reported in this paper gives further support to the view that available advanced CFD tools are in fact able to simulate combined scenarios of release of combustible gas, entrainment by air, and subsequent gas explosion. Validation of the computational tools against good experiments is crucial. Published experimental data from experiments of the kind conducted by FZK are very scarce, and therefore the availability of these data in the present investigation was decisive. However, the scale of the FZK experiments is comparatively small in relation to large industrial scales, and the resulting explosions correspondingly less severe. Hence, any future possibility of validating advanced computational tools like FLACS against results from this type of combined experiments in lager scales should indeed be welcomed.

7 Predicting Deflagration to Detonation Transition (DDT) with FLACS

7.1 Introduction

It is well-known that deflagration to detonation transition (DDT) may be a significant threat for hydrogen explosions. Due to the high reactivity of hydrogen, DDT is likely in a variety of scenarios involving H_2-air mixtures and result in large-scale damage. The situation is exacerbated in the presence of obstacles, which induce turbulence that accelerates flames to a high speed. This rapid turbulent flame acceleration can lead to DDT when sufficiently intense turbulent mixing is achieved at the reaction zone. The determination of the conditions for the transition from deflagration to detonation has been a subject of several studies for hydrogen explosion safety. Also, considerations of mixture sensitivity and geometric dimensions are important as a stable detonation front will only be formed if the concentration lies within the detonability limit and the geometric dimensions exceed the detonation cell size. Even if it is possible to initiate detonation directly, this is not a cause of worry for typical safety applications as explosions normally start as a result of weak ignition sources e.g. an electrical spark. Under certain conditions, the flame can accelerate and undergo a transition to detonation. The flame acceleration phenomenon is separate from the actual initiation of detonation and is equally important to study.

Transition to detonation can occur in a variety of situations, many of which are commonly employed in industrial settings. These include flame propagation in smooth tubes or channels (e.g. Urtiew & Oppenheim, 1966), flame acceleration as a result of repeated obstacles (e.g. Peraldi, Knystautas & Lee, 1986), and jet ignition (e.g. Knystautas, Lee & Wagner, 1979). This is a common problem in industrial process piping as it is typically designed to withstand only moderate over-pressurization (due to cost reasons) and catastrophic failure is mitigated by the use of venting devices. However, these devices are insufficient to limit the rapid pressure rise from a fast flame and/or detonation and therefore, it is important to understand and avoid the conditions for a transition to detonation. A common feature of any future "hydrogen economy" will be a hydrogen filling station. If a significant hydrogen release were to occur, it could form an explosive hydrogen-air mixture. The possibility of a transition to detonation upon ignition must be accounted for when planning for the location of the filling station in relation to other facilities and buildings. Further, the actual design of the storage facility and handling procedures all require the issue of DDT to be understood in a quantitative manner. The nuclear industry has also been very interested in these investigations as the consequences from nuclear accidents are global as opposed to offshore oil exploration accidents, and it is very important to keep confinement in case of a hydrogen explosion. In particular, during the Three Mile Island accident, there was a partial meltdown of the reactor core resulting in the production and release of a large amount of hydrogen gas into the containment building (Henrie & Postma, 1983). During the accident, the combustion of the hydrogen resulted in several pressure spikes but the pressure rise was fortunately not large enough to compromise the integrity of the containment. Thankfully, a transition to detonation (DDT) did not occur in this case but this accident led many countries with nuclear power plants to initiate extensive research programs investigating hydrogen detonation related phenomena.

Transition to detonation in an explosive mixture has been studied for more than 65 years to obtain a qualitative and quantitative understanding of the phenomenon (e.g. Lee & Moen, 1979; Lee, Soloukhin & Oppenheim, 1969). It is very challenging to fully understand the phenomena behind high-speed turbulent deflagrations and the transition to detonation (Shepherd & Lee,

1992). There have been several experimental studies in recent years. Some of them have been basic studies of high-speed turbulent flame propagation in detonation tubes (e.g. Chao & Lee, 2003; Lee, Knystautas & Freiman, 1984, etc.). The goal of these studies is to show that the maximum steady-state turbulent flame speed that can be achieved in the experiments depends only on the properties of the mixture and is governed only by the chemical kinetics and energetics. A transition to detonation (or quasi-detonation since losses may result in a speed less than the CJ velocity) can occur for more "sensitive" mixtures. These speeds can then form a basis for the development of models for understanding DDT. Other studies have focused on the development of necessary criteria for "effective flame acceleration". These have examined the effect of basic flame parameters (expansion ratio, Lewis number, Zeldovich number, etc.) and geometry (tube diameter, blockage ratio, etc.) on the possible development of fast combustion regimes that can eventually transition to a detonation. These have mostly been performed by Dorofeev and coworkers in this decade (Dorofeev, Sidorov, et al., 2000; Dorofeev, Kuznetsov, et al., 2001; Kuznetsov, Alekseev, Matsukov, & Dorofeev, 2005; etc.). Several other large-scale tests in a congested area have been carried out to simulate the conditions of a process facility. These tests are often not directly useful for the development of models as detailed measurements of e.g. turbulence parameters is not carried out.

There are several different mechanisms that have been propounded to explain the DDT phenomenon. In the CJ theory, the detonation wave is treated as a discontinuity with infinite reaction rate. Based on this one dimensional theory, it is possible to calculate detonation velocity, pressure, etc. if the composition of the gas mixture is known. The values calculated from this simple theory agree surprisingly well with observations. Therefore, a detonation front was initially thought to be one dimensional and the 3D structure was discovered only later. However, understanding the actual mechanisms for the formation of the detonation wave is much more complex. The widely prevailing "Gas Dynamic" explanation for DDT is essentially one-dimensional wherein the volume expansion of hot burned gases move into the unburned gas and generate shock waves. These shock waves preheat the unburned mixture, thus increasing the burning rate and forming further shock waves. The resultant shock fronts can merge into a wave that is strong enough to cause a local explosion that transforms into a steady detonation (Sherman, Tieszen & Benedick, 1989). Under this scenario, the study of the flame acceleration leading to the development of the "right" conditions leading up to detonation initiation is as important as the actual onset of the detonation event. Oppenheim (1970) have shown an additional mechanism to be prevalent in many cases wherein the transition begins with a local explosion in a region of high turbulence, even though the compression heating of the unburned gas due to shock waves is not sufficient. The interactions of flame with the wall have also been found to be important. Lee, Knystautas & Yoshikawa (1978) have propounded the shock-wave amplification by the coherent energy release (SWACER) mechanism where induction time gradients associated with temperature and pressure gradients in the system produce a compression wave that can gradually get amplified into a strong shock wave. This shock wave can auto-ignite the mixture and produce DDT. Instabilities near the flame front as well as interaction between the flame and another flame, a shock wave or a secondary explosion (local quenching and then re-ignition), may also lead to DDT. Further details and a fairly exhaustive list of references for the mechanisms involved in DDT can be found in Breitung et al. (2000) and Ciccarelli & Dorofeev (2008).

Although there has been a strong debate on the mechanisms underlying the transition to detonation and it is still an active research area, there is no doubt that it is very important to study this phenomenon from a process safety perspective. Detailed description of all processes following ignition that may lead to DDT is extremely challenging. This is due to a complicated interaction of compressible flow, chemical reaction, and turbulence that needs to be described at very high spatial and temporal resolution. Therefore, much theoretical effort has been focused on

development of criteria for DDT (Breitung, et al., 2000). As described above, researchers have tried to establish the initial and boundary conditions, and geometric and process parameters under which a transition to detonation can be expected. However, these criteria and scaling arguments are difficult to apply in a process setting where exact numerical results are much more valuable.

With the advance in scientific computing, research on DDT has been shifted toward the use of computational approaches. Numerical simulations can be a powerful tool to obtain detailed analyses of the underlying phenomena and can provide a picture of the basic DDT process from flame ignition, acceleration and transition to detonation. Before the beginning of this work, the standard versions of FLACS could only handle the deflagration mode of combustion, in which the flame propagates because hot flame products heat and ignite the unburned gas ahead. In situations with very fast flames and/or very strong pressure waves a deflagration to detonation transition (DDT) may change the propagation mode so that shockwaves will ignite unburned gas and lead to faster flame propagation (1500–2000 m/s). In this work, the use of FLACS to simulate hydrogen explosions in different geometries and get indications about the likelihood of DDT is described. The study of this phenomenon is very critical as the overpressures in detonation front can cause losses which are much more severe as compared to those seen with blast waves produced by a deflagration. Therefore, efforts have been carried out to extend FLACS in this area.

The work carried out is described in two papers:

Paper 9: Prediction of Deflagration to Detonation Transition (DDT) in hydrogen explosions

This paper (Middha, Hansen & Storvik, 2006) is published in the Proceedings of the 40th Annual Loss Prevention Symposium. This work studied scenarios reported in literature where high-speed deflagrations transition to detonation and implemented the first models in FLACS to predict DDT. The main goal was to carry out hydrogen explosion simulations in various practical scenarios. FLACS explosion simulations were performed for four different scenarios reported in recent literature. Numerical simulations in diverse geometries showed that FLACS is able to indicate the areas where detonations have been observed in experiments. In general, the simulations are able to predict detonation pressures, run-up distances, and speeds reasonably well. The following geometries were used: (a) Sandia FLAME facility (Sherman, Tieszen & Bendick, 1989), (b) McGill Detonation Tubes (Peraldi, Knystautas & Lee, 1986), (c) FZK/Kurchatov Institute Smooth Tube (Kuzentsov, Alekseev, Matsukov & Dorofeev, 2005) and (d) KOPER facility (Dorofeev, Bezmelnitsin & Sidorov, 1995).

Some details and justification of the methodology that has been developed are provided below:

The DDT phenomena can be usually divided into two separate phases (Lee & Moen, 1980; Shepherd & Lee, 1992): (1) the creation of conditions for the onset of detonation by processes of flame acceleration, mixing of products and reactants, etc. and (2) the actual formation of the detonation wave itself or the onset of detonation. Processes in the first phase are particular to the specific initial and boundary conditions of the problem. Different physical mechanisms dominate the process of flame acceleration in obstructed channels, smooth tubes or large volumes filled with combustible mixtures. However, the actual formation of the detonation appears to be a more universal phenomenon and the basic structure of the detonation front is well known. The methodology used is based on this underlying structure of a detonation front. The structures of deflagration and detonation waves are contrasted in Figure 7.1 (James, 2001; Nicholls, 1998). In a detonation, a high pressure shock front travels only about 1 to 10 mm ahead of the reaction zone / flame (in a fast deflagration, the reaction zone lags much further behind the shock front). Therefore, for all practical purposes, it can be assumed that the flame and pressure front travel together. Early work by Bone (1931) has also indicated that a shock wave, independently started,

should precede the flame and observed that, as the accelerated flame front caught up with the shock wave, detonation set in ahead of the flame.

Based on the discussion above, the likelihood of DDT is illustrated in terms of a parameter proportional to the spatial pressure gradient across the flame front (Tegnér & Sjögreen, 2002; Lee & Moen, 1980). This parameter is able to visualize when the flame front captures the pressure front, which is the case in situations when fast deflagrations transition to detonation. It is proposed that the presence of these spatial pressure gradients represents the indication of a possibility of the deflagration front transiting to detonation.

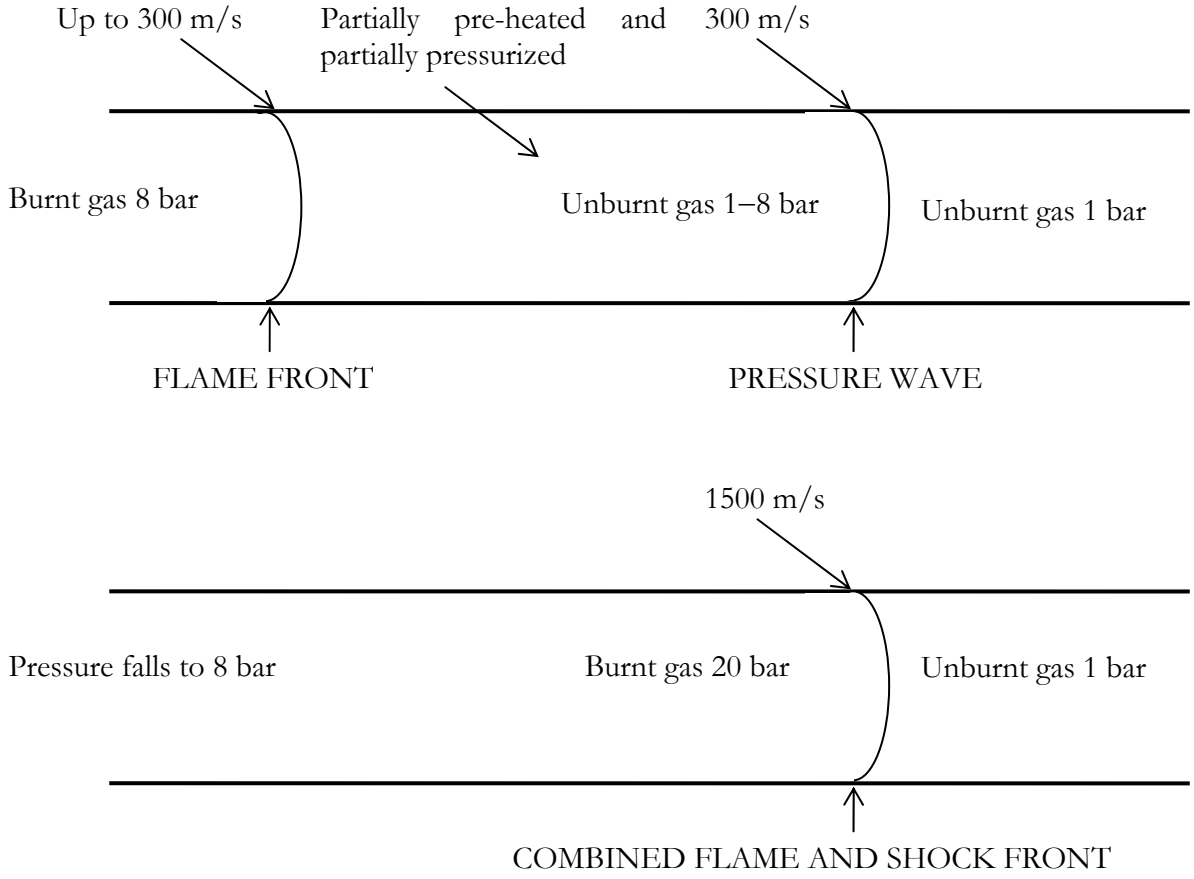

Figure 7.1 – A schematic diagram showing the underlying structure of a detonation front.

However, it should be pointed out that this approach was still in its nascent stage when this work was presented. The methodology needed careful study in terms of the role of flame thickness, geometry, and process parameters on the magnitudes of these gradients and the impact on actual DDT likelihood. As a part of this work, the parameter spatial pressure gradient (dP/dx) described above has been normalized. The dimensionless spatial pressure gradient can be expressed as:

$$\left.\frac{dP}{dx}\right|_{normalized} = \left.\frac{dP}{dx}\right|_{actual} \frac{X_{CV}}{P_0} \tag{7.1}$$

where P_0 is the initial pressure and X_{CV} represents the grid resolution. It is proposed that a magnitude of the pressure gradients of order 1 indicates that DDT is likely, with values around 10 or larger indicate strong possibility of DDT. One consequence of this normalization is that the values of normalized pressure gradient will decrease if we have very fine grid, but this is not

the case in general for large-scale situations. The parameter has also been related to detonation cell sizes in a more thorough manner. This work is described in:

Paper 10: Predicting Deflagration to Detonation transition in hydrogen explosions

This paper has been published in the journal Process Safety Progress (Middha & Hansen, 2008). In previous work described in **Paper 9**, FLACS was extended to identify whether DDT is likely in a given scenario and indicate the regions where it might occur. The likelihood of DDT has been expressed in terms of spatial pressure gradients across the flame front. This parameter is able to visualize when the flame front captures the pressure front, which is the case in situations when fast deflagrations transition to detonation. Reasonable agreement was obtained with experimental observations in terms of explosion pressures, transition times, and flame speeds. The DDT model was extended as a part of this work to develop a more meaningful criterion for estimating the likelihood of DDT by comparison of the geometric dimensions with the detonation cell size. This article discussed the new models to predict DDT, and compared predictions with relevant experiments. One of the experiments that have received attention as a part of this work is the jet-ignited hydrogen explosion experiments in a partial confinement (Pförtner & Schneider, 1984). The simulation details and comparison with experimental data for this study are also described in a presentation at the 12th International Loss Prevention Symposium in Edinburgh (Middha, Hansen & Schneider, 2007).

7.2 Shock Ignition Model

A "shock-ignition model" has also been implemented in FLACS as a part of this work in order to represent a detonation front. This has been implemented by modeling ignition ahead of the merged shock-flame front (based on the criteria described above). The ignition is implemented by artificially increasing the burning rate in the grid cells ahead of the flame front. Some limited testing of this shock ignition model has been carried out in the RUT facility geometry (Dorofeev, Sidorov, Breitung & Kotchourko, 1997). The schematic of the geometry used is shown in Figure 7.2.

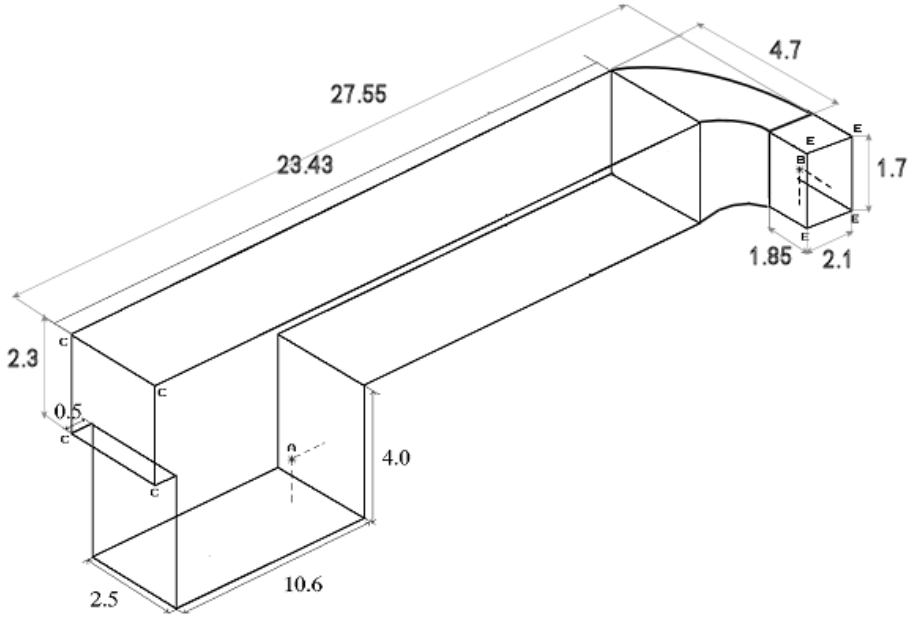

Figure 7.2 – Schematic of the RUT facility.

Figure 7.3 shows the flame front and the pressure front during the simulations. Figure 7.4 shows the propagation of flame front as a function of time. Each sensor point is 1 m apart and it can be seen that a constant velocity (equal to approximately 1800 m/s) is achieved. The maximum overpressures achieved in this case are around 15 bar. These values are in reasonably good agreement with the theoretical C-J values. However, this model is still at an initial stage and there is a need to develop this model needs further and validate it against available experimental data.

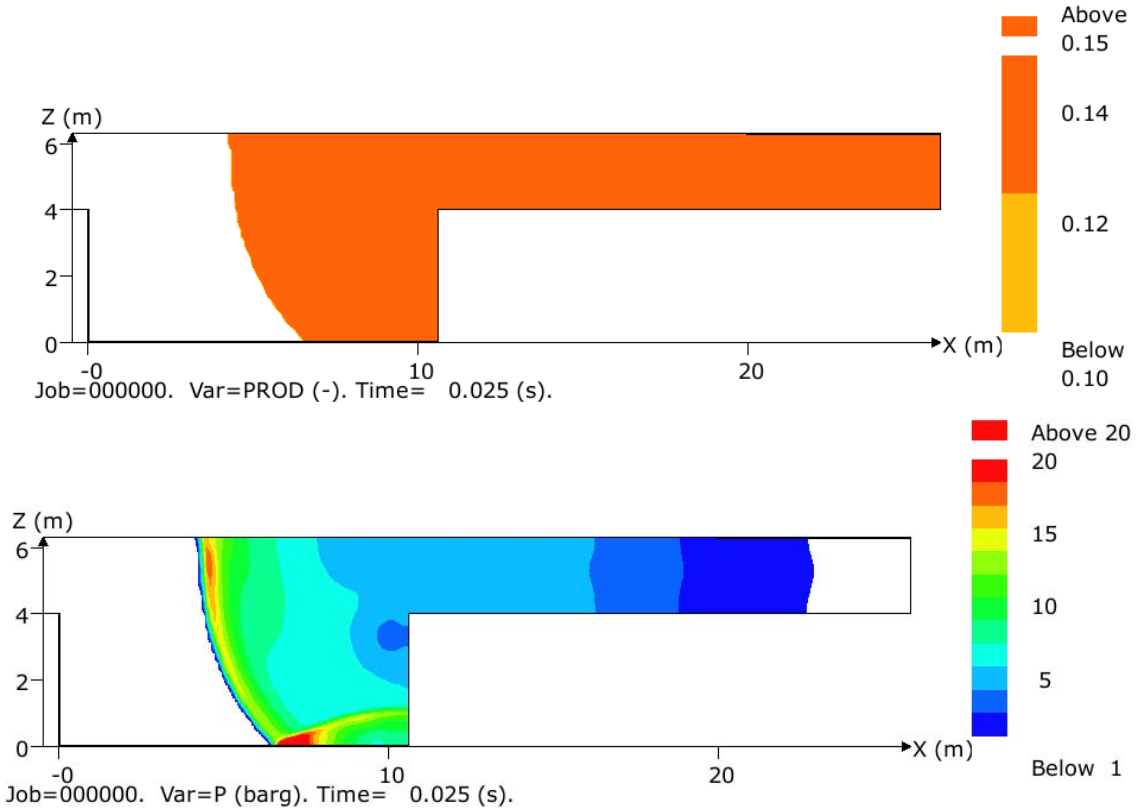

Figure 7.3 – Flame front (top) and pressure front (bottom) for detonation simulations in the RUT facility.

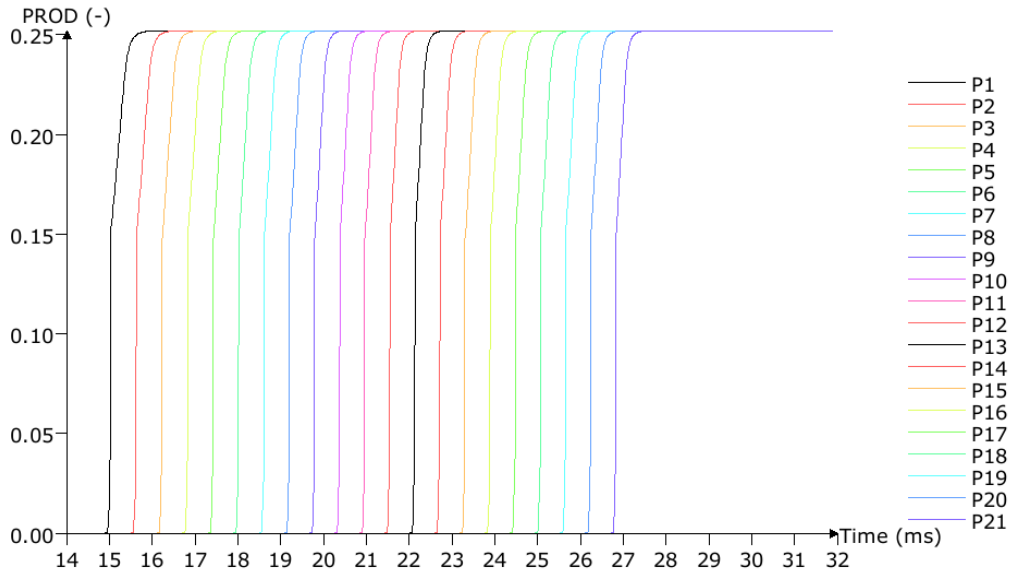

Figure 7.4 – Flame arrival times for detonation simulations in the RUT facility.

7.3 Final Remarks

The possibility of DDT represents a severe danger for hydrogen explosions due to its high reactivity. This chapter presents the work that has been carried out to enable FLACS to indicate the possibility, location, and time of occurrence of a transition to detonation. As a part of this work, the spatial pressure gradient has been used to predict the likelihood of DDT. Numerical simulations in diverse practical geometries have shown that FLACS is able to pick up significant pressure gradients in areas where detonations have been observed in experiments. In general, the modelling results are able to capture the experimental observations, including pressure traces and locations of DDT, reasonably well. The dimensions of a given geometry have been compared with the detonation cell size in order to estimate whether the propagation of any initiated detonation front is possible.

However, this model still needs to be developed further, especially the shock ignition model. But in any case, this work represents an important step forward for the development of a numerical tool to predict this highly complex phenomenon in real-scale geometries, even if it is on an "average" basis. The current model, when coupled with the additional features currently under development, can be used by the process industry to get a fair idea of the danger of DDT.

8 Risk Assessment for Hydrogen Applications

8.1 Introduction and Methodology

In recent years, CFD has been increasingly used to perform quantitative risk assessments, especially in the oil and gas industry. As guidance to the NORSOK standard (2001) it is described how a quantitative explosion risk assessment should preferably be carried out with the use of CFD for ventilation, dispersion and explosion calculations. Based on predicted consequences of a range of potential accident scenarios a risk level is predicted. The importance of establishing methods for carrying out Quantitative Risk Assessment (QRA) for installations involving the use of hydrogen has increased by a large extent in recent years, primarily because of the expected large-scale use of hydrogen as an energy carrier in the future (LaChance, Tchouvelev & Ohi, 2007). Due to the very high reactivity of hydrogen, safe handling is critical. For most applications it is not realistic to perform an extensive risk assessment similar to what is done for large petrochemical installations. On the other hand, simplified methods, like venting guidelines, may have a questionable validity for hydrogen. The use of simple methods, if these actually are conservative, will in general predict too high consequences for the majority of scenarios, as these are not able to represent actual geometry and physics of the explosion.

As a part of this doctoral study, CFD-based risk assessment methods for hydrogen applications have been developed based on the NORSOK criteria:

Paper 11: CFD-based risk assessment for hydrogen applications (Hansen & Middha, 2008)

In this paper a 3-step approach is proposed, in which the CFD-tool FLACS is used to estimate the risk. The initial approach will be to carry out a "worst-case" calculation evaluating the consequences if a full stoichiometric gas cloud is ignited. Mitigation measures can also be considered. As a second step, if potential consequences of the initial approach are not acceptable, the assumptions are refined and more calculations are performed to make the evaluations more realistic and reduce unnecessary conservatism of the chosen worst-case scenarios. Typically a number of dispersion calculations will be performed to generate likely gas clouds, which are subsequently ignited. If estimated consequences are still not acceptable, a more comprehensive study, including ventilation, dispersion and explosion, is performed to evaluate the probability for unacceptable events. Calculation examples are used to illustrate the different approaches. The proposed approach is thus very flexible, and can be tailored to the scenario under consideration.

8.2 Risk analysis of hydrogen vehicles in a traffic tunnel

When introducing hydrogen-fuelled vehicles, an evaluation of the potential change in risk level should be performed. It is widely accepted that outdoor accidental releases of hydrogen from single vehicles will disperse quickly, and not lead to any significant explosion hazard. The situation may be different for more confined situations such as parking garages, workshops, or tunnels. Experiments and computer modelling are both important for understanding the situation better.

A simulation study has been performed by the author to examine what, if any, is the explosion risk associated with hydrogen vehicles in tunnels. This work is described in:

Paper 12: CFD simulation study to investigate the risk from hydrogen vehicles in tunnels (Middha & Hansen, 2009b)

Its aim was to further our understanding of the phenomena surrounding hydrogen releases and combustion inside road tunnels, and furthermore to demonstrate how a risk assessment methodology developed above could be applied to the current task. There have been other studies involving CFD modelling of release from hydrogen vehicles and subsequent explosion (e.g. Venetsanos, et al., 2008). The study described in this section is more detailed and makes an attempt to estimate the overall risk. The effect of other vehicles is also considered. Its aim was to further our understanding of the phenomena surrounding hydrogen releases and combustion inside road tunnels, and furthermore to demonstrate how a risk assessment methodology developed for the offshore industry could be applied to the current task. This work is contributing to the EU Sixth Framework (Network of Excellence) project HySafe, aiding the overall understanding that is also being collected from previous studies, new experiments and other modelling activities.

Releases from hydrogen cars (containing 700 bar gas tanks releasing either upwards or downwards or liquid hydrogen tanks releasing only upwards) and buses (containing 350 bar gas tanks releasing upwards) for two different tunnel layouts and a range of longitudinal ventilation conditions have been studied. The largest release modelled was 20 kg H_2 from four cylinders in a bus (via one vent) in 50 seconds, with an initial release rate around 1000 g/s. Comparisons with natural gas (CNG) fuelled vehicles have also been performed.

The study suggests that for hydrogen vehicles a typical worst-case risk assessment approach assuming the full gas inventory being mixed homogeneously at stoichiometry could lead to severe explosion loads. However, a more extensive study with more realistic release scenarios reduced the predicted hazard significantly. The flammable gas cloud sizes were still large for some of the scenarios, but if the actual reactivity of the predicted clouds is taken into account, moderate worst-case explosion pressures are predicted. As a final step of the risk assessment approach, a probabilistic QRA study is performed in which probabilities are assigned to different scenarios, time dependent ignition modelling is applied, and equivalent stoichiometric gas clouds are used to translate reactivity of dispersed non-homogeneous clouds. The probabilistic risk assessment study is based on over 200 dispersion and explosion CFD calculations using the commercially available tool FLACS. The risk assessment suggested a maximum likely pressure level of 0.1-0.3 barg at the pressure sensors that were used in the study. Somewhat higher pressures are seen elsewhere due to reflections (e.g. under the vehicles). Several other interesting observations were found in the study. For example, the study suggests that for hydrogen releases the level of longitudinal tunnel ventilation has only a marginal impact on the predicted risk, since the momentum of the releases and buoyancy of hydrogen dominates the mixing and dilution processes.

8.3 Further Work

In order to address some of the questions left unanswered by the work described above, additional simulations have been carried out. These have primarily considered wide bridge scenarios where "realistic" ceilings have been used instead of the smooth ceiling assumption used in the previous work. As mentioned above, this is expected to have a significant influence on the results as hydrogen gas can get collected between beams and other associated support structures. These structures, as well as armature fittings, can also act as "turbulizers" and contribute to flame acceleration and higher overpressures.

The situation considered is a hydrogen release from a bus travelling in an underpass (dimension 42 × 15 × 6 m) below a highway. No other vehicles assumed to be present except the hydrogen bus. It is also assumed that the bus remains upright after the incident (and at the same position). Ambient Conditions of 15 °C temperature and 1 bar pressure are used. Quiescent atmospheric conditions (with no wind) are assumed. The ceiling supports included 0.8 m deep I-beams every

3 m (1 cm thick web with 50 cm ends; shown in red). Stiffeners on each beam on both sides of web at crossbracing positions and mid-way between braces (blue) and cross bracing at supports, mid-span, and quarter-span (blue) were also present. A bus (12 × 2.55 × 3.2 m) was located at position (10, 8, 0). Light armature units (4 × 0.4 × 0.2 m) were located every 2.5 m in the width (X) direction and every 8 m in the length (Y) direction. Snapshots of the geometry are presented in Figure 8.1. More details on stiffeners and bracings are presented in Middha (2008a).

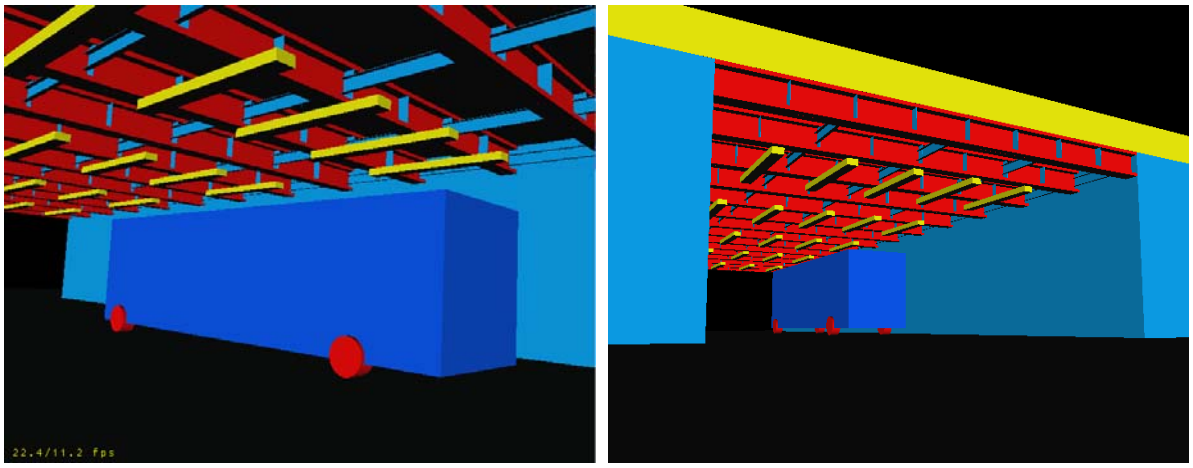

Figure 8.1 – Snapshots of the geometry used for the wide bridge study.

8.3.1 Dispersion simulations

The release is a PRD release (4 PRDs) into a 20 mm vent line (the storage arrangement is the same as one presented in **Paper 12**). 20 kg (contained in 4 tanks) is assumed to be released from a CGH_2 tank (pressure 350 bar, ambient temperature). The release direction is upwards and the release position is (9 m, 20 m, 3.3 m). 10 monitor points are assumed to be located at X=7.5 m, Z=5.8 m and Y=3, 7, etc every 4 m. Based on the above information, the nozzle diameter is 4 mm (1 cylinder and 4 cylinder releases) and the diameter of the expanded jet (based on Birch notional nozzle concept) is 12 cm (6 cm for 1 cylinder release).

Four separate simulations are considered. The base case (scenario 1) involved the release of 20 kg hydrogen upwards from position (9, 20, 3.3). The first sensitivity involved moving the release position such that the jet hit the light armature present in the "tunnel" (scenario 2). The second sensitivity was study of the effect of changing the ceiling to one that was completely flat (scenario 3). The last one studied the effect of total hydrogen released (and hence initial release rate). Herein, only one hydrogen tank was supposed to empty with 5 kg hydrogen released (scenario 4). These are summarized in Table 8.1 below. A structured cartesian grid was used in the simulations (default grid resolution was 50 cm). The grid was refined near the H_2 release. The total number of cells ranged from about 240.000 to 340.000 depending on the release rate (1 cylinder or 4 cylinder release) and the geometry (flat or with beams).

The concentrations at the sensors are shown below in Figure 8.2 for all four scenarios considered. Significant concentrations are seen just after the release at some sensor locations but the cloud is quickly diluted to very dilute concentrations that are at or below the lower flammability limit (LFL). More details on the size of the flammable gas cloud are shown below in Figure 8. where the flammable volume is presented as a function of time. The left figure depicts the total flammable volume (in the range 4–75 %) in the underpass as a function of time for all four scenarios. The second figure converts this total flammable volume to an equivalent stoichiometric volume according to the formulation given in **Paper 12**.

Table 8.1 – Dispersion simulations for the wide bridge scenario

#	Simulation	Type
1	20 kg released from a tank with pressure 350 bar (position 9m, 20m, 3.3m)	Base Case
2	Jet hits light armature (move release to 10m, 20m, 3.3m)	Sensitivity 1
3	Original release location Define flat ceiling at z=5m (move sensors to 4.8m)	Sensitivity 2
4	5 kg H_2 (1 tank) released Original geometry and release point	Sensitivity 3

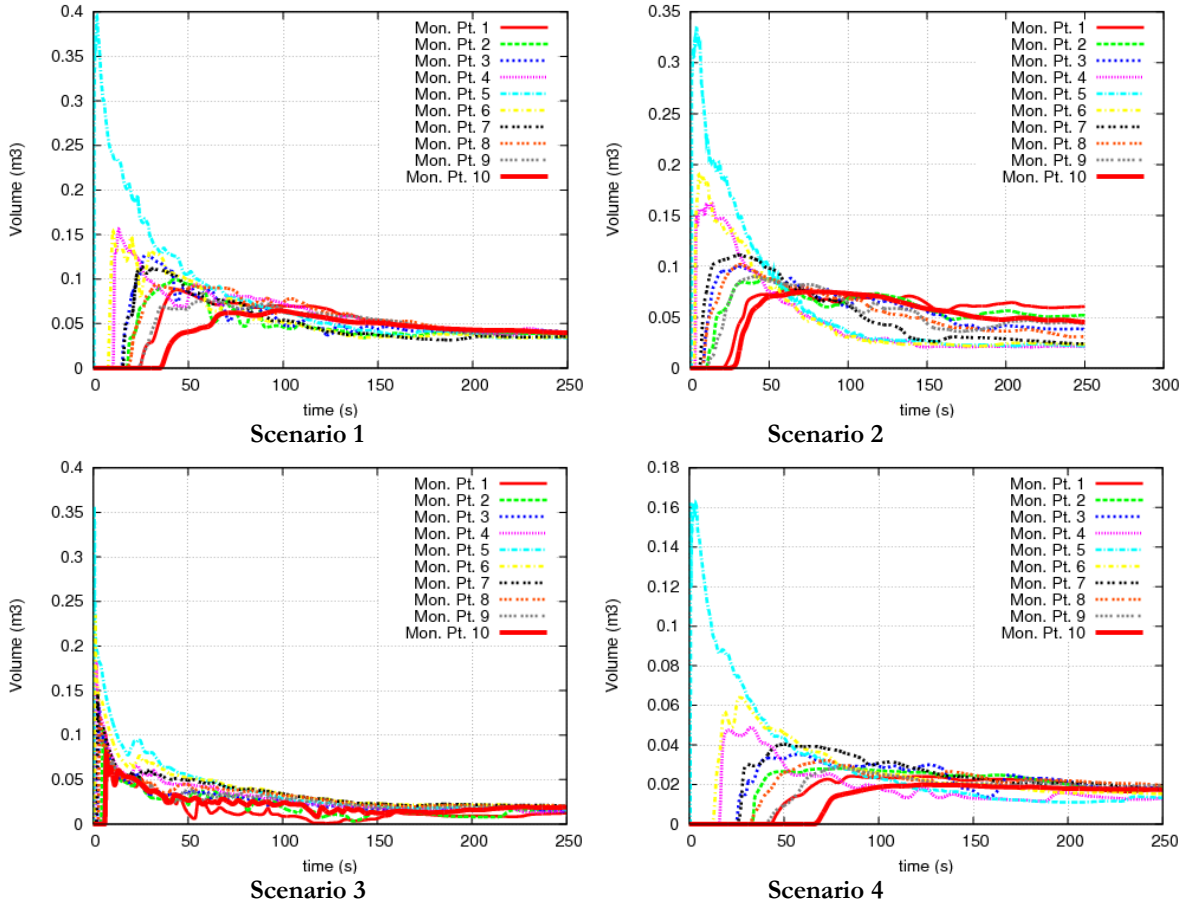

Figure 8.2 – Concentration profiles as a function of time for all sensor locations for all four different dispersion scenarios for the wide bridge study.

It can be seen from these figures that the maximum flammable gas cloud is around 2200 m^3 for the base case scenario (scenario 1) and occurs around 60 seconds after the start of the release. To get an indication of expected explosion severity following a release, it can be more useful to consider the FLACS estimated equivalent stoichiometric gas cloud (Q9). The equivalent

stoichiometric gas cloud concept has been developed through previous work towards quantitative risk assessment (QRA) for oil and gas applications. Herein, the dispersed gas clouds with non-homogenous distribution of gas and turbulence from jet are normally replaced by smaller equivalent stoichiometric gas clouds, *Q9* (NORSOK, 2001). *Q9* cloud is a scaling of the non-homogeneous gas cloud to a smaller stoichiometric gas cloud that is expected to give similar explosion loads as the original cloud (provided conservative shape and position of cloud, and conservative ignition point). It is defined as $Q9 = \sum V \times S_L \times \sigma \; / \; (S_L \times \sigma)_{\max}$. Here, V is the flammable volume, S_L is the laminar burning velocity (corrected for flame wrinkling/Lewis number effects), σ is volume expansion caused by burning at constant pressure in air, and the summation is over all control volumes. More details can be found in **Paper 12**. The corresponding value for the equivalent stoichiometric gas cloud is only 120 m^3 occurring much earlier (10-15 seconds after the start of the release). This shows that the cloud is fairly dilute. The size of the gas cloud is somewhat reduced (by around 20 %) if the release is shifted to impinge on the armature. In this case, the corresponding values for the total flammable gas cloud and the *Q9* cloud are 1800 m^3 and 100 m^3 respectively. This is due to the decrease in the effective height of the tunnel before the hydrogen jet impinges on a surface. As expected, the use of a flat ceiling reduces the gas cloud sizes significantly as the gas cannot get collected between the various support structures. In this case, the corresponding values for the total flammable gas cloud and the *Q9* cloud are 1300 m^3 and 30 m^3 respectively. This means that the gas cloud is also significantly less reactive than that obtained for a "rough" ceiling. If it is assumed that only 5 kg of hydrogen is released (scenario 4), then the flammable gas cloud is clearly smaller (425 m^3 and 7 m^3 respectively).

Thus, the ceiling structure, release mass, and release position each have a significant effect on the size and reactivity of the gas cloud. Also, it can be seen from the plots above showing the concentrations at each monitor point that the steady state concentrations are fairly dilute. This is confirmed by the second figure for each scenario which presents the values of the equivalent stoichiometric gas cloud (described above). It can be seen that the equivalent stoichiometric gas cloud size (*Q9*) is only about 100 m^3 for scenarios 1 and 2, while it is even smaller for scenario 3. This suggests that the danger of these clouds is not very high.

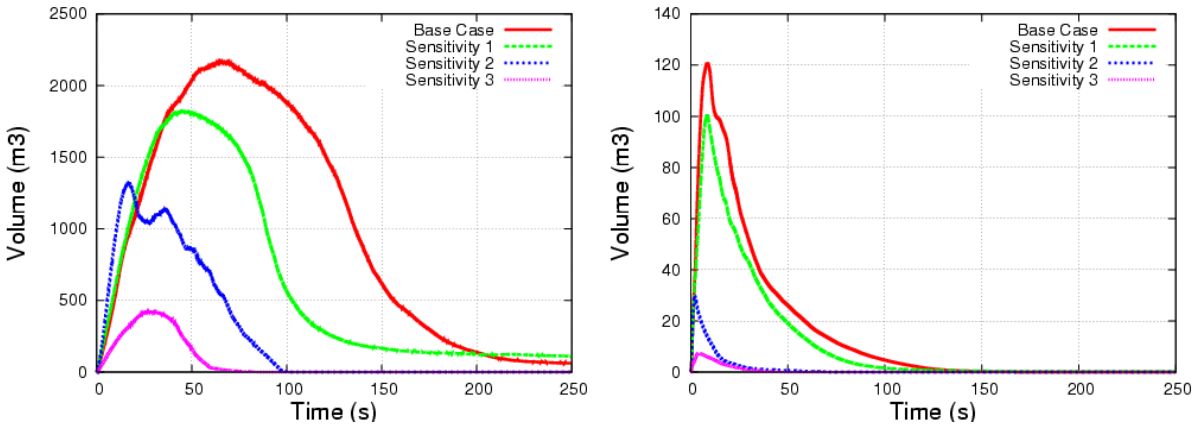

Figure 8.3 – Total flammable (left) and equivalent stoichiometric (right) gas cloud sizes as a function of time all four different dispersion scenarios for the wide bridge study.

These simulations were carried out as a part of a benchmark study developed by the author (in collaboration with O.R. Hansen). Other modellers have also carried out these simulations and an inter-comparison of the results is published (Venetsanos, Papanikolau, Middha, Hansen, Garcia, Heitsch, et al., 2010).

8.3.2 Explosion simulations

For explosion calculations, the geometry was exactly the same as that described above (and used for dispersion simulations). 20 sensors were defined in order to measure the combustion overpressure, including 10 monitor points at "sidewalk" (X = 1 m, Z = 1 m and Y = 3, 7, etc every 4 m) and 10 monitor points at ceiling (X = 7.5 m, Z = 5.8 m and Y = 3, 7, etc every 4 m). A summary of the simulations that were performed is presented in Table 8..

Table 8.2 – Explosion simulations for the wide bridge scenario

#	Simulation	Type
	Explosion of gas cloud of different sizes	Base Case
1	All released inventory (ca. 20 kg stoich.cloud X = 0-15m, Y = 0-42m, Z = 4.8-6m)	
2	Smaller clouds 1.9 kg (10%) filling space between beams at Y = 18 & 24m (Ignition point at: X = 12.5m, Y = 22m and Z = 5.25m)	
	Repeat with flat ceiling at 5m (move sensors to 4.8m) (Ignition point changed to Z = 4.25m)	Sensitivity
3	Full stoichiometric gas cloud (ca. 20 kg cloud at X = 0-15m, Y = 0-42m, Z = 3.8-5m)	
4	10% cloud (same shape as above, but moved down below 5m)	

A structured Cartesian grid was used. The grid resolution was 10 cm (12 cm for flat ceiling), and the total number of cells was 2–3 million. The grid was extended outside the "tunnel" opening in order to represent the external flow.

The results are presented next. Figure 8. presents the pressure as a function of time for the monitor points 1-10 (near the ceiling) for scenarios 1 (full cloud, beams), 2 (10 % cloud, beams), 3 (full cloud, flat ceiling) and 4 (10 % cloud, flat ceiling). In this case, a maximum pressure level around 6 barg is seen for scenario 1 which reduces to around 2 barg for the 10 % cloud. The corresponding level for scenario 3 is 0.5 barg which clearly shows the effect of turbulence generated by the obstacles in the ceiling. For scenario 4, the pressure level is about 0.06 barg. Figure 8. presents a similar plot monitor points 11-20 (near the "sidewalk", X, Z = 1 m). In this case, the pressure level for scenario 1 is even higher (10 barg) due to long travel distance. However, the pressures for scenario 2 are significantly smaller. The corresponding pressure levels for scenario 3 and 4 are 0.15 and 0.05 barg.

Two different ignition positions were attempted in order to find the worst case for the pedestrian (scenario 4) at (1, 2, 1). However, it turned out that the ignition position used in scenario 2 actually gave the highest pressure levels. Scenario 3 was also attempted (worst-case after the release in case of ceiling with obstacles) and pressure levels around 0.6–0.7 barg were seen. More details on the results are given in Middha (2008b).

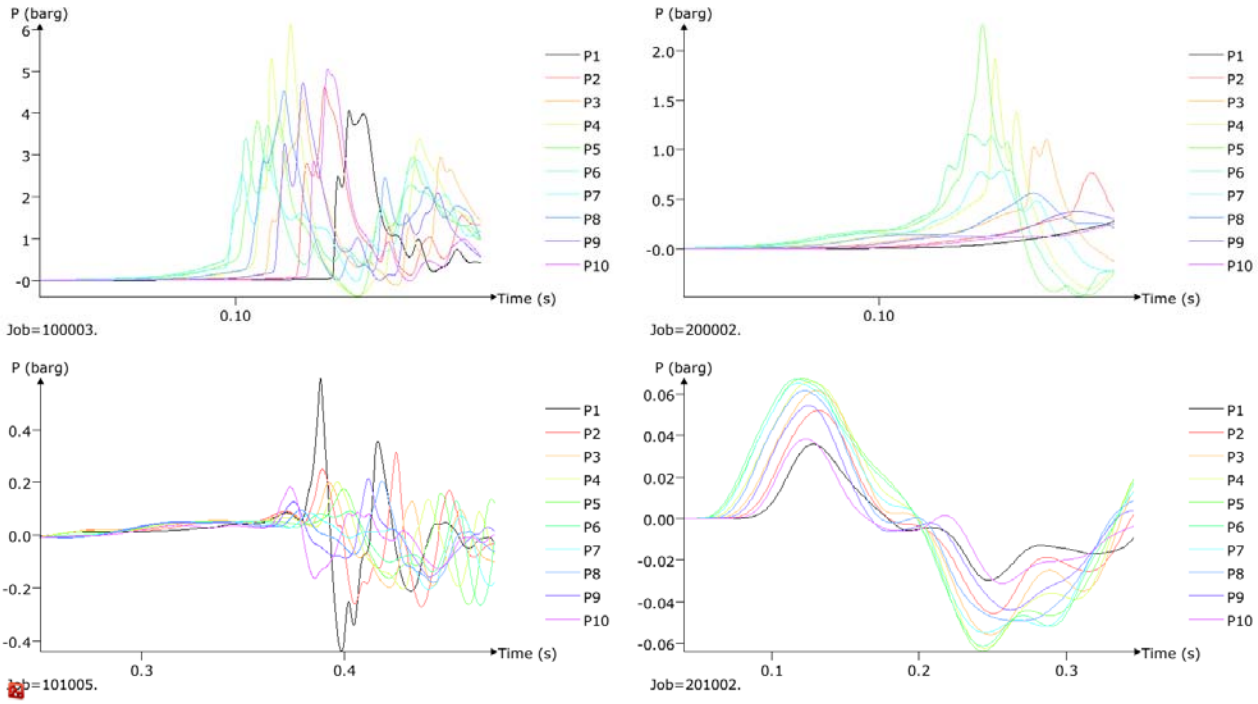

Figure 8.4 – Overpressure as a function of time for monitors 1-10 for scenarios 1 (top left), 2 (top right), 5 (bottom left) and 6 (bottom right)

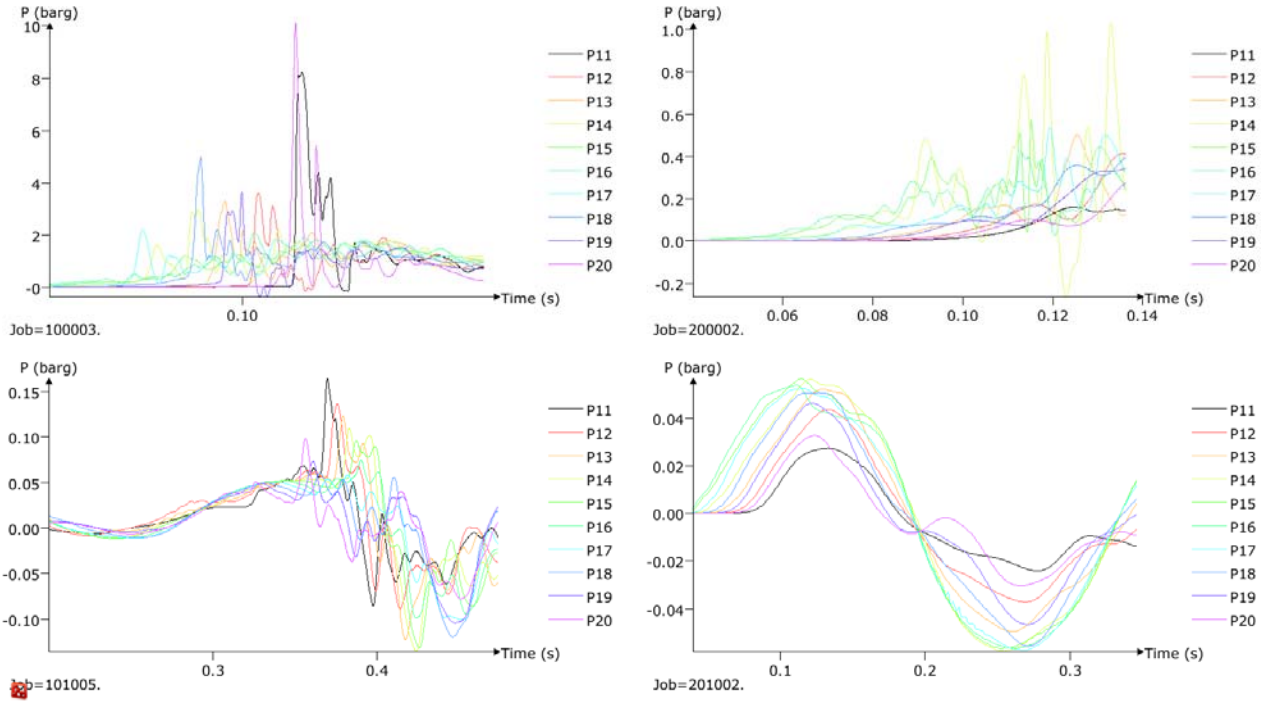

Figure 8.5 – Overpressure as a function of time for monitors 11-20 for scenarios 1 (top left), 2 (top right), 5 (bottom left) and 6 (bottom right)

It is evident from the results presented above that unacceptably high pressures are obtained from the explosion calculations. However, these clouds are certainly not realistic. The volume of the gas cloud used for scenario 1 is 756 m^3. This is more than a factor of 6 larger than that obtained in the base case dispersion calculation. The gas clouds obtained as a result of dispersion

calculations have also been ignited in order to obtain a more realistic value of the overpressures. Sensitivity to ignition locations and times has been investigated. In this case, two scenarios were considered: 20 kg hydrogen released for the case of "rough" and smooth ceiling. The maximum overpressure obtained for the rough ceiling scenario was found to be around 0.7–0.75 barg. For the case of smooth ceiling, the maximum overpressure was found to be 0.1–0.15 barg. Thus, the overpressure increases by a factor of 5–6 due to turbulence generating objects in the ceiling. The overpressure obtained for the smooth ceiling case compares well with the value reported in part 1 of the CFD simulation study where a maximum pressure of the order of 0.1–0.3 barg was reported. Thus, it may be deduced that if a rough ceiling were present in those calculations, a pressure of 0.6–1 barg could be expected.

8.4 Effect of addition of hydrogen to natural gas on explosion risk

One of the main benefits sought by including hydrogen in the alternative fuels mix is emissions reduction – eventually by 100 %. However, in the near term, there is a very significant cost differential between fossil fuels and hydrogen. Hythane (a blend of hydrogen and natural gas) can act as a viable next step on the path to an ultimate hydrogen economy as a fuel blend consisting of 8–30 % hydrogen in methane by volume can reduce emissions of pollutants such as NO_x (and greenhouse gases such as CO_2) while not requiring significant changes in existing infrastructure (more information is available on http://www.hythane.com). The use of hythane is able to provide the immediate emissions benefits that can justify the required investment in infrastructure. Depending upon the blend, many of the vehicles currently running on Compressed Natural Gas (CNG) will not have to have any modifications to run on hythane. Due to this and other advantages, there is a significant focus to introduce hythane in public transport infrastructure worldwide. However, the author has not been able to find many relevant safety studies on the use of hythane in literature. With this purpose, a computational study has been carried out.

This work was presented in the 3rd International Conference on Hydrogen Safety and is in press in the International Journal for Hydrogen Energy (Middha, Engel & Hansen, 2009). This work seeks to evaluate whether hythane may be safer than both hydrogen and methane under certain conditions. This is due to the fact hythane combines the positive safety properties of hydrogen (strong buoyancy, high diffusivity) and methane (much lower flame speeds and narrower flammability limits as compared to hydrogen). For this purpose, several different mixture compositions (e.g. 8 %, 20 % and 30 % hydrogen) are considered. The evaluation of (a) dispersion characteristics (which are more positive than for methane), (b) combustion characteristics (which are closer to methane than hydrogen), and (c) Combined dispersion + explosion risk is performed. This risk is expected to be comparable to that of pure methane, possibly lower in some situations, and definitely lower than for pure hydrogen.

The first part of the work involved validating the flame speeds and flammability limits predicted by FLACS against values available in literature. The next part of the work involved validating the overpressures predicted by the CFD tool for combustion of premixed mixtures of methane and hydrogen with air against available experimental data. In the end, practical systems such as vehicular tunnels, garages, etc. are used to demonstrate positive safety benefits of hythane with comparisons to similar simulations for both hydrogen and methane. Details can be found in Middha, Engel & Hansen (2009). This article is not included in the appendix for brevity.

8.5 Final Remarks

CFD has become increasingly accepted for risk assessment and explosion safety studies in offshore oil platforms worldwide. Due to the increasing focus on hydrogen safety, significant use of the tool is seen in evaluating the viability of new and existing establishments in terms of probability and consequences of accidental events. It is expected that CFD will be used in carrying out risk assessments for hydrogen risk with the same frequency as that for oil and gas applications. However, the CFD tool needs to be well validated to be able to evaluate risk of hydrogen applications in a truly predictive way.

This work described in this chapter presents a rigorous methodology for carrying out quantitative risk assessment calculations using a validated CFD tool such as FLACS. Three different approaches are presented, with an increasing degree of complexity. This methodology enables the user to estimate the complete risk arising from a hydrogen release in a given geometry in a quantitative fashion. Detailed examples of using the methodology are also presented. The examples demonstrate how the complete risk of a given system in terms of the likely explosion pressure load and the frequency with which it is expected to occur can be estimated in a rigorous fashion starting from possible release scenarios.

This proposed CFD based risk analysis method for explosion (and fire) risk is advantageous in many respects. These include:

- Physically sound methods will help minimize risk in cost efficient way
- Transparent method will facilitate the identification of knowledge gaps
- Methods and competence developed within oil and gas should be looked to
- More accurate calculation tools and faster computers should be exploited
- Extensive use of simplified methods prevent progress towards more intelligent solutions

It is therefore recommended that such approaches are actively used as a part of the risk "toolbox", and that any RCS being developed will stimulate their use.

9 Conclusions

It has been established that the use of hydrogen represents many potential hazards even if it does have some favourable properties such as high buoyancy. This points to the need for establishing viable tools to carry out the required safety and risk analyses connected with the use of hydrogen infrastructure. It is possible to use both simplified methods (venting guidelines, etc.) and advanced tools such as those based on Computational Fluid Dynamics (CFD) in order to carry out the required safety analyses. For safety analysis of hydrogen systems, there is also a significant focus on regulations, codes, and standards (RCS) e.g. safety distance rules. However, only CFD tools have the potential to model the relevant physics involved in safety analyses. With CFD, it is possible to take account of effects of buildings, mitigation measures, piping and vessel arrangements, etc. which have been found to have a strong influence on the consequences of any accident or unwanted incident. A primary requirement for the use of any such tool, in addition to the models capturing the correct physics, is extensive validation against available small- and large-scale experiments (with studies on variations of various important parameters that may affect explosion loads and hence risk). The validation should be an integrated part of development. Clear user guidelines must exist to enable user independency, even when predicting blind. Without proper user guidelines based on extensive validation work, very mixed prediction capability can be expected.

The validation carried out before the start of the study was missing several key elements, notably dispersion scenarios, situations involving combined dispersion and explosion phenomena, etc. These and several other scenarios are considered as a part of the current work. FLACS has been thoroughly validated for natural gas and such a validation exercise is carried out for hydrogen applications to some extent to raise the confidence level in carrying out predictions with FLACS-HYDROGEN.

Further to the validation work, several improvements have been made to FLACS regarding the simulation of hydrogen-air explosions. These have included changes in flammability limits and the effect of inert. Efforts have also been made to improve the handling of small-scale phenomena. A thorough evaluation of the laminar burning velocity of hydrogen-air mixtures as a function of concentration has been carried out. Turbulent burning velocity models have also been evaluated in general and suggestions have been made for future improvements. FLACS uses a utility program in order to model releases from high-pressure reservoirs. The utility program provides the release rate and the leak diameter (expanded to the atmosphere) as a function of time. Work has been carried out in order to extend the models in the utility program in order to include real gas effects.

Extensive validation work has been carried out in the area of dispersion of hydrogen. Modelling results are compared to experimental data, and in general, reasonable agreement is seen for many different kinds of release conditions. Examples of subsonic and sonic gas releases (free space and impinging) as well as liquid hydrogen releases are presented. A range of different experiments is simulated, including low momentum releases in a garage, sub-sonic jets in a garage with stratification effects and subsequent slow diffusion, low momentum and subsonic horizontal jets influenced by buoyancy, and free jets from high-pressure vessels. LH_2 releases are also considered. Several of the simulations are performed as blind predictions. Similar validation effort has been carried out for hydrogen explosions. Some of the simulations are performed as blind simulations. Modelling results are compared to experimental data, and in general, reasonable agreement is seen for many different kinds of geometries and conditions. These have included tunnel geometry, refueling station geometry, obstructed and unobstructed channels and pipes, unconfined "lane" geometry, etc.

It must be pointed out that the typical accident scenario is usually more complicated, possibly involving time varying releases impinging on equipment, with delayed ignition of a non-homogenous and possibly turbulent mixture. When aiming for increased precision in risk assessment methods there is a need to validate consequence tools for this added complexity. For post-accident simulations, it is obvious that there is a need to reproduce the complex physics of the accident scenario, and validation of tools for the combined release and ignition scenarios is important. For that reason, validation against combined release and explosion experiments carried out by FZK has been carried out. These involved vertically upwards hydrogen releases with different release rates and velocities impinging on a plate in two different geometrical configurations. The dispersed cloud was subsequently ignited and pressures recorded. In the weeks prior to the planned experiments, several blind CFD simulations were performed to predict the outcome of the proposed experiments, and if possible, to help the planning. After the experiments were reported, the quality of the blind predictions was evaluated. In general, the blind prediction of various scenarios of hydrogen release and dispersion and subsequent ignition were in good agreement with the results of the subsequent FZK experiments. The explosion pressures predicted by FLACS were quite similar to those obtained in the experiments, both for ignition of non-homogeneous clouds during releases, but equally importantly, the explosion pressures from the estimated equivalent gas clouds (*Q9*-method) also corresponded well with the observations in the experiments. It seems justified to conclude that the results reported in this chapter gives further support to the view that available advanced CFD tools are in fact able to simulate combined scenarios of release of combustible gas, entrainment by air, and subsequent gas explosion.

Deflagration to detonation transition (DDT) may be a significant threat for hydrogen explosions. Due to the high reactivity of hydrogen, DDT is likely in a variety of scenarios involving H_2-air mixtures and result in large-scale damage. With the advance in scientific computing, research on DDT has been shifted toward the use of computational approaches. Before the beginning of this work, the standard versions of FLACS could only handle the deflagration mode of combustion, in which the flame propagates because hot flame products heat and ignite the unburned gas ahead. In this work, the use of FLACS to simulate hydrogen explosions in different geometries and get indications about the likelihood of DDT is described. The study of this phenomenon is very critical as the overpressures in detonation front can cause losses which are much more severe as compared to those seen with blast waves produced by a deflagration. The likelihood of DDT is illustrated in terms of a parameter proportional to the spatial pressure gradient across the flame front. This parameter is able to visualize when the flame front captures the pressure front, which is the case in situations when fast deflagrations transition to detonation. The methodology was then validated against available experimental data using several practical systems. In general, the modelling results are able to capture the experimental observations, including pressure traces and locations of DDT, reasonably well. The current model, when coupled with the additional features currently under development, can be used by the process industry to get a fair idea of the danger of DDT.

CFD has become increasingly accepted for risk assessment and explosion safety studies in offshore oil platforms worldwide. Due to the increasing focus on hydrogen safety, significant use of the tool is seen in evaluating the viability of new and existing establishments in terms of probability and consequences of accidental events. It is expected that CFD will be used in carrying out risk assessments for hydrogen risk with the same frequency as that for oil and gas applications. A rigorous methodology for carrying out quantitative risk assessment calculations using a validated CFD tool such as FLACS is presented. Three different approaches are presented, with an increasing degree of complexity. This methodology enables the user to estimate the complete risk arising from a hydrogen release in a given geometry in a quantitative fashion. Detailed examples of using the methodology are also presented. The examples

demonstrate how the complete risk of a given system in terms of the likely explosion pressure load and the frequency with which it is expected to occur can be estimated in a rigorous fashion starting from possible release scenarios.

Finally, it can be concluded that the work done in this dissertation has made FLACS a more complete tool for simulating problems relevant to hydrogen safety with reasonable confidence.

Bibliography

1. Abdel-Gayed, R.G., Bradley, D. and Lawes, M., (1987). Turbulent burning velocities: A general correlation in terms of straining rates. *Proc. R. Soc. Lond. A*, 414, 389-413.
2. Al-Hassan, T., Johnson, D.M., (1998). Gas explosions in large-scale offshore module geometries: Overpressures, mitigation and repeatability, presented at OMAE-98, Lisbon, Portugal.
3. Arntzen, B.J., (1998). Modelling of turbulence and combustion for simulation of gas explosions in complex geometries. Dr. Ing. Thesis, NTNU, Trondheim, Norway.
4. Aung K. T, Hassan M. I., Faeth G. M., Flame Stretch Interactions of Laminar Premixed Hydrogen/Air Flames at Normal Temperature and Pressure, Combustion and Flame 109:1-24, 1997.
5. Birch, A.D., Brown, D.R., Dodson, M.G., Swaffield, F., (1984). The Structure and Concentration Decay of High Pressure Jets of Natural Gas, *Combust. Sci. Tech.*, 36, 249-261.
6. Birch, A.D., Hughes, D.J., Swaffield, F., (1987). Velocity Decay of High Pressure Jets, *Combust. Sci. Tech.*, 52, 161-171.
7. Balonov, M.I., (2007). The Chernobyl Forum: major findings and recommendations, *J. Environ. Radioact.*, 96(1-3), 6-12.
8. Baraldi, D., Kotchourko, A., Lelyakin, A., Yanez, J., Middha, P., Hansen, O.R., Gavrikov, A., Efimenko, A., Verbecke, F., Makarov, D., Molkov, V., (2009). An inter-comparison exercise on CFD model capabilities to simulate hydrogen deflagrations in a tunnel. *Intl J. Hyd. Ener.*, 34(18), 7862-7872.
9. Baraldi, D., Venetsanos, A.G., Papanikolaou, E., Heitsch, M., Dallas, V., (2009). Numerical analysis of release, dispersion and combustion of liquid hydrogen in a mock-up hydrogen refuelling station, *J. Loss Prevent. Proc. Ind.*, 22(3), 303-315.
10. Becker, T. & Ebert, F., 1985. Vergleich zwischen experiment und theorie der explosion grober, freier gaswolken. Chem.-Ing.-Tech., V.57, N.1, 42-45 (in German).
11. Bjerketvedt, D., Bakke, J. R., and van Wingerden, K., (1997) Gas Explosion Handbook, *J. Hazard. Mat.*, 52, 1-150.
12. Bone, W. A., (1931) *Phil. Trans. A*, 230, 363.
13. Bradley, D. (2000), Flame propagation in a tube: The legacy of Henri Guénoche. *Comb. Sci. Tech.*, 158, 15-33.
14. Bradley, D., Lawes, M., Liu, K., (2008). Turbulent flame speeds in ducts and the deflagration/detonation transition. *Comb. Flame*, 154, 96-108.
15. Bradley, D., Sheppard, C.G.W. & Wolley, R., (2001). Unstable explosion flames and acoustic oscillations. In: Proceedings of the 18th ICDERS, Seattle, WA, USA, July 29–August 3, 2001.
16. Bray, K. N. C., (1990). Studies of the turbulent burning velocity. *Proc. R. Soc. Lond. A*, 431, 315-335.
17. Breitung W. et al., (2000). Flame Acceleration and Deflagration-to-Detonation Transition in Nuclear Safety, State-of-the-Art Report by a Group of Experts, OECD, Nuclear Energy Agency Committee on The Safety of Nuclear Installations, NEA/CSNI/R(2000)7.
18. Breitung, W., et al., (2005), Integral large scale experiments on hydrogen combustion for severe accident code validation-HYCOM. *Nuc. Engg. Des.* 235, 253–270.
19. Butler, T.D., O'Rourke, P.J., (1976). Numerical method for two-dimensional unsteady reacting flows. In: 6th Symposium on detonation, San Diego, CA, USA, 24 Aug 1976.
20. Catlin, C., Gregory, C.A.J, Johnson, D.M., Walker, D.G., (1993). Explosion mitigation in offshore modules by general area deluge, *Trans. IChemE*,. 71, Part B.

21. Chaineaux, J. (1999). Leak of hydrogen from a pressurized vessel. Workshop on dissemination of goals, preliminary results and validation of methodology. Brussels, March 11, 1999.
22. Ciccarelli, G., Dorofeev, S. B., 2008, Flame acceleration and transition to detonation in ducts. *Prog. Ener. Comb. Sci.*, 34 (4), 499-550.
23. Dagba, Y., Perette, L., Venetsanos, A.G., (2005). Description of INERIS-test-6 experiment and requirements for corresponding blind SBEP in the framework of the InsHyde internal project. HYSAFE report, 24 October 2005.
24. Davis, S., Hansen, O.R., Ichard, M., (2009). Validation of FLACS for vapour dispersion from LNG spills: Model Evaluation Protocol. In: Mary Kay O'Connor Process Safety Symposium, College Station, TX, USA, October 27-28, 2009.
25. Davis S.G, Searby, G., (2002). The use of counterflow flames for the evaluation of burning velocities and stretch effects in hydrogen/air mixtures, *Comb. Sci. Tech.*, 174(11-2), 93-110.
26. Dempsey, J., (2001). Hydrogen fuel cell engines and related technologies. College of the Desert, Energy Technology Training Center, Palm Desert, CA, USA, Revision 0, December 2001.
27. Dorofeev, S.B., Bezmelnitsin, A.V., Sidorov, V.P., (1995). Transition to detonation in vented H_2-air explosions. *Comb. Flame*, 103, 243-246.
28. Dowdy, D.R., Smith, D.B., Taylor, S.C., Williams, A., (1990). The use of expanding spherical flames to determine burning velocities and stretch effects in hydrogen/air mixture. In: Twenty-Third Symposium (International) on Combustion, The Combustion Institute, Pittsburgh, 1990, p. 325.
29. Fairweather, M., Ormsby, M.P., Sheppard C.G.W., Woolley, R., (2009). Turbulent burning rates of methane and methane-hydrogen mixtures. *Comb. Flame*, 156, 780-790.
30. Friedrich, A., Grune, J., Kotchourko, N., Kotchourko, A., Sempert, K., Stern, G., Kuznetsov, M., 2007. Experimental study of jet-formed hydrogen-air mixtures and pressure loads from their deflagrations in low confined surroundings. In: Proceedings of 2nd International Conference on Hydrogen Safety, San Sebastian, Spain.
31. Gallego, E., García, J., Migoya, E., Crespo, A., Kotchourko, A., Yanez, J., Beccantini, A., Hansen, O.R., Baraldi, D., Høiset, S., Voort, M.M. and Molkov, V., 2005. An Inter-comparison Exercise on the Capabilities of CFD Models to Predict Deflagration of a Large-Scale H2-Air Mixture in Open Atmosphere. In: Proceedings of the 1st International Conference on Hydrogen Safety, Pisa, Italy.
32. Groethe, M., Colton, J., & Chiba, S. (2002). Hydrogen deflagration safety studies in a confined tube. In: Proceedings of the 14th World Hydrogen Energy Conference, Montreal, Que´bec, Canada.
33. Gupta, S., Brinster, J., Studer, E. & Tkatschenko, I., 2007. Hydrogen related risks within a private garage: Concentration measurements in a realistic full scale experimental facility. In: Proceedings of the 2nd International Conference on Hydrogen Safety, San Sebastian, Spain.
34. Hansen, O.R., Melheim, J.A., Storvik, I.E., (2008). Validating the data, LNG Industry Magazine, Spring 2008.
35. Hansen, O.R., Middha, P., (2007). GexCon blind simulations compared to FZK experiments. GexCon Technical Note Ref. Nr. GexCon-07-F46207-TN-1.
36. Hansen, O.R., Middha, P., (2008a). CFD-based risk assessment for hydrogen applications. *Proc. Safety Prog.*, 27(1), 29-34.
37. Hansen, O.R., Middha, P., (2008b). Blind prediction of dispersion and explosion experiments using CFD. In: 2nd World Conference on Safety of Oil & Gas Industry, College Station, TX, October 28-29, 2008.
38. Hansen, O.R., Renoult, J., Sherman, M.P., Tieszen, S.R., (2005). Validation of FLACS-Hydrogen CFD Consequence Prediction Model Against Large Scale Hydrogen Explosion

39. Hansen, O.R., Storvik, I.E., (2005). SBEP-V2: Fh-ICT Balloon Test – FLACS-Hydrogen Calculations. GexCon Report GexCon-05-F46207-TN-2, 16 February 2005.
40. Hansen, O. R., Storvik, I. E., Renoult, J., (2005). Hydrogen R&D at GexCon, experiments and simulations, Fire Bridge Second International Conference. Belfast, Northern Ireland, UK, May 2005.
41. Hansen, O.R., Storvik, I.E., van Wingerden, C.J.M., (1999). Validation of CFD-models for gas explosions, where FLACS is used as example; model description and experiences and recommendations for model evaluation. Proceedings European Meeting on Chemical Industry and Environment III, Krakow, Poland.
42. Harlow, F.H., Nakayama, P.I., (1967). Turbulence Transport Equations. *Phys. Fluids*, 10, 2323-2332.
43. Heitsch, M., Huhtanen, R., Techy, Z., Fry, C., Kostka, P., Niemi, J., Schramm, B., (2010). CFD evaluation of hydrogen risk mitigation measures in a VVER-440/213 containment, *Nuclear Engineering and Design*, 240(2), 385-396.
44. Henrie, J.O., Postma, A.K., (1983). Analysis of the Three Mile Island (TMI-2) Hydrogen Burn, In: Joint ANS/AMSE/AIChE meeting, The Second International Topical Meeting on Nuclear Reactor Thermal-Hydraulics, Santa Barbara, CA., January 1983, Published as Thermal-Hydraulics of Nuclear Reactors, Vol. 2, ANS Order No 700081.
45. Herrmann, D. (2007). Why Use CFD for Explosion Studies? Proceedings of the 41st Annual Loss Prevention Symposium, Houston, TX.
46. Hjertager, B.H. (1985). Computer simulation of turbulent reactive gas dynamics. *J. Model. Identification Control*, 5, 211–236.
47. Hjertager, B.H., (1986). Three-dimensional modeling of flow, heat transfer, and combustion. Handbook of Heat and Mass Transfer. Gulf Publishing Company, P.O. Box 2608, Houston, Texas 770011, pp. 304–350 Chapter 41.
48. Hjertager, B.H., Bjørkhaug, M., Fuhre, K., (1988a). Gas explosion experiments in 1:33 scale and 1:5 scale; offshore separator and compressor modules using stoichiometric homogeneous fuel–air clouds. *J. Loss. Prev. Process Ind.* 1, 197–205.
49. Hjertager, B.H., Bjørkhaug, M., Fuhre, K., (1988b). Explosion propagation of non-homogeneous methane-air clouds inside an obstructed 50 m^3 vented vessel. *J. Haz. Mater.* 19, 139–153.
50. Holen, J (2001). Comparison of Five Corresponding Explosion Risk Studies Performed by Five Different Consultants, ERA Conference, London, UK.
51. Holtappels, K., (2005). Report on the experimentally determined explosion limits, explosion pressures and rates of explosion pressure rise – Part 1: methane, hydrogen and propylene. Project SAFEKINEX: SAFe and Efficient hydrocarbon oxidation processes by KINetics and Explosion eXpertise. EU Programme "Energy, Environment and Sustainable Development"
52. Hord, J., (1978). Is Hydrogen a safe fuel?, *Intl. J. Hyd. Ener.*, 3, 157-176.
53. Hu, E., Huang, Z., He, J., Jin, C., Miao, H., Wang, X., (2009). Measurement of laminar burning velocities and analysis of flame stabilities for hydrogen-air-diluent premixed mixtures. *Chin. Sci. Bull.*, 54(5), 846-857.
54. James, H., (2001). Detonations, HSE guidance note ref. TD5/039. Available from http://www.hse.gov.uk/foi/internalops/hid/din/539.pdf.
55. Johnson, D.M., Cleaver, R.P., Puttock, J.S., van Wingerden, C.J.M., (2002). Investigation of Gas Dispersion and Explosions in Offshore Modules, Offshore Technology Conference, Paper 14134, Houston, TX.

56. Jordan, T., et al., (46 authors), (2009). Achievement of the EC Network of Excellence HySafe, In: Proceedings of 3rd International Conference of Hydrogen Safety, Corsica, France, September 16-18, 2009. *Intl. J. Hyd. Ener.*, Under review.
57. Jordan, T., Xiao, J., Middha, P., Travis, J., Garcia, J., Hansen, O.R., Molkov, V., Verbecke, F., Venetsanos, A.G., (2007). Results of the HySafe CFD validation Benchmark SBEP-V5, In: 2nd International Conference of Hydrogen Safety, San Sebastian, Spain, September 11-13, 2007.
58. Kikukawa, S., (2007). Consequence analysis and safety verification of hydrogen fueling stations using CFD simulation. *Intl. J. Hyd. Ener.*, 33(4), 1425-1434.
59. Kitagawa, T., Nakahara, T., Maruyama, K., Kado, K., Hayakawa, A., Kobayashi, S., (2008). Turbulent burning velocity of hydrogen-air premixed propagating flames at elevated pressures. *Intl. J. Hyd. Ener.*, 33, 5842-5849.
60. Kim, Y., Nam, J.H., Shin, D., Chung, T.-Y., Kim, Y-.G., (2009). Computational fluid dynamics simulations for hydrogen dispersion and exhaust in residential fuel cell systems, *Current Applied Physics*, In Press, DOI: 10.1016/j.cap.2009.11.048.
61. Kuo, K. K., (2005). Principles of Combustion. 2nd Edition, ISBN 0-471-04689-2. John Wiley & Sons, New Jersey.
62. Kuzentsov, M., Alekseev, V., Matsukov, I., Dorofeev, S., (2005). DDT in a smooth tube filled with a hydrogen-air mixture. *Shock Waves*, 14, 205-215.
63. Kwon, O.C., Faeth, G.M., (2001). Flame/stretch interactions of premixed hydrogen-fuelled flames: measurements and predictions, *Comb. Flame*, 124(4), 590-610.
64. LaChance, J., Tchouvelev, A. V. & Ohi, J. (2007). Risk-Informed Process and Tools for Permitting Hydrogen Fueling Stations. In: Proceedings of 2nd International Conference on Hydrogen Safety, San Sebastian, Spain.
65. Lacome, J.M., Dagba, Y., Jamois, D., Perrette, L., Proust, Ch., (2007). Large-scale hydrogen release in an isothermal confined area. In: 2nd International conference on hydrogen safety, 11–13 September 2007, San Sebastian, Spain.
66. Launder, B.E. & Spalding, D.P., (1974). The numerical computation of turbulent flows. *Comp. Meth. Appl. Mech. Eng.*, 3(2), 269-289.
67. Lee, J.H.S., Moen, I.O., (1980). The mechanism of transition from deflagration to detonation in vapor cloud explosions. *Proc. Energy Comb. Sci.*, 6, 359-389.
68. Makarov, D., Verbecke, F., Molkov, V., Roe, O., Skotenne, M., Kotchourko, A., Lelyakin, A., Yanez, J., Hansen, O.R., Middha, P., Ledin, S., Baraldi, D., Heitsch, M., Efimenko, A. Gavrikov, A., (2009). An inter-comparison exercise on CFD model capabilities to predict a hydrogen explosion in a simulated vehicle refuelling environment. *Intl. J. Hyd. Ener.,* 34(6), 2800-2814.
69. Marinescu-Pasoi, L., Sturm, B., (1994). Messung der Ausbreitung einer Wasserstoff-und Propanwolke in bebautem Gelaende" und "Gasspezifische Ausbreitungsversuche", Battelle Ingenieurtechnik reports R-68202 and R-68264.
70. Melheim, J.A., Ichard, M., Pontiggia, M., (2009). Towards a computational fluid dynamics methodology for studies of large scale LNG releases. In: Hazards XXI, 10-12 November, 2009, Manchester, UK.
71. Mercx, W.P.M., (1996). Extended Modelling and Experimental Research into Gas Explosions, Final Summary Report, CEC EMERGE Project Report, EV5VCT930274 (TNO)
72. Middha, P., (2008a). HySafe SBEP V11: Dispersion Simulations with Hydrogen Bus in an Underpass below a Highway. GexCon Technical Note Ref. Nr. GexCon-08-F46207-TN-4.
73. Middha, P., (2008b). HySafe SBEP V15: Explosion Simulations with Hydrogen Bus in an Underpass below a Highway. GexCon Technical Note Ref. Nr. GexCon-08-F46207-TN-6.
74. Middha, P., Engel, D., Hansen, O.R., (2009). Can the addition of hydrogen to natural gas reduce the explosion risk? 3rd International Conference of Hydrogen Safety, Ajaccio,

75. Middha, P., Hansen, O.R., (2005). FZK Combustion Experiments: FLACS calculations of H2 release and subsequent ignition in low confinement situations. GexCon Technical Note Ref. Nr. GexCon-05-F46207-TN-1.
76. Middha, P., Hansen, O.R., (2008). Predicting deflagration to detonation transition in hydrogen explosions, *Proc. Safety Prog.*, 27(3), 192-204; In: Proceedings of the AIChE Spring National Meeting and 41st Annual Loss Prevention Symposium, Houston, USA, April 22-26, 2007.
77. Middha, P., Hansen, O.R., (2009a). Using computational fluid dynamics as a tool for hydrogen safety studies *J. Loss Prevent. Proc. Ind.*, 22(3), 295-302.
78. Middha, P., Hansen, O.R., (2009b). CFD simulation study to investigate the risk from hydrogen vehicles in tunnels. *Intl. J. Hyd. Ener.*, 34(14), 5875-5886.
79. Middha, P., Hansen, O.R., Groethe, M., Arntzen, B.J., (2007). Hydrogen Explosion Study in a Confined Tube: FLACS CFD Simulations and Experiments, Presented at 21st International Colloquium of Dynamics of Explosions and Reactive Systems, Poitiers, France, July 23-27, 2007.
80. Middha, P., Hansen, O.R., Grune, J., and Kotchourko, A., (2010). Validation of CFD calculations against impinging jet experiments. *J. Haz. Mat.*, 179(1-3), 84-94.
81. Middha, P., Hansen, O.R., Schneider, H., (2007). Deflagration to Detonation Transition (DDT) in Jet Ignited Hydrogen-Air Mixtures: Large Scale Experiments and FLACS CFD Predictions. In: 12th International Loss Prevention Symposium, Edinburgh, UK, May 22-24, 2007.
82. Middha, P., Hansen, O.R., Storvik, I.E., (2006). Prediction of deflagration to detonation transition in hydrogen explosions. Proceedings of the AIChE Spring National Meeting and 40th Annual Loss Prevention Symposium, Orlando, FL, April 23-27, 2006.
83. Middha, P., Hansen, O.R., Storvik, I.E., (2009). Validation of CFD-model for hydrogen dispersion. *J. Loss Prevent. Proc. Ind.*, 22(6), 1034-1038.
84. Middha, P., Ichard, M., Arntzen, B.J., (2009). Validation of CFD modelling of LH_2 spread and evaporation against large-scale spill experiments. In: 3rd International Conference of Hydrogen Safety, Ajaccio, Corsica, France, September 16-18, 2009; *International Journal of Hydrogen Energy*, doi:10.1016/j.ijhydene.2010.03.122.
85. Middha, P., Skjold, T., Dahoe, A.E., (2006). Turbulent and Laminar Burning Velocities of Hydrogen-Air Mixtures from Constant Volume Explosions in a 20-litre Vessel. In: 31st International Symposium on Combustion, Heidelberg, Germany, August 6-11, 2006.
86. Middha, P., van Wingerden, C.J.M., (2009). On the use of consequence models for accident investigations. In: 43rd Annual Loss Prevention Symposium, Tampa, FL, USA, April 26-30, 2009.
87. Muppala, S.P.R., Nakahara, M., Aluri, N.K., Kido, H., Wen, J.X., Papalexandris, M.V., (2009). Experimental and analytical investigation of the turbulent burning velocity of two-component fuel mixtures of hydrogen, methane and propane. *Intl J. Hyd. Ener.,* 34, 9258-9265.
88. Ng, H.D., Lee, J.H.S., (2008). Comments on explosion problems for hydrogen safety. *J. Loss Preven. Proc. Ind.*, 21(2), 136-146.
89. Nicholls, F., (1998). PIPEX Project - flame acceleration in pipelines, Presented at 23rd UKELG Discussion Meeting on Deflagration to Detonation Transition, ICI Runcorn, UK.
90. NORSOK Standard Z-013. (2001). Risk and emergency preparedness analysis, Norwegian Technology Center, Oslo, Norway Rev. 2. Available from www.standard.no/pronorm-3/data/f/0/01/50/3_10704_0/Z-013.pdf.
91. Oran, E. S. And Gamezo, V. N., (2007). Origins of the deflagration-to-detonation transition in gas-phase combustion. *Comb. Flame*, 148, 4-47.

92. Papanikolaou, E.A., Venetsanos, A.G., Heitsch, M., Baraldi, D., Huser, A., Pujol, J., Makarov, D., Molkov, V., Garcia, J., Markatos, N., (2009). HYSAFE SBEP-V20: Numerical predictions of release experiments inside a residential garage with passive ventilation. In: 3rd International Conference of Hydrogen Safety, Ajaccio, Corsica, France, September 16-18, 2009.
93. Patankar, S.V., (1980). Numerical heat transfer and fluid flow. Hemisphere Pub, ISBN: 0070487405.
94. Peraldi, O., Knystautas, R., Lee, J.H.S., (1986). Criteria for transition to detonation in tubes. *Proc. Comb. Inst.*, 21, 1629-1637.
95. Pförtner, H., Schneider, H. (1984). Tests with jet ignition of partially confined hydrogen air mixtures in view of the scaling of the transition from deflagration to detonation, Final report for Interatom GmbH, Bergisch Gladbach, Germany, Oct. 1984, Fraunhofer ICT Internal Report.
96. Qiao, L., Kim, C.H., Faeth, G.M., (2005). Suppression effects of diluents on laminar premixed hydrogen/oxygen/nitrogen flames, *Comb. Flame*, 143 (1-2), 79-96.
97. Renoult, J., Wilkins, B.A., (2003a). Hydrogen Explosion Safety Phase 2 – Small scale dispersion experiments, GexCon-03-F46201-1, GexCon, Bergen, Norway (confidential).
98. Rehm, W., Gerndt, M., Jahn, W., Semler, F., Jones, I., (1998). CFD simulation of deflagration-detonation processes usingvector- and parallel computing systems. *App. Math. Modelling*, 22, 811-822.
99. Rehm, W., Nae, C., Jahn, W., Vogelsang, R., Wang, B.L., (2002). CFD simulations of turbulent reactive flows with supercomputing for hydrogen safety. *Comp. Phys. Comm.*, 147, 522–525.
100. Renoult, J., Wilkins, B.A., (2003b). Hydrogen Explosion Safety Phase 2 – Small scale explosion experiments, GexCon-03-F46201-2, GexCon, Bergen, Norway (confidential).
101. Roberts, P.T., Shirvill, L.C., Roberts, T.A., Butler, C.J., Royle, M., (2006). Dispersion of hydrogen from high-pressure sources. In: Proceedings of the XIX Hazards Conference, 27-30 March, 2006, Manchester, UK.
102. Royle, M., Shirvill, L.C., & Roberts, T.A. (2007). Vapour Cloud explosions from the ignition of methane/hydrogen/air mixtures in a congested region. In: Proceedings of 2nd International Conference on Hydrogen Safety, San Sebastian, Spain.
103. Sato, Y., Merilo, E., Groethe, M., Colton, J., Chiba, S., Iwabuchi, H. (2006). Homogeneous hydrogen deflagrations in a sub-scale vehicle tunnel. In: Proceedings of 15th World Hydrogen Energy Conference, Lyon, France.
104. Selby, C. & Burgan, B., (1998). Blast and fire engineering for topside structures, Phase 2, Final summary report, Steel Construction Institute, UK, SCI Publication Number 253.
105. Shepherd, J.E., Lee, J.H.S., (1992). On the transition from deflagration to detonation. In: P. Hussaini, P. Kumar and P. Voigt, Editors, Major research in combustion, Springer, USA, pp. 439–471.
106. Sherman, M.P., Tieszen, S.R. & Benedick, W.B, (1989). FLAME Facility, The Effect of Obstacles and Transverse Venting on Flame Acceleration and Transition to Detonation for Hydrogen-Air Mixtures at Large Scale, Sandia National Laboratories, Albuquerque, NM 87185, USA, NUREG/CR-5275, SAND85-1264, R3.
107. Shirvill, L.C., Royle, M., Roberts, T.A. (2007). Hydrogen releases ignited in a simulated vehicle refuelling environment. In: Proceedings of 2nd International Conference on Hydrogen Safety, San Sebastian, Spain.
108. Statharas, J.C., Venetsanos, A.G., Bartzis, J.G., Würtz, J., Schmidtchen, U., (2000). Analysis of data from spilling experiments performed with liquid hydrogen, *J. Haz. Mat.*, 7, 57-75.
109. Swain, M.R., Grilliot, E.S., Swain, M.N., (1998). Phase 2: Risks in indoor vehicle storage, in Addendum to Hydrogen Vehicle Safety Report: Residential Garage Safety Assessment, U.S.

110. Taylor, S. C., (1991). Burning velocity and the influence of flame stretch. Ph.D. Thesis, University of Leeds.
111. Tegnér, J., Sjögreen, B., (2002). Numerical investigation of deflagration to detonation transitions. *Comb. Sci. Tech.*, 174(8), 153-186.
112. Tse S.D., Zhu D.L., Law C.K., (2000). Morphology and burning rates of expanding spherical flames in H_2/O_2/inert mixtures up to 60 atmospheres. *Proc. Comb. Inst.*, 28(2), 1793-1800.
113. Turns, S.R., (2000). An introduction to combustion. McGraw Hill, New York.
114. Vaagsaether, K., Knudsen, V., Bjerketvedt, D., (2007). Simulation of flame acceleration and DDT in H2–air mixture with a flux limiter centered method. *Intl. J Hyd. Ener.*, 32, 2186–91.
115. Venetsanos, A.G., et al., (2006). Report on CFD-experimental matrix design for internal project InsHyde. HySafe Deliverable D38.
116. Venetsanos, A.G., Baraldi, D., Adams, P., Heggem, P.S., Wilkening, H., (2008). CFD modelling of hydrogen release, dispersion and combustion for automotive scenarios, *J. Loss Prevent. Proc. Ind.*, 21(2), 162-184.
117. Venetsanos, A.G., Bartzis, J.G., (2007). CFD modelling of large-scale LH_2 spills in open environment, *Intl. J Hyd. Ener*, 32(13), 2171-2177.
118. Venetsanos, A.G., Huld, T., Adams, P., Bartzis, J.G., (2003). Source, dispersion and combustion modelling of an accidental release of hydrogen in an urban environment, *J. Haz. Mat.*, 105(1-3), 1-25.
119. Venetsanos, A.G., Papanikolaou, E., Delichatsios, M., Garcia, J., Hansen, O.R., Heitsch, M., Huser, A., Jahn, W., Jordan, T., Lacome, J.-M., Ledin, S., Makarov, D., Middha, P., Studer, E. Tchouvelev, A.V., Teodorczyk, A., Verbecke, F., Van der Voort, M.M., (2009). An inter-comparison exercise on the capabilities of CFD models to predict the short and long term distribution and mixing of hydrogen in a garage. *Intl. J Hyd. Ener*, 34(14), 5912–5923.
120. Venetsanos, A.G., Papanikolaou, E., Middha, P., Hansen, O.R, Garcia, J., Heitsch, M., Baraldi, D., Adams, P., (2010). HySafe Standard benchmark Problem SBEP-V11: Predictions of hydrogen release and dispersion from a CGH2 bus in an underpass. *Intl. J Hyd. Ener*, Accepted (2010).
121. Wilkening, H., Baraldi, D., (2007). CFD modelling of accidental hydrogen release from pipelines. *Intl. J. Hyd. Ener.*, 32(13), 2206-2215.
122. Williams, F. A., (1986). Lectures on applied mathematics in combustion: Past contributions and future problems in laminar and turbulent combustion. *Physica D*, 20D (1): 21-34.
123. Witcofski, R.D., (1981). Dispersion of flammable clouds resulting from large spills of liquid hydrogen, NASA Technical Memorandum 83131.
124. Witcofski, R. D., Chirivella, J. E., (1984). Experimental and analytical analyses of the mechanisms governing the dispersion of flammable clouds formed by liquid hydrogen spills, Int. J. Hydrogen Energy, 9(5), 425-435.
125. Zabetakis, M.G., (1965). Flammability characteristics of combustible gases and vapours (Buletin 627), US Bureau of Mines, Washington, D.C.
126. Zbikowski, M., Makarov, D., Molkov, V., (2008). LES model of large scale hydrogen–air planar detonations: Verification by the ZND theory. *Intl. J. Hyd. Ener.*, 33, 4884-4892.